DEPARTMENT OF PHYSICS
UNIVERSITY OF JYVÄSKYLÄ
RESEARCH REPORT No. 4/2014

QUANTUM FLUCTUATIONS IN SUPERCONDUCTING NANOSTRUCTURES

BY
JANNE LEHTINEN

Academic Dissertation
for the Degree of
Doctor of Philosophy

To be presented, by permission of the
Faculty of Mathematics and Natural Sciences
of the University of Jyväskylä,
for public examination in Auditorium FYS-1 of the
University of Jyväskylä on June 13, 2014
at 12 o'clock noon

Jyväskylä, Finland
June 2014

ABSTRACT

LEHTINEN, JANNE
QUANTUM FLUCTUATIONS IN SUPERCONDUCTING NANOSTRUCTURES
Jyväskylä: University of Jyväskylä, 2014, 126 p.
(Research report/Department of Physics, University of Jyväskylä
ISSN 0075-465X)
ISBN 978-951-39-5688-2 (nid.)
ISBN 978-951-39-5689-9 (PDF)
Diss.

Modern nanofabrication technology enables fabrication of very narrow quasi-1-dimensional superconducting nanowires demonstrating finite resistivity within the range of experimentally obtainable temperatures. The observations were reported in ∼10 nm nanowires of certain superconducting materials. The effect has been associated with quantum phase slip process - the particular manifestation of quantum fluctuations of the order parameter. In titanium, the phenomenon can be observed already at dimensions ∼35 nm where the fabrication is well reproducible and the dimensions of samples can be characterized with high accuracy. We have performed systematic study of the size dependence of transport properties for superconducting ultra-narrow titanium nanowires utilizing method of gradual size reduction by low energetic ion beam milling. The method enables the study of the same nanowire with 1 nm effective diameter reduction between measurement cycles. The experiments demonstrated clear crossover to fluctuation dominated regime when the dimensions are reduced below a certain threshold. All available at our disposal microscopic analyses indicate no damage or contamination of the bulk of the nanowire due to the ion milling.

The next stage of the work was to demonstrate experimentally the quantum duality between the physics of Josephson junction and superconducting nanowire governed by quantum fluctuations. We showed that sufficiently narrow nanowires embedded in high-impedance environment demonstrate the insulating state - Coulomb blockade. The system can be considered as a single Cooper pair transistor without any dielectric barriers. Irradiation of the nanowire with external RF drive leads to formation of the Bloch steps on the IV characteristics - the phenomenon dual to the well-known Shapiro effect, currently used as quantum standard of electric voltage. We have performed experiments demonstrating the corresponding current singularities which confirm the hypothesis. The observation is of significant importance for both scientific and metrological communities.

Keywords: superconductor, fluctuation, phase slip, Bloch oscillation, QPS-transistor, 1-dimensional, titanium, ion milling

Author

Janne Lehtinen
Department of Physics
University of Jyväskylä
Finland

Supervisor

Docent Konstantin Arutyunov
Department of Physics
University of Jyväskylä
Finland

Reviewers

Prof. Alexey Ustinov
Department of Physics
Karlsruhe Institute of Technology
Germany

Prof. Hervé Courtois
CNRS and UJF
Institut Néel
France

Opponent

Prof. Alexey Bezryadin
Department of Physics
University of Illinois
USA

ACKNOWLEDGEMENTS

The past four years I've been working on my dissertation there are several people who I wish to acknowledge. I would like to express my very great appreciation to my supervisor Docent Konstantin Arutyunov for his guidance in the project. I would like to offer my special thanks to Mrs. Terhi Hongisto for helping me in the beginning of the project by getting me familiar with nanofabrication equipment and dilution fridge.

I am particularly grateful for the assistance given by Taneli Rantala by fabricating samples and participating in measurements and Hannu-Pekka Auraneva for help with the Kelvinox dilution fridge and Leena Leino for help with taking AFM-images of the samples. I wish also to acknowledge the help provided by other co-workers in the group Pasi Jalkanen, Igor Lyakhov and Miika Leppänen.

My special thanks are extended to the staff of NanoScience Center and physics department of University of Jyväskylä. Especially I would like to offer my special thanks to the laboratory engineers Tarmo Suppula, Antti Nuottajärvi and Kimmo Kinnunen for help with the cryostats, constant helium supply even when it has been challenging and keeping the equipment in operation.

I would also like to acknowledge our departmental secretaries Riitta-Liisa Kuittinen and Soili Leskinen for making the bureaucracy easier for us and organizing the practical matters with efficiency. I'm grateful for the national graduate school in materials physics for financing my studies and finally, I wish to thank my family and friends for their support and encouragement throughout my study.

It has been a pleasure, sincerely,

The main results of the thesis have been reported in following articles:

A. I: J. S. Lehtinen, T. Sajavaara, K. Yu. Arutyunov, M. Yu. Presnjakov, and A. L. Vasiliev, Evidence of quantum phase slip effect in titanium nanowire, Phys. Rev. B 85, 094508 (2012).

A. II: J. S. Lehtinen and K. Yu. Arutyunov, The quantum phase slip phenomenon in superconducting nanowires with a low-Ohmic environment, Supercond. Sci. Technol. 25, 124007 (2012).

A. III: J. S. Lehtinen, K. Zakharov and K. Yu. Arutyunov, Coulomb Blockade and Bloch Oscillations in Superconducting Ti Nanowires, Phys. Rev. Lett. 109, 187001 (2012).

A. IV: J. S. Lehtinen, T. Rantala and K. Yu Arutyunov, Insulating state of a Quasi-1-Dimensional Superconductor, submitted to Phys. Rev. Lett. (2013).

Author has also contributed in work by fabricating samples and participating in measurements:

A. V: K. Yu. Arutyunov, T. T. Hongisto, J. S. Lehtinen, L. Leino and A. L. Vasiliev, Quantum phase slip phenomenon in ultra-narrow superconducting nanorings, Sci. Rep. 2, 213 (2012).

Patents:

P. I: K. Yu. Arutyunov, and J. S. Lehtinen, "Nanostructure and method for determining a dc electric current", patent, International Publication Number WO 2013/072568 A1

Conferences/workshops/seminars(presenter underlined):

C. I: J. Lehtinen, T. Rantala and K. Arutyunov, "Quantum fluctuations in superconducting nanostructures", invited talk, Superstripes 2013, Ichia, Italy, 2013.

C. II: J. Lehtinen, T. Rantala and K. Arutyunov, "Quantum fluctuations in superconducting nanostructures", talk, Physics days 2013, Espoo, Finland, 2013.

C. III: J. Lehtinen and K. Yu. Arutyunov, "Supercondcuting nanowire as a quantum standard of electric current", invited talk, EURAMET meeting, Madrid / Tres Cantos, Spain, 2013.

C. IV: J. S. Lehtinen, T. Rantala, K. Yu. Arutyunov, "Quantum fluctuations in 1D supercondcutors: physics and applications", talk, VORTEX-III, Rhodes-Greece, 2013.

C. V: K. Yu. Arutyunov and J. S. Lehtinen, "Superconducting nanowire as junctionless transistor and/or qautum standard of electric current", talk, 11th European Conference on Applied Superconductivity EUCAS 2013, Genova, Italy, 2013.

C. VI: J. Lehtinen, T. Rantala and K. Arutyunov, "Duality between physics of Josephson junction and superconducting ultra-narrow nanowire", invited talk, CECAM workshop 2012: Control and enhancement of superconductivity in conventional and high Tc nanostructures, Lausanne, Switzerland, 2012.

C. VII: J. Lehtinen, T. Rantala and K. Arutyunov, "Duality between physics of Josephson junction and superconducting ultra-narrow nanowire", poster, Nanoscience days 2012, Jyväskylä, Finland, 2012.

C. VIII: J. Lehtinen, and K. Arutyunov, "Duality between physics of Josephson junction and superconducting ultra-narrow nanowire", talk, Physics days 2012, Joensuu, Finland, 2012.

C. IX: K. Yu. Arutyunov and J. S. Lehtinen, "Quantum phase slip junction",invited talk, International Workshop "Superconducting NanoHybrids", San Sebastian, Spain, 2012.

C. X: J. Lehtinen and K. Arutyunov, "Duality between physics of Josephson junction and superconducting ultra-narrow nanowire", poster, Doctoral Training Session: Frontiers of Condensed Matter, Les Houches, France, 2011.

C. XI: J. Lehtinen and K. Arutyunov, "Bloch oscillations in a superconducting nanowire governed by quantum fluctuations", poster, Nanoscience days 2011, Jyväskylä, Finland, 2011.

C. XII: K. Yu. Arutyunov and J. Lehtinen, "Physics and applications of quantum phase slip effect in superconducting nanostructures", talk, European conference on applied superconductivity EUCAS-2011, Hague, Netherlands, 2011

C. XIII: J. Lehtinen and K. Arutyunov, "Electric current standard based on quantum fluctuations of the superconducting order parameter", poster, Physics days 2011, Helsinki, Finland, 2011.

C. XIV: J. Lehtinen, T. Hongisto and K. Arutyunov, "Quantum Fluctuations in superconducting nanowires and nanorings", CECAM workshop 2010, superconductivity in nanosized systems, invited talk, Lausanne, Switzerland, 2010.

C. XV: J. Lehtinen and K. Arutyunov, "Quantum standard for electric current", poster, Nanoscience days 2010, Jyväskylä, Finland, 2010.

CONTENTS

1 INTRODUCTION

More than hundred years after the discovery of superconductivity the phenomenon can be considered known but not yet completely understood. The strangeness of quantum physics is fully realized in it even though superconductivity is easily observable in simple demonstration experiments. Some manifestations of superconductivity phenomena are counterintuitive without theoretical understanding (e.g. Meissner effect). During my studies I've had to reformulate many of the facts that I thought I knew. I can't even imagine the surprise for Kamerlingh Onnes in 1911 when he was able to cool down a Hg-sample below the superconducting critical temperature and notice the sudden and absolute disappearance of resistivity!

Comprehensive theory for conventional superconductivity [1, 2] was formulated some forty years after the discovery and no significant improvements were made for next thirty years. Only after the discovery of high-T_c superconductors roughly thirty years ago, the research in the field reignited. Then for next ten to twenty years the superconductor research was mainly about high-T_c superconductors. Only after development of micro- and nanofabrication methods the conventional superconductor research became active again. By reducing the dimensions of a superconductor or by making more exotic structures utilizing the unique features related to superconductivity, several new types of devices were made.

Our research is about quasi-1-dimensional superconductivity. In strict sense, a 1-dimensional conductor never can be a true superconductor as there is always finite dissipation due to inevitable fluctuation effects. The research related to 1-dimensional superconductors began already in 1967 by pioneering work of W. Little [3] who analyzed the impact of fluctuations on the phase of superconducting order parameter, so called, phase slip (PS). The research was about how a finite temperature affects the shape of R(T) in transition from normal to superconducting state. At that time in realistically obtainable sample the thermal effects were small, only measurable few millikelvin range below the transition temperature, and never had significant contribution to superconductivity at temperatures $T \ll T_c$.

Two decades later, an idea of quantum tunneling in addition to thermally activated fluctuations was introduced by N. Giordano.[4] The requirements for observation of macroscopic tunneling of the order parameter or quantum phase slips (QPS) are strict. Thus systematic research required modern fabrication methods. The next round of experiments claiming the existence of quantum fluctuations were published in 2000 by A. Bezryadin, C. Lau and M. Tinkham.[5] Their method utilized suspended insulating carbon nanotubes, which were covered with thin layer of amorphous 5-nm-thick $Mo_{79}Ge_{21}$ film.

Uncertainty originating from uniqueness of nanoscale samples, fabricated in different experimental runs, gives rise to speculations: whether to associate the claimed effect to size-dependent 'physics' or to particular strange artefacts? In the group I've been doing my Ph.D. research, Quantum Nanoelectronics group in university of Jyväskylä, a method for progressive reduction of dimensions of a pre-fabricated superconducting nanowire was invented.[6, 7] The approach allows systematic study of a size effect in a same sample. With this method, aluminum nanowires were studied by M. Zgirski.[8] The results supported the quantum fluctuation hypothesis.[9, 10]

At the same time in our group, T. Hongisto studied size dependent decay of persistent currents in superconducting nanorings due to the QPS. My contribution to the project was to fabricate samples and participate in the measurements. The experiment was the first non-transport measurement studying the QPS-phenomenon and it demonstrated that the QPS affects the magnitude, the period and the shape of the current-phase relation of a superconducting nanoring.[11] The discovery was the first experimental observation of the impact of quantum fluctuations on the ground state of a macroscopically coherent system. Additionally to the basic science importance, the research contributed to the development of QPS-based qubit.[12]

The transport experiments with aluminum nanowires with diameters ~ 10 nm[8, 9, 10] gave promising results, but the dimensions of the those samples were at the limit of available fabrication. For more practical utilization and more conclusive study of the phenomenon, the rate of the fluctuations should be a) higher and b) the fabrication more controllable compared to 10 nm scales for aluminum. Theory predicts that for high QPS-rate high resistivity and low transition temperature is preferable. Suitable material satisfying these criteria is titanium. Other materials were also tested, but titanium had several advantages compared to the rest of the tested materials, one of most important being that from technological point of view Ti is easy-to-use material.

The first part of my experiments concentrates on systematic study of size dependent superconductivity of titanium nanowires in low-ohmic environment. At this stage, suitable methods for fabrication and measurement were developed. Second part of the studies deals with titanium nanowires embedded into high-ohmic environment, where QPS-stimulated charge phenomena lead to two intriguing applications: QPS junctionless transistor and quantum standard of electric current.

In Chapter 2 is the relevant theoretical background for understanding the

experiments starting from conventional superconductivity and fluctuations in 1-dimensional superconductors to duality between thin superconducting nanowire and Josephson junction. Sample fabrication, including the method of reducing pre-fabricated sample dimensions, and measurement methods are briefly discussed in Chapter 3. The results, which of large portion is yet unpublished, are presented in Chapter 4 followed by conclusions in Chapter 5.

2 THEORETICAL BACKGROUND

2.1 Introduction to superconductivity

Originally, superconductivity, a sudden loss of electrical resistivity below a certain threshold temperature, was discovered by Kamerlingh Onnes in 1911 when he studied the temperature dependencies of resistivity of various metals. The discovery of superconductivity became available solely due to developments of cryogenics. Actually the Nobel prize awarded to K. Onnes was not for the discovery of superconductivity, but for the method of helium liquefaction. It even could be said that after reaching the certain temperature range the discovery of superconductivity was inevitable: there are number of metals with high enough superconducting critical temperature.

At first, Onnes studied materials that were good conductors, gold and platinum. Luckily for him he switched to more easily refinable material: mercury. Much later with development of the microscopic theory, it became clear that typically the better conductor the metal is at room temperature, the lower critical temperature of superconductivity it has. This is due to the electron-phonon interactions which will be discussed later. For mercury the superconducting critical temperature is 4.2 K. At this temperature there is infinitely sharp drop in the resistance, as Onnes reported, "Mercury has passed into a new state, which on account of its extraordinary electrical properties may be called the superconductive state".[13]

Superconductors are more than a perfect conductors of electricity. In 1933 Walther Meissner and Robert Ochsenfeld discovered that a superconductor excludes applied magnetic fields within its interior (Meissner effect). The magnetic field induces circulating currents that oppose and repel the buildup of magnetic field in the bulk. In a solid, this effect is called diamagnetism, and in a perfect conductor – superconductor – perfect diamagnetism. It should be noted that repulsion of magnetic field from a hypothetical 'perfect conductor' and a superconductor (Meissner effect) are qualitatively different. In the former the repulsion happens only for a time-dependent magnetic field, while in superconductors the

Meissner state can be reached in a static field just by cooling the superconductor below the critical temperature.

2.1.1 Overview of theories in superconductivity

The London theory, developed in 1935 by brother Heinz and Fritz London, was the first phenomenological description of superconductivity. The London equations were able to describe the Meissner effect and were based on intuitive logic to treat the superconducting electrons as free electrons under the influence of a uniform external electric field. Nowadays the London model is the starting point in introductory courses on superconductivity but does not provide any insight on the origin of the effect.

In 1950 Ginzburg and Landau (GL) theory was published. It was an attempt to describe conventional superconductivity based on Landau's theory of second-order phase transitions. It doesn't give explanations for the microscopic origin of the phenomena, but examines the macroscopic properties of superconductivity with the aid of thermodynamic arguments. The theory can be used to describe both type-I and type-II superconductors. It has been proven that the GL theory is valid near T_c being in fact a limited form of the microscopic description of superconductivity.

Only few years after the GL-theory, in 1957, Bardeen, Cooper and Schrieffer (BCS) published two papers [1, 2], which provided the microscopic theory of superconductivity. The model describes the second-order phase transition at critical temperature T_c, the exponential dependence of electronic specific heat near $T = 0$, the Meissner effect, the infinite conductivity and the isotope effect i.e. why the lattice atoms mass affects the critical temperature. The model gives good quantitative agreement for specific heat and magnetic penetration depth and their temperature dependencies. The Nobel prize in 1972 was awarded to Bardeen, Cooper and Schrieffer for the development of their theory.

The rigorous derivation of BCS theory can be found in numerous papers, including the original articles, but for this work qualitative understanding of the theory is enough. The model is based on three main insights: the attractive force between electrons; the bound states formed by electrons outside the Fermi surface by the weak attractive force (no matter how weak); and the construction of the many-particle wavefunction, which has all the electrons near the Fermi surface paired up. From this frame, all necessary consequences and features of the BCS theory can be derived. Here we are only going to utilize the results derived from BCS model, mainly equations for the superconducting energy gap Δ, coherence length ξ and critical temperature T_c.

2.1.2 Electron-phonon coupling and Cooper pairs

The electrons are fermions and obey the Pauli exclusion principle, but when paired they behave like bosons, which can condense into the same quantum state. In classical (BCS) superconductivity the pairing is attained by phonon-electron

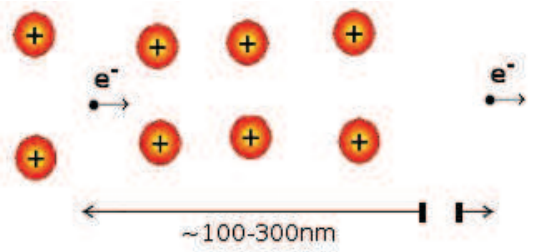

FIGURE 1 Qualitative picture of the electron - electron pairing by the distortion trail within the ion lattice. Note the long distance between electrons in a e-e pair (∼100 nm) compared to the distance between atoms in typical metallic lattice (∼0.5 nm).

coupling. The electron causes local polarization a material by attracting positive ions in the vicinity. This leaves a distortion trail. Such distortions have higher ion-density resulting an attractive influence to nearby electrons. This attraction is delayed by the difference of the time-scales of the electronic and the ionic motion (Fig. 1). The deformation is at maximum when the distance to the electron is approximately $d \approx \frac{v_F 2\pi}{\omega_D} \approx 100 - 300nm$, where v_F is the Fermi velocity of the electron, typically $(1\ to\ 3) * 10^6 \frac{m}{s}$, and ω_D the Debye frequency, which measures the response of the ionic sub-system and is about $(2\ to\ 8) * 10^{13}$ Hz. This sets the average electron pair separation, typically of the scale of hundreds inter-atomic distances screening the Coulomb repulsion between the paired electrons almost completely.

The energy of the pairing interaction is weak, of the order of 10^{-5} to 10^{-3} eV. This means that only at low temperatures a significant number of paired electrons (Cooper pairs), having the same state with respect to both relative and center-of-mass coordinate, are Bose condensed. The tendency for all the Cooper pairs to 'condense' into the same ground quantum state is responsible for the peculiar properties of superconductivity. The pair formalisms is adequate for classical superconductors (e.g. single element metals) and it probably includes also high-T_C superconductors with the exception that the pairing mechanism responsible for the Cooper pair formation in high-T_C superconductors is (probably) different. However, the only requirement for the superconductivity is that the potential is attractive regardless of its origin.

2.1.3 Dimensionality of a superconductor

Superconductivity in 1-dimension can be argued not to exist. By definition a 'conventional' superconductor doesn't dissipate energy. This is not true in 1-dimensional (1D) case. Actually in 1D there is always finite dissipation and non-zero electrical resistance. This is due to the fluctuations. There is always a finite probability that the modulus of the order parameter approaches zero allowing the phase of the order parameter to change by 2π. In practice this phase slippage is short dynamic process where a section of a 1D superconductor looses superconductivity for time $\sim \frac{\hbar}{\Delta}$. It is important to notice that this effect is enabled only for

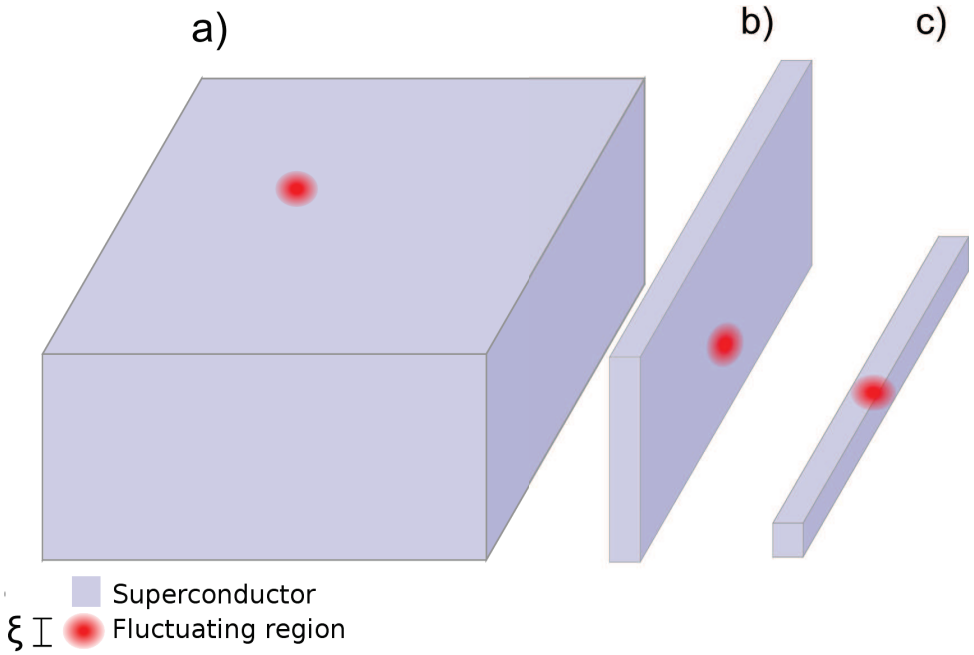

FIGURE 2 Picture of a a) 3D- b) 2D- and c) 1D-superconductor. The fluctuating region - the red dot - is shunted by neighboring superconducting area in the 3D and 2D case. In 1D-case there are no shunting regions.

1D limit. In 2- or 3-dimensional superconductor a fluctuation-driven momentary suppression of superconductivity is shunted by surrounding superconducting regions.(Figure 2) Thus only in 1-dimensional superconductor the fluctuations should have a measurable effect on the electric transport properties.

The dimensionality of the superconductor is defined by a characteristic length called coherence length ξ. The coherence length is the smallest length scale at which the superconducting electron density cannot change significantly. In typical conventional superconductor, ξ roughly defines the size of a Cooper pair. Thus the smallest length scale in which the suppression of superconductivity can happen is the coherence length. The BCS coherence length is given by expression

$$\xi = \frac{\hbar v_f}{\pi \Delta}, \tag{1}$$

where v_f is the Fermi velocity and Δ is the temperature dependent superconducting energy gap, which for weak coupling superconductors $\frac{\hbar\omega_D}{kT_c} \gg 1$ can be evaluated assuming continuous density of states from the following integral equation:

$$\frac{1}{N(0)V} = \int_0^{\hbar\omega_D} \frac{\tanh(\frac{1}{2}\beta(\delta^2+\Delta^2)^{\frac{1}{2}})}{(\delta^2+\Delta^2)^{\frac{1}{2}}} d\delta, \tag{2}$$

where $\beta = \frac{1}{k_b T}$, $\hbar\omega_D$ is the Debye cut-off energy, N_0 is the density of states at T $\rightarrow$ 0 and V_0 is a term related to electron-phonon coupling strength.

2.2 Superconductivity in quasi-1-dimensional limit

2.2.1 Concept of a phase slip

The concept of phase slips was introduced by W. Little [3]. He considered that thermodynamic fluctuations in a very thin superconducting wires could be detectable. The basis of the calculations were made within the GL model minimizing the free energy expressed by the GL functional in one dimension.

$$F(\Phi) = \int [a|\Psi(x)|^2 + b|\Psi(x)|^4 + c|\Delta\Psi(x)|^2]dx. \tag{3}$$

The order parameter $\Psi(x)$ is a complex function with real amplitude $\Delta(x)$ and phase $e^{i\phi(x)}$. In the equilibrium the fluctuations are ignored and the equilibrium value for $\Psi(x)$ is calculated by minimizing $\Delta(x)$ and $\phi(x)$. Other functional forms of $\Delta(x)$ and $\phi(x)$ are still possible with a probability proportional to the Boltzman factor $e^{-\beta F(x)}$. This means that in the vicinity of transition temperature there is a finite probability that the temperature fluctuations allow the order parameter to diffuse to higher free-energy states.

The concept of a phase slip can be easily understood for a loop geometry. The requirement for persistent current in a ring-shaped superconductor is that the line integral of the order parameter around the ring is multiple of 2π. The supercurrent is due to the gradient of the phase and the phase can only change an integer times 2π. When supercurrent decays, it can only decay by a discrete amount due to the change of the winding number. When the results are translated into a singly connected superconducting wire, the conclusion is that the ends of the wire retain a constant relative phase ϕ_{12} while the perfect conductivity requires that the potential difference between the ends of the wire is zero.

If to consider a current carrying superconducting nanowire having a finite resistance (whatever the cause), the averaged phase difference ϕ_{12} should increase steadily with time in order to retain the zero potential difference between the wire ends. The solution for this apparent inconsistency is that phase-slip events occur, in which the phase coherence is momentarily broken at some point(s) of the superconductor allowing the phase to change by 2π. To maintain the steady state, according to the Josephson relation (41), such events should occur with frequency

$$f_j = \frac{2eV}{h}, \tag{4}$$

where the V is the time-averaged voltage. This means that the relative phase difference increases in time until a phase slip process occurs reducing the phase difference ϕ_{12}. When the phase-slip occurs, with the current being constant (kept by external source), the result is a finite voltage across the sample.

The steady-state order parameter of a current carrying superconductor is depicted in figure 3a, where the solutions $\Psi_0 e^{iqx}$ of the GL complex function Ψ(x) are expressed in polar coordinates. The solutions for $J < J_c$ is can be presented

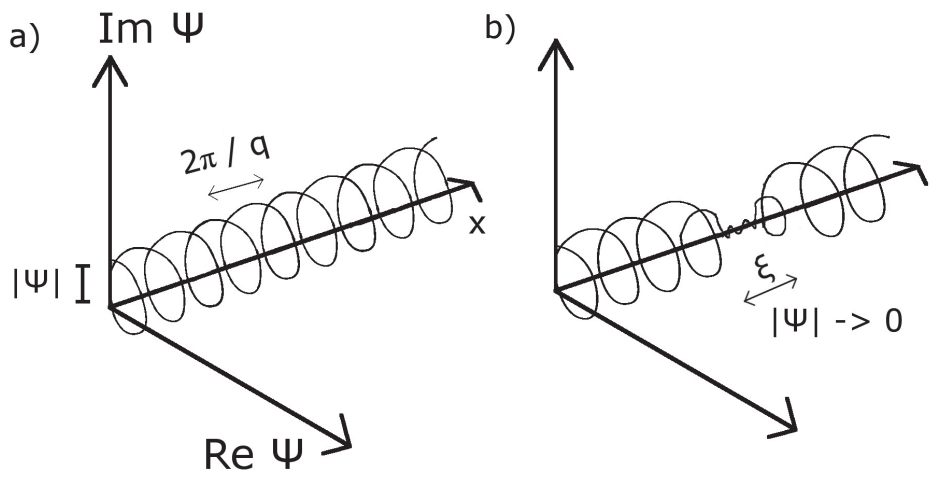

FIGURE 3 After M. Tinkham.[14] a) Uniform solution of complex current-carrying GL equation in one dimensional superconductor presented as Argand diagram. b) Non-uniform solution where the helix is tightened $|\Psi| - > 0$ just before the phase-slip happens.

by helices of pitch $\frac{2\pi}{q}$ and radius Ψ_0. The presented equilibrium solution is for current-carrying superconductor at zero voltage.

If a voltage is applied the relative phase difference between wire ends increases at steady rate 2eV/h as has been just discussed. This can be schematically presented by tightening of the helix until it 'looses' one turn presented in figure 3b. This process can be formally understood as acceleration of the supercurrent explained by the London equation

$$\frac{\partial \mathbf{j_s}}{\partial t} = \frac{n_s e^2}{m} E, \tag{5}$$

which means that the presence of voltage increases q until the phase difference between the ends of wire obeys $\phi_{12} = qL$ or from the London equation

$$\frac{\partial \mathbf{v_s}}{\partial t} = \frac{e\mathbf{E}}{\mathbf{m}} \quad (j_s = n_s e v_s), \tag{6}$$

where the supercurrent density j_s is related to velocity v_s through the concentration of 'superconducting' electrons n_s. When the velocity v reaches the critical limit of v_c the uniform solution is no longer possible. The phase slip processes maintain the steady state at $v_s < v_c$, in the presence of non-zero voltage, if the turns of the helix are annihilated at the same rate of the new ones are cranked.

Langer and Ambegaokar presented the theory that is based on the Ginzburg-Landau equation constructed in analogy with the droplet model of a supersaturated vapor.[15] Just as in the droplet model, the fluctuations are extremely improbable and play no role determining the bulk properties of system. The model equates the constantly increased current caused by non-zero voltage with fluctuations reducing the phase difference.

Neglecting the possible contribution of normal current, the conservation of the current requires that the supercurrent is constant. According to G-L model the supercurrent is proportional to the gradient of phase and the density of superconducting electrons:

$$|\Psi|^2 \frac{d\phi}{dx} = I \tag{7}$$

which serves as constraint on variations of the order parameter. If the amplitude of the order parameter is small at some point, the gradient $d\phi/dx$ must be large. Thus when $|\Psi| \to 0$, it is easy to subtract or add a turn of a helix (fig. 3).[3] Langer and Ambegaokar used this idea and found a path through function space where two uniform solutions with different amount of turns have the lowest free-energy barrier to overcome. That way, they found the saddle point barrier of the GL free energy. By this, they calculated the saddle-point free-energy increment

$$\Delta F_0 = \frac{\sqrt{2} H_c(T)^2}{3\pi} \sigma \xi, \tag{8}$$

where σ is the area of the conductor and ξ is the coherence length and H_C is the temperature-dependent critical magnetic field. It can be thus deducted that the free-energy barrier is reduced when the wires cross section is reduced. The energy ΔF_0 is of the same order as the condensation energy of the length of wire of $\sim \xi$, which is plausible since one can argue that the Ψ cannot vary on scales smaller than the coherence length.

In the absence of net current, the phase slips $\pm 2\pi$ are equally probable. When a finite current is applied the slips in one direction become more probable than in the other. The energy difference between the initial and the final state is unequal depending on the direction in the phase space. This difference stems from the electrical work done in the process. The situation can be qualitatively described by modeling the phase slip within a model of resistively and capacitively shunted Josephson junction.[14] The model is discussed in more details section 2.3.1 in context of Josephson junctions. For a phase slip of 2π the energy difference is

$$\delta F = \Delta F_+ - \Delta F_- = \frac{h}{2e} I. \tag{9}$$

McCumber showed that Langer and Ambegaokar arguments can be used as well with in current and voltage bias regimes.[16]

The phase slip rate can be easily calculated with accuracy of an unknown prefactor Ω

$$\frac{d\phi_{12}}{dt} = \Omega [e^{\frac{-\Delta F_0 - \frac{\delta F}{2}}{k_B T}} - e^{\frac{-\Delta F_0 + \frac{\delta F}{2}}{k_B T}}] = \frac{2eV}{\hbar}. \tag{10}$$

The prefactor is often called attempt frequency. The attempt frequency is dependent on the wire length since one could expect that in the simplest case of non-interacting phase slips, the phase slips should happen independently from each other.

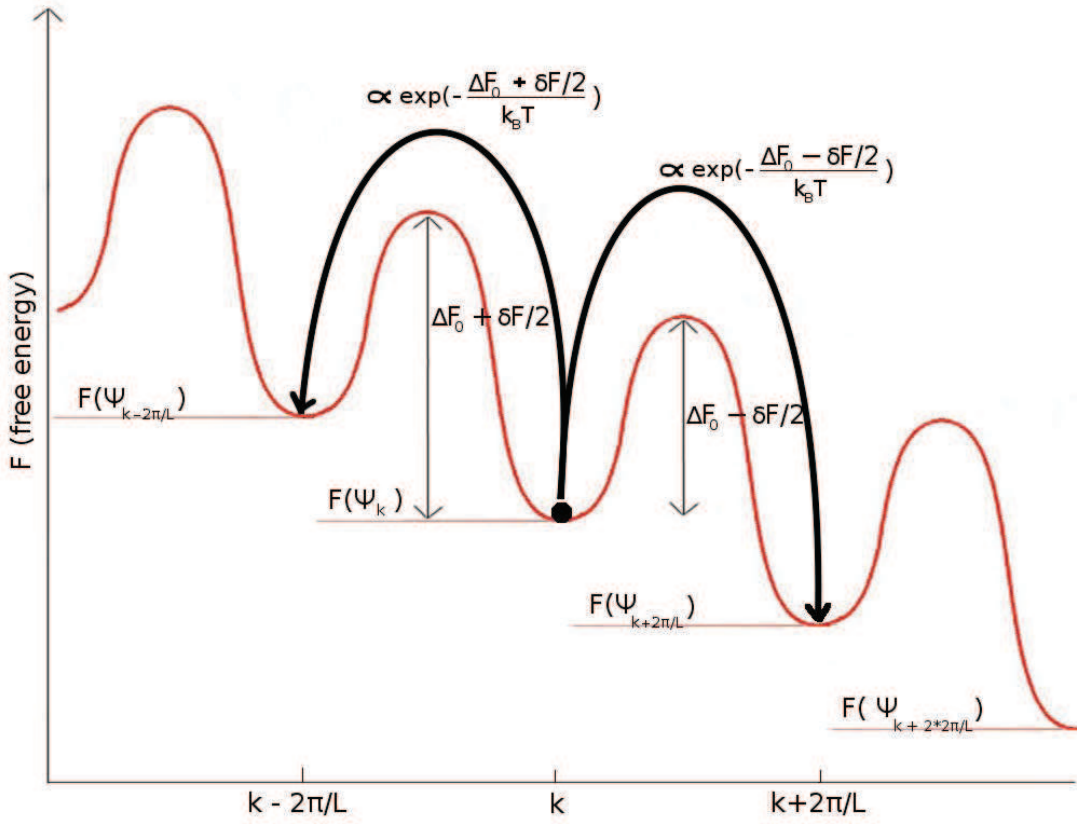

FIGURE 4 The washboard model with finite current describing the thermal phase-slips energy scale and escapes to different directions.

The correlation between voltage and current for a wire undergoing phase slips can be resolved from the equation (10) using the result (9). Figure 4 schematically depicts the corresponding energy-phase relation at finite current: tilted wash-board potential.

McCumber and Halperin derived equation for the attempt frequency using time dependent GL theory (TDGL) [17]

$$\Omega = \frac{L}{\xi}(\frac{\Delta F_0}{k_B T})^{\frac{1}{2}}\frac{1}{\tau_s}, \tag{11}$$

where τ_s is the characteristic relaxation rate of the supercurrent in the TDGL. Thus an attempt frequency is resolved and using equations (10) and (9) for voltage-current relation, one gets:

$$V = \frac{\hbar\Omega}{e} e^{\frac{-\Delta F_0}{k_B T}} \sinh(\frac{hI}{4ekT}). \tag{12}$$

The model is called LAHM (Langer-Ambegaokar-Halperin-McCumber).

For comparison with experiment the resistance caused by the TAPS needs to be calculated. For simplicity we can assume small current approximation which replaces the hyberbolic sine by its argument and by using the Ohm's law the resistance can be calculated

$$R_{TAPS} = \frac{V}{I} = \frac{\Omega\pi\hbar^2}{2e^2k_BT}\exp\left(\frac{-\Delta F_0}{k_BT}\right). \quad (13)$$

The approximation is valid when $I < I_0$, where $I_0 = 4ek_BT/h$. At lowest temperature used to measure R(T) dependencies in our experiments $\sim$ 20 mK the maximum current is I_0(T= 0.020 K) $\approx$ 0.27 nA which is much larger than the AC-currents used in the R(T) measurements, typically 50 pA.

The LAHM model has been verified by several experiments. The most well known experiments are the measurements of the resistive transition and the current-voltage characteristics of single-crystal tin whiskers.[18, 19] The thermally activated phase slips proposed by Langer and Ambegaokar were observed and their contribution, determined by the rate of phase slippage, was verified with the modification of the attempt frequency proposed by McCumber and Halperin.

The peculiar point of the model is that it only works at temperatures just below the transition temperature. The LAHM theory doesn't work when temperature approaches T_c since the attempt frequency and free-energy barrier go to zero at T_c. On the other hand, the model is based on GL theory which works only at values $T/T_c \approx 1$. For thermally activated phase slips the constraint is unimportant since the effects are noticeable only sufficiently close to the critical temperature, but for the phase slips of quantum origin, expected to be observable well below the T_c, GL formalism is not applicable even qualitatively.

2.2.2 Microscopic model of Quantum Phase Slips (QPS)

When the temperature is lowered, the probability of thermally activated phase slips reduces exponentially and no measurable resistance should be expected when T is much smaller than T_c (13). However, certain experiments on ultra-narrow nanowires [4, 5, 9, 10, 20, 21, 22, 23, 24, 25, 26] have shown the opposite: resistance has a finite value even at T $\rightarrow$ 0. Several phenomenological models were suggested to explain the phenomena.[23, 27, 28, 29] Instead of the thermally activated phase slips, the phase slips originating from quantum tunneling of the phase of the order parameter start to be of essence.

The first estimate for the QPS tunneling rate $\sim e^{-S_{QPS}}$ lead to a disappointing conclusion, that couldn't explain the experimental results, because of an overestimated QPS action term. The term was assumed to be equal to the number of transverse channels $S_{QPS} \sim N_{ch} = {k_F}^2\sigma$ in a wire of cross section σ [4, 22]. That assumption leads to a huge value for S_{QPS} in experimentally achievable samples. When the diameter is about $\sim$ 10 nm the S_{QPS} would be about $10^2 - 10^3$ and therefore the QPS should be virtually non-existent.

Golubev and Zaikin (GZ) argued that the estimation needs qualitative improvement.[30] The first approximation they made was to take into consideration the finite dimension $l < 10$ nm of the experimentally obtainable nanowires falling into the dirty limit $l \ll \xi_0$. The coherence length $\xi \sim \sqrt{l\xi_0} << \xi_0$ can be considered as the typical QPS lateral dimension. They also argued that the role of electromagnetic field should be smaller than that was calculated earlier.

Third revision was to presume that dissipative currents should not have a strong impact on the QPS rate when temperature is significantly smaller than T_c. They used microscopic approach contrary to the TDGL-model used in the earlier estimations.

The GZ model gives the QPS rate in the following form:

$$\Gamma_{QPS} = \Omega e^{-S_{QPS}} = \Omega e^{-(S_{out}+S_{core})}. \tag{14}$$

The action S_{QPS} is divided into two terms. The term S_{core} considers the 'stand alone' phase slip, and it is determined by the condensation energy and the dissipation of the normal currents. The S_{out} is a hydrodynamic part which depends on propagation of electromagnetic fields originating from each phase slip event. Estimation of the S_{out} can be simplified by the fact that outside the core the absolute value of the order parameter remains equal to some mean value and only the phase of the order parameter changes. The S_{out} saddlepoint action can be written in the form

$$S_{out} = \mu \ln [\frac{\min (c_0\beta, X)}{\max (c_0\tau_0 x_0)}], \tag{15}$$

where $c_0 = \frac{1}{L_s C_l}$ is the Mooij-Schön plasmon velocity [31], C_l and L_s are the wire's capacitance and inductance per unit length, the x_0 and τ_0 are the typical length and time scales of the QPS event.

$$\mu = \frac{\pi}{4\alpha}\sqrt{\frac{C_l}{L_s}} \tag{16}$$

is a dimensionless parameter describing the characteristic damping of the electromagnetic excitations, where α is the fine structure constant. For infinitely long wire the S_{out} at the limit of $T \to 0$ diverges logarithmically towards zero making the contribution of the S_{out} term dominant.

The other part of the S_{QPS} is the core contribution. The calculation of the core action parameter is a complicated task. However, if a dimensionless prefactor, which can be obtained from the experimental data, is utilized, the calculations are much simplified. The approach allows to approximate the order parameter field inside the QPS core by two types of fluctuations. The absolute value of the the order parameter should vanish at limits $x = 0$ and $\tau = 0$ and coincide with the mean field value outside the QPS core. The phase flips at $x = 0$ and $\tau = 0$ provide change of the net phase 2π. This leads to a trial function describing the dynamics of the phase slip [32]

$$|\delta\Psi(x,\tau)| = \Psi_0 exp(-\frac{x^2}{2{x_0}^2} - \frac{\tau^2}{2{\tau_0}^2}). \tag{17}$$

By minimizing the action S_{core} with respect to x_0 and τ_0 it is possible to get intuitively expected results:

$$x_0 = a\sqrt{\frac{D}{\Psi_0}} \approx \xi \tag{18}$$

$$\tau_0 = \frac{b}{\Psi_0} \approx \frac{\Delta_0}{h} \tag{19}$$

The above estimations give the net result:

$$S_{core} = \pi A N_0 \sigma \sqrt{D\Psi_0} = A\frac{R_q L}{R_N \xi}, \tag{20}$$

where a, b, A are the dimensionless prefactors, R_N is the total normal state resistance, $R_q = \frac{\pi\hbar}{2e^2} = 6.453\ k\Omega$ is the quantum resistance. The QPS rate can be approximated $S_{QPS} \approx S_{core}$ for sufficiently short nanowire with length L in which the capacitive effects are small enough and thus $S_{out} << S_{core}$. The limit of the validity of the approximation is

$$L \ll L^* = \xi\frac{e^2 N_0 \sigma}{C_l}. \tag{21}$$

For a typical dirty superconductor this limit is around 10 μm. In longer wires the capacitative effects start to affect the core part and the separation of the action terms into S_{core} and S_{out} isn't an ideal approximation. In our experiments, the wires are of the order of the characteristics length L^* and the approximation works well enough compared to the experimental accuracy. In the opposite limit for sufficiently long nanowires $L > 100\ \mu m$ the core action takes more complicated form

$$S_{core} = \frac{DR_q}{R_N}(\frac{L}{\xi})^{\frac{3}{2}}\sqrt{\frac{D}{e^2 N_0 \sigma}}, \tag{22}$$

where D is the numerical prefactor.

The model [30] gives for S_{QPS} action the value about $\sim$ 2 orders of magnitude smaller than the first estimates [23, 29] supporting the expectation that QPS should be observable for sufficiently thin wires.

The prefactor Ω can be calculated by instanton technique:

$$\Omega = \frac{BS_{QPS}L}{\tau_0 x_0} \tag{23}$$

where B is the numerical constant of the order of unit. The QPS rate for sufficiently short nanowires can be approximated using equations (14), (18), (19) and (20) and $A, B \approx 1$

$$\Gamma_{QPS} = \frac{\Delta_0}{h}\frac{R_Q}{R_N}(\frac{L}{\xi})^2 \exp\,(-\frac{R_Q}{R_N}\frac{L}{\xi}). \tag{24}$$

2.2.3 Resistance of a superconducting nanowire below T_c

The QPS rate for the nanowires in the zero current limit is set by the equations (14) and (24). A heuristic model for calculating the resistance caused by the QPS with small currents can be build up by using the same approach as in the LAHM model for TAPS. The approach leads to the relation, which is relatively close to the one obtained by more advanced calculations, but the derivation is more easily understandable. Let's write the action in the form

$$S_{QPS} = \frac{\Delta F_0}{E_{ch}}, \tag{25}$$

where E_{ch} is the characteristic energy scale of the QPS process. Using the result for the tunneling rate calculated for non-zero current

$$\Gamma_{QPS} = \Gamma_- - \Gamma_+ = \Omega \exp\left(-[\frac{\Delta F_0 - \delta F/2}{E_{ch}}]\right) - \Omega \exp\left(-[\frac{\Delta F_0 + \delta F/2}{E_{ch}}]\right)$$

$$= 2\Omega \sinh\left(\frac{\delta F}{2E_{ch}}\right) \exp\left(\frac{-\Delta F_0}{E_{ch}}\right). \tag{26}$$

The effective dc voltage can be derived in full analogy with the LAHM model (12):

$$V_{QPS} = \frac{h}{2e\tau_{QPS}} = \Omega \frac{h}{e} \sinh\left(\frac{hI}{4eE_{ch}}\right) \exp\left(\frac{-\Delta F_0}{E_{ch}}\right). \tag{27}$$

The effective resistance in the linear limit $R_{QPS} = \frac{V_{QPS}}{I}$ $(I \to 0)$ is

$$R_{QPS} \equiv \frac{V_{QPS}}{I} = \frac{\Omega R_q h}{E_{ch}} \exp\left(-S_{QPS}\right). \tag{28}$$

Note that E_{ch} appears only in the prefactor Ω. Making an assumption $E_{ch} \approx \Delta$ one arrives to a simple expression

$$R_{QPS} = R_q \frac{h\Omega}{\Delta} \exp(-S_{QPS}). \tag{29}$$

The expression used for fitting our experimental data is more complicated compared to (29) and has been based on the microscopic model.[30, 32] The heuristic model presented above gives almost identical results at high temperature limit $1/2T_c < T < T_c$. The equation used for the fitting the data is [32]:

$$R_{QPS} = b{S_{QPS}}^2 \Delta(T) \frac{L}{\xi(T)} \exp\left(-2S_{QPS}\right). \tag{30}$$

Note the coefficient "2" under exponent originating from pairs of phase slips $\pm\, 2\pi$. The expression (30) is based on model for QPS only taking into account the core action being the valid approximation for sufficiently short wires. The fitting parameter b isn't dimensionless. Likely it has the form of $b \cong \frac{R_N}{\Delta_0}$. However,

note that due to strong exponential dependence the exact coefficient in the prefactor of (30) is not so that important. Using expression (20) for the core action, the equation (30) can be written in form utilizing the parameters obtainable from the experiment

$$R_{QPS} = R_N(A\frac{R_qL}{R_N\xi(T)})^2\frac{\Delta(T)}{\Delta_0}\frac{L}{\xi(T)}\exp\left(-2A\frac{R_qL}{R_N\xi(T)}\right). \quad (31)$$

The parameter $A \approx 1$ is dimensionless and describes the magnitude of the QPS action. In this work the coefficient A has been used as the fitting parameter when comparing our data with the model.[30, 32] It should be noted that all above derivations consider the phase slips to be rare events, ie. $R_{QPS} << R_N$. To our best knowledge no theory has been proposed so far to describe the limit of "strong" phase slips $R_{QPS} \approx R_N$ reachable in the experiments (see Chapter 4).

2.2.4 Superconductor to insulator transition (SIT)

Extensive experiments conducted on short ultra-thin superconducting MoGe wires, fabricated with molecular templating method [33], have showed SIT transition when two conditions are met: the wire length is short $L \ll \xi\sqrt{N_T}$, where N_T is number of transverse channels, and the resistance of the wire is higher than the superconducting resistance quantum $R_Q = h/4e^2 \approx 6.5$ kΩ.[21, 34] MoGe nanowires with slightly lower resistance have transitions that can be explained by LAHM [3, 16] and G-Z [30] models.

The SIT transition in short superconducting MoGe nanowires is accounted for Chakravarty-Schmid-Bulgadaev (CSB) dissipative phase transition [35, 36, 37] and later generalized for thin nanowires.[38, 39, 40] It is not clear whether the SIT occurs in ultra-thin short superconducting wires or is it a crossover from wires with small QPS rate to wires in which the QPS rate so large that it drives the wire to normal state.

The shape of the transitions of the short ultra-thin MoGe nanowires, when compared to our experiments with Ti-nanowires, is qualitatively different. In addition, we have observed only very weak (barely observable) Coulomb blockade in titanium nanowires with low-ohmic environment, even when the wire resistance has been of the order higher than the superconducting resistance quantum. Our nanowires embedded in high-ohmic environment show pronounced Coulomb blockade but the observations cannot be accounted to CSB mechanism, applicable only to short nanowires.[40] Furthermore, the temperature and magnetic field dependencies of the Coulomb blockade are qualitatively different. In our wires, observed Coulomb blockades are likely to be associated with coherent QPS discussed in the following section.

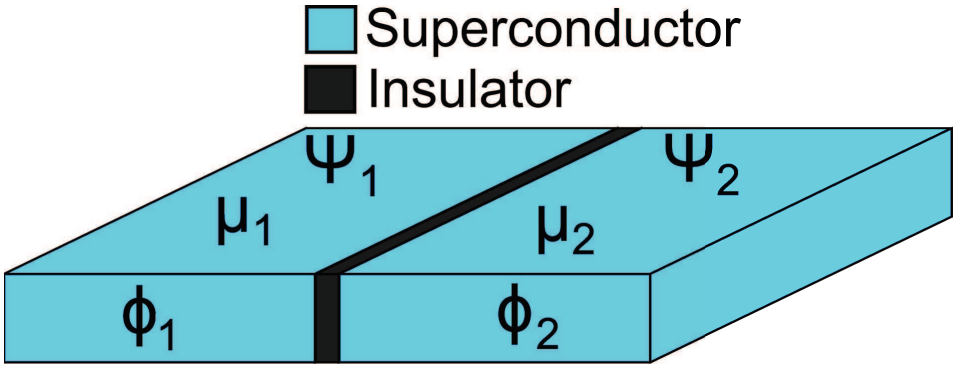

FIGURE 5 Qualitative image of a Josephson junction, two superconducting electrodes separated by a thin dielectric layer.

2.3 Josephson effect and quantum phase slip junction

2.3.1 The Josephson effect

In 1962 Josephson made a prediction [41] that a finite supercurrent should exist between two superconducting electrodes separated by very thin insulating layer (fig. 5). Each of the superconducting electrodes can be described by G-L complex order parameter Ψ. The derivation of Josephson relations follows the Feynman lecture series,[42] which is much simpler compared to the original paper of Josephson [41]. Let us consider the superconducting order parameter

$$\Psi_m = |\Psi_m| \exp(i\phi_m) = \sqrt{n_m} \exp(i\phi_m), \tag{32}$$

where m = 1,2 is the index of the left and right electrode and n_m is the concentration of "superconducting" electrons. One can write following time-dependent Schödinger equations for each electrode

$$(1)\quad i\hbar \frac{d\Psi_1}{dt} = \mu_1 \Psi_1 + K\Psi_2, \tag{33}$$

$$(2)\quad i\hbar \frac{d\Psi_2}{dt} = \mu_2 \Psi_2 + K\Psi_1, \tag{34}$$

where μ_m is the chemical potential and K is a coupling term defined by the properties of the junction. For a thick insulating layer the K approaches zero and the equations describe just energy states of two uncoupled superconductors.

Grouping the imaginary parts of equations (33), (34) and utilizing expression (32), the equations can be written in following forms:

$$(1)\quad \mathrm{Im}[i\hbar \frac{d\Psi_1}{dt}] = \frac{1}{2}\hbar \frac{dn_1}{dt} + K\sqrt{n_1 n_2}\sin(\phi_2 - \phi_1), \tag{35}$$

$$(2)\quad \mathrm{Im}[i\hbar \frac{d\Psi_2}{dt}] = \frac{1}{2}\hbar \frac{dn_2}{dt} + K\sqrt{n_1 n_2}\sin(\phi_1 - \phi_2), \tag{36}$$

$$(1)\quad \mathrm{Re}[i\hbar\frac{d\Psi_1}{dt}] = n_1\hbar\frac{d\phi_1}{dt} + \mu_1 n_1 + K\sqrt{n_1 n_2}\cos(\phi_2 - \phi_1), \tag{37}$$

$$(2)\quad \mathrm{Re}[i\hbar\frac{d\Psi_2}{dt}] = n_2\hbar\frac{d\phi_2}{dt} + \mu_2 n_2 + K\sqrt{n_1 n_2}\cos(\phi_1 - \phi_2). \tag{38}$$

The current through the junction is

$$I_J = \frac{dQ}{dt} = (\mu_1 - \mu_2)\frac{dn_1}{dt} = (\mu_2 - \mu_1)\frac{dn_2}{dt}, \tag{39}$$

and utilizing the imaginary parts (35), (36) with the current relation above we obtain equation for the current through the junction

$$I_J = \frac{2K\Delta\mu}{\hbar}\sin(\phi_2 - \phi_1) = I_c\sin(\Delta\phi). \tag{40}$$

The equation corresponds to so called DC Josephson effect. By reducing the real parts of the equations (37) and (38) and keeping in mind that the difference between chemical potentials is equal to the applied voltage $2eV = \mu_2 - \mu_1$ we obtain the AC Josephson effect:

$$\frac{\Delta\phi}{dt} = \frac{-\Delta\mu}{\hbar} = \frac{2eV}{\hbar}, \tag{41}$$

where V is the voltage difference over the junction. The equations (40) and (41) have very interesting implications. The DC Josephson effect equation states that a phase difference $\Delta\phi$ leads to a finite supercurrent. If the current (set by external source) doesn't exceed the critical current I_c the phase-difference over the junction stays constant. From the AC-effect equation (41) it can be seen that only time dependent phase difference results in finite voltage. Thus at small currents the transport through the junction is dissipationless: the voltage across the junction is zero until the critical current is exceeded. If to apply voltage over the junction the phase varies in accordance with the AC-relation (41), i.e. constant voltage results in phase/current oscillations.

The Josephson effect, even though originally based on theoretical analysis of quantum mechanical tunneling of electrons through an insulating barrier, can be generalized. In reality the effect is much more general. Any "weak link" between superconducting electrodes behaves as Josephson junction. For example, Josephson junctions can be made just by having normal metal region or even constriction between two 'massive' superconducting electrodes.

2.3.2 Semi-classical approach

To describe electrodynamics of a Josephson junction with classical arguments, the model of resistively and capacitively junction (RCSJ) is typically used. In this model, the physical junction is modeled by an ideal junction following equations (40) and (41) shunted by a resistance R and a capacitance C (fig 6a). The impact of resistance R is important only after the critical current is exceeded, i.e. in the finite

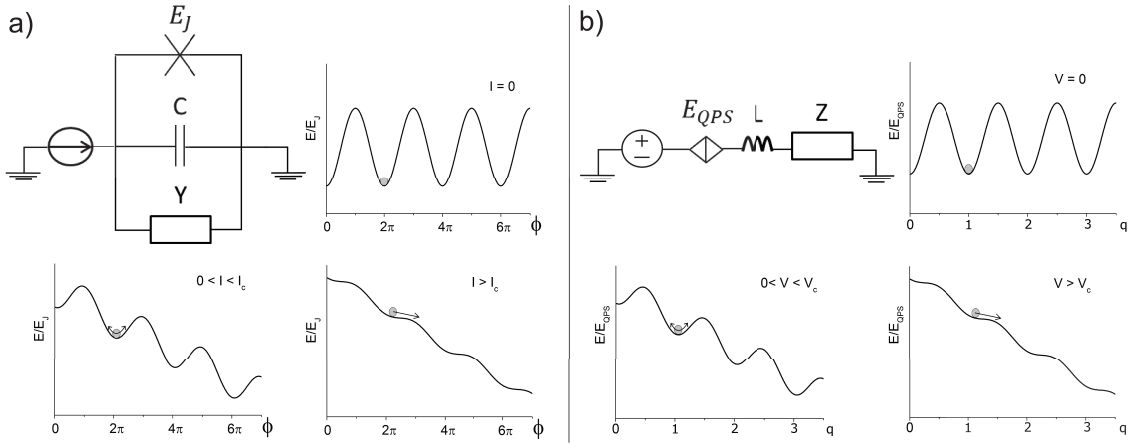

FIGURE 6 a) RCSJ-model for current biased Josephson junction. The washboard potentials energy vs. phase correspond to three limits: zero bias current, small bias current $0 < I < I_C$ and large bias current situations. The system is either trapped in one of the minima (zero current or small current) or slides down (with friction) the potential (large bias current). b) Corresponding model for voltage biased QPSJ. As above, the washboard potentials energy vs. charge correspond to zero voltage, small bias voltage $0 < V < V_C$ and large bias voltage situations. The system is trapped in one of the minima if the volt-age doesn't exceed the critical voltage V_C. At larger bias voltages the charge slides down the potential.

voltage regime, when the resistance is responsible for the dissipation. The resistance R is approximately the normal state resistance R_N of the junction. In high quality junctions, where the freeze-out of quasi-particles at low temperatures is the dominant factor, the R increases as $\sim R_N \exp(\Delta/k_bT)$. The capacitance C is the geometrical shunting capacitance between the superconducting electrodes, which depends on the insulating layer thickness and the junction area. The total current from the three parallel channels is

$$I(t) = I_C \sin\phi + \frac{\Phi_0}{2\pi}(C\frac{d^2\phi}{dt^2} + \frac{1}{R}\frac{d\phi}{dt}). \tag{42}$$

The differential equations (42) is formally identical to a mechanical model where a particle of mass $(\frac{\hbar}{2e})^2 C$ moves along the phase axis in an effective potential (fig. 6a).

$$U(\phi) = -E_J \cos(\phi) - (\frac{\hbar I}{2e})\phi, \tag{43}$$

where $E_J = \frac{\hbar I_c}{2e}$ is Josephson energy, ie. the energy accumulated in the junction by the flow of the supercurrent. The critical current I_C for a superconductor-insulator-superconductor junction can be determined using Ambegaokar-Baratoff relation $I_C R_N = \frac{\pi}{2e}\Delta(T)\tanh(\frac{\Delta(T)}{2k_BT})$. Time independent solution corresponds to the zero-voltage state where the system is trapped in a potential minimum. When current exceeds $I_c = 2\pi E_J/\Phi_0$ the wash-board potential is "too tilted" and no minima trapping the phase are left. Even in the limit $I << I_c$ the system can

change its quantum state by thermal activation over the barrier or by tunneling through the barrier. Both processes will cause finite voltage.[43, 44] Already at this stage one can notice the resemblance of Josephson physics with the phase slippage (fig. 6).

2.3.3 QPS junction

If to model a narrow superconducting nanowire in the regime of strong quantum fluctuations and with high-impedance environment in a similar way, the current bias needs to be replaced by voltage bias, the parallel resistor by series resistor and the series capacitance by parallel inductance.[45] The series resistance R is the normal state resistance of the nanowire and the inductance L is the kinetic inductance of the nanowire. The quantum phase slips in this context can be conceptually considered as the passages of a quantized vortexes through the system resulting in changes of phase by 2π. In the limit where the energy related to the phase/vortex tunneling is larger than the inductive energy $E_S = \hbar\Gamma_{QPS} >> E_L = \frac{\phi^2}{2L}$ and the high-impedance environment provides charge isolation so that the charge is the well defined quantum variable, the assumptions lead to reversed properties compared to a classical JJ (42):

$$V(t) = V_C \sin\frac{2\pi q}{2e} + (L\frac{d^2q}{dt^2} + R\frac{dq}{dt}), \tag{44}$$

where q is the quasicharge corresponding to accumulated charge in the nanowire.

Instead of critical current now the system is characterized by a critical voltage resulting in Coulomb blockade. The system enters a finite current regime when the bias voltage exceeds the critical voltage

$$V_C = 2\pi E_{QPS}/2e. \tag{45}$$

The solution to the differential equation (44) leads to a result where the charge is trapped in the effective potential (fig. 6b)

$$U(q) = -E_{QPS}\cos\frac{2\pi q}{2e} + (\frac{\hbar V}{R_q})\frac{q}{2e}. \tag{46}$$

The nanowire in this context can be called quantum phase slip junction (QPSJ) in analogy with conventional Josephson junction. The reversed properties are the result of the fact that the phase ϕ and quasicharge q in superconductors are quantum mechanical conjugate variables $[\hat{q}, \hat{\phi}] = -i$. Utilizing the uncertainty principle $\delta q \delta\phi > e$ one recovers the expected result, if one is well defined the other fluctuates. In a current biased Josephson junction the phase difference over the physical barrier is well defined, but the charge over the junctions fluctuates. In case of a voltage-biased QPSJ the reverse is true, the wire has a well defined charge but due to the QPS, the phase along the wire fluctuates. QPSJ biased with small voltage $V < V_c$ demonstrates Coulomb blockade behaving as a perfect insulator. Even though we tried to describe QPSJ and JJ in terms of classical variables (and with aid of some quantum mechanical arguments) the

underlaying reason for the duality, and even more so, proper understanding of the effects requires quantum mechanical model.

2.3.4 From semi-classical model to quantum mechanics

Though the presented above semi-classical model can be considered adequate, it lacks the power to explain the phenomenon properly. The quantum effects and dissipation needs proper quantum mechanical approach. In the following section we follow the reasoning of Mooij and Nazarov.[45] Starting from the well known Josephson junction Hamiltonian, the duality between Hamiltonians of JJ and QPSJ can be demonstrated. In the simplest case the Hamiltonian for a JJ can be written as

$$\hat{H}_{JJ} = E_c\hat{q} - E_J\cos(\hat{\phi}) + \hat{H}_{env} + \hat{H}_{coupling}, \tag{47}$$

where $\hat{H}_{env}$ describes the boson-like environment and $\hat{H}_{coupling}$ is a coupling term taking into account the effect of fluctuations and is different for voltage and current bias

$$\hat{H}_{coupling} = \begin{cases} \frac{\phi_0}{2\pi}(I - \hat{I}_r) & \text{for current bias} \\ -2e(V - \hat{V}_r) & \text{for voltage bias} \end{cases}, \tag{48}$$

where the operators $\hat{I}_r = \frac{-i\omega\hbar}{2e}Y(\omega)\phi(\omega)$ and $\hat{V}_r = -i\omega(2e)Z(\omega)q(\omega)$ are current and voltage fluctuations. The $Z(\omega)$ and $Y(\omega)$ are the resistance and the admittance of the serial and parallel resistor, respectively.

The Hamiltonian (47) describes the circuit from figure 6a. For the QPSJ-circuit (fig. 6b) we can utilize the JJ Hamiltonian and do the canonical transformation of the phase and charge $(\hat{q}, \hat{\phi}) \rightarrow (\frac{\hat{\phi}}{2\pi})$, $2\pi\hat{q})$, replace the corresponding energies, $E_J \rightarrow E_S$, $E_C \rightarrow E_L$, change the current bias to voltage bias $I \rightarrow R_q^{-1}V$ and change the parallel resistor (admittance) to serial resistor $Y(\omega) \rightarrow R_q^{-2}Z(\omega)$. Thus the Hamiltonian for a QPSJ is

$$\hat{H}_{QPSJ} = \frac{E_L}{(2\pi)^2}\hat{\phi}^2 - E_S\cos(2\pi\hat{q}) + \hat{H}_{env} + \hat{H}_{coupling}. \tag{49}$$

This duality relation allows the exact mapping of any transport characteristics of a Josephson junction to a QPSJ. In the following sections we will discuss the QPSJ I(V)-characteristics based on the theory of Josephson junctions.

2.3.5 Energy bands and Bloch oscillations

For conventional Josephson junction with large capacitance and hence small charging energy $E_c = e^2/2C$, other characteristic energies k_BT and eV are typically larger and, hence, Coulomb effect are suppressed. On the contrary, in a small Josephson junction (=small capacitance and, hence, large E_c) Coulomb phenomena should be pronounced in an experimentally reachable limit $E_c > k_BT$.[46] To our best knowledge, so far a microscopic theory dealing with electrodynamics

of a QPSJ has not been developed. Anticipating equivalence of a Josephson tunneling and a phase slip,[45] one may conjecture that electrodynamics of a JJ and QPSJ should be similar. Hereafter we continue the presentation considering a JJ, but keeping in mind the duality between a JJ and a QPSJ.

In this section we follow the review by Schön and Zaikin.[47] Let's first consider a dissipationless Josephson junction for which the Hamiltonian is

$$\hat{H}_0 = \frac{\hat{Q}^2}{2C} + U(\hat{\phi}). \tag{50}$$

In the classical limit the dissipationless Hamiltonian reduces to the equation of motion described by the washboard model. The dissipation can be added following the Caldeira-Legget approach where the junction is coupled to a bath of harmonic oscillators.[48]

Following the graphical presentation in fig. 6 the system can escape from one of the local minima to another by quantum mechanical tunneling through the barrier. In this process the macroscopic variable phase ϕ changes by 2π. The process is known as macroscopic quantum tunneling (MQT) and has been experimentally studied in JJs about thirty years ago.[46, 49] The rate of the tunneling can be written as

$$\Gamma_{MQT} = \frac{\omega_q}{2\pi} \exp(-A). \tag{51}$$

where the prefactor and the exponent in the weak Ohmic dissipation limit are $w_q = c\omega_0\sqrt{A}$ and $A = (\frac{a\Delta U}{\hbar\omega_0^2})(\frac{1+b}{R_sC\omega_0})$ and in the strong dissipation limit $w_q = c'\omega_0\sqrt{A}(R_sC\omega_0)^{-3}$ and $A = \frac{a'\Delta U}{\hbar\omega_0^2 R_sC}$. The ΔU is the height of the barrier, ω_0 the plasma frequency in the local minimum and a, b, c, c′ are numerical constants depending on the form of the potential. Do not confuse with parameters from sections 2.2.2 and 2.2.3!

Within each minimum energy-phase relation can be approximated by harmonic potential

$$U(\phi) = \frac{1}{2}C\omega_0^2(\frac{\hbar\phi}{2e})^2. \tag{52}$$

while within each minima the spectrum is degenerated into discrete states (fig. 7).

The Hamiltonian (50) is analogous to the solid state Hamiltonian of a particle in a periodic potential. Thus the eigenfunctions should resemble Bloch states. The spectrum depends on parameter Q_x denoted as "quasicharge" in analogy with the quasimomentum [50] of Bloch states in a periodic lattice

$$\Psi_{n,Q_x}(\phi + 2\pi) = exp(\frac{i2\pi Q_x}{2e})\Psi_{n,Q_x}(\phi). \tag{53}$$

The physical meaning of Q_x, is that of an external charge on the junction electrodes created by the flow of electric current. To enable the charge to behave as a classical variable one should provide the current biasing regime embedding

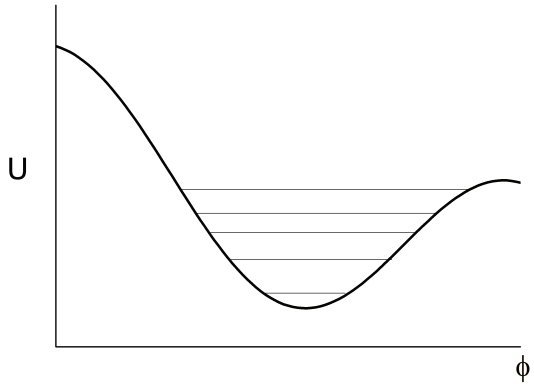

FIGURE 7 Each potential minimum in phase is divided to discreet eigen states. The phase is no longer well defined but spreads to larger range, the "phase" particle is no longer strongly localized near the minimum of the potential.

the junction into a high impedance environment consisting of e.g. resistors [51] or arrays of JJs [52].

The discrete energy levels E_n in figure 7, relevant for a single minimum, develop into energy bands $E_n(Q_x)$ [53, 50], where the first Brillouin zone extends over the range $-e \leq Q_x \leq e$. The form of $E_n(Q_x)$ depends on the ratio of $\frac{E_C}{E_J}$. The energy levels can be obtained by numerical solution utilizing the 'plane waves' eq. (53) and the Mathieu equation that is a time independent Schrödinger equation for the Hamiltonian (50):

$$4\frac{\partial \Psi}{\partial \phi} + (\frac{E}{E_C} + \frac{E_J}{E_C}\cos(\phi))\Psi = 0. \tag{54}$$

In "nearly free-electron" limit $E_J \ll E_C$, the energy bands can be approximated by a parabola

$$E_n(Q_x) \simeq \frac{Q_x^2}{2C}. \tag{55}$$

The energy levels are built up from the infinite set of parabolas. The Josephson energy couples the neighboring charge states opening the gap in the degeneracy points $\pm$e (fig. 8). The energy gap between the bands "n" and "n - 1" is

$$\delta E_n \approx E_C(\frac{E_J}{E_C})^n / n^{n-1}. \tag{56}$$

The energy gap δE_n decreases with the increase of the quantum number "n" being maximum for the lowest bands $\delta E_1 = E_J$.

In the opposite case of a small-capacitance Josephson junction, where $E_J \gg E_C$. The energy bands $E(Q_x)$ degenerate into quasi-sinusoidal pattern(fig. 8) with the ground state energy

$$E_0(Q_x) = -\Delta_0 \cos(\frac{2\pi Q_x}{2e}), \tag{57}$$

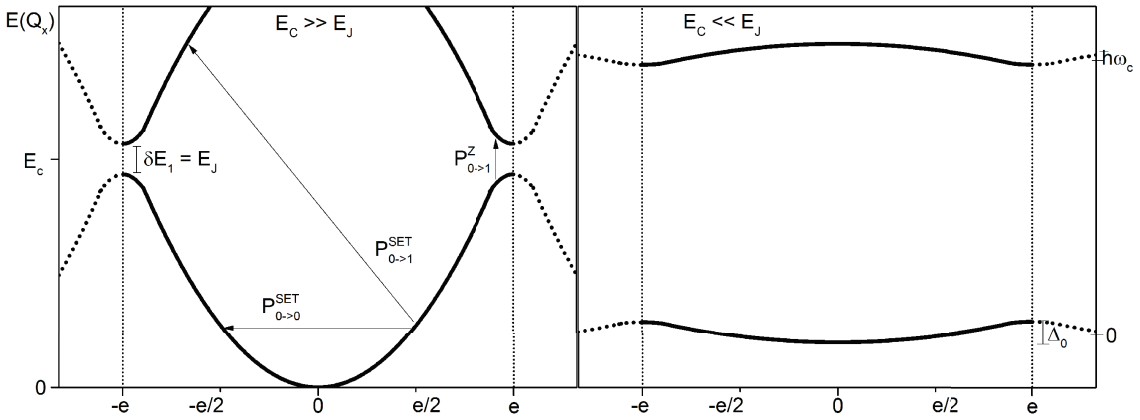

FIGURE 8 The band structure as a function of the quasicharge Q_x. The first Brillouin zone covers the range $-e \leq Q_x \leq e$. The bands are infinite and periodic and thus the situation can be always reduced to the first zone. In the left side is the "nearly free electron" limit $E_J \ll E_c$. On the right side is the "tight-binding" limit $E_J \gg E_C$. Transitions due to Zener tunneling or quasiparticle tunneling are indicated with arrows.

where the bandwidth is

$$\Delta_0 = 16(\frac{E_J E_C}{\pi})^{\frac{1}{2}}(\frac{E_J}{2E_C})^{\frac{1}{4}} \exp\left[-(\frac{8E_J}{E_C})^{\frac{1}{2}}\right] \tag{58}$$

and the energy gap between the lowest (n=0) and the next (n=1) bands

$$\delta E_1 = \hbar\omega_0 = (8E_J/E_C)^{1/2}. \tag{59}$$

The two limits $E_C \gg E_J$ and $E_C \ll E_J$ are depicted in the left and the right panels of figure 8. In the following section we mainly focus on the "nearly free electron" limit, $E_C \gg E_L$, keeping in mind the experimentally achievable case for a dual system – the QPSJ. If the value of the quasicharge is small $Q_x \ll |e|$, the lowest energy state has expectation value for charge $\langle 0\,|\widehat{q}|\,0\rangle \approx q$ and for energy $E_0(Q_x) \approx \frac{Q_x}{2C}$. When the $Q_x \simeq |e|$ the Cooper pair tunneling removes the degeneracy mixing the states. As the result $\langle 0\,|\widehat{q}|\,0\rangle$ diminishes and the energy is lowered by E_J resulting in opening of the gap in the energy spectrum. If the Q_x is increased beyond $|e|$, the Cooper pair tunnels in way that the charge remains small. Thus also the energy of the ground state remains small. The process makes the energy bands 2e-periodic in quasicharge representation.

If at low temperatures, $k_B T$ is much smaller than the band splitting δE_1, the quasicharge is increased adiabatically so that $\hbar\frac{dQ_x/2e}{dt} \ll \delta E_1$, the system will stay in its lowest energy and follow the neighboring energy parabola down. As the energy bands are periodic and infinite, there are two equally valid approaches: either the quasicharge can have any value, or the charge is restricted to the first Brillouin zone and the Cooper pair tunneling at $q = e(q = -e)$ brings it back to $q = -e(q = e)$. The energy and other observables, for example voltage

$$V = \frac{dE_0}{dq} \tag{60}$$

vary in time. If the variation of charge in time, being equal to the current $I = \frac{dQ_x}{dt}$, is a constant, then the voltage oscillates with frequency $f_B = \frac{I}{2e}$. The process, named as Bloch oscillations, is analogue to oscillations of an electron confined in a periodic potential and driven by constant electric field: the motion of a Bloch electron in a perfect crystal lattice.

If the junction is driven by both dc-current and ac-current

$$I(t) = I_{dc} + I_{ac}\sin(2\pi f_{ac}t), \tag{61}$$

there are resonances when the frequency of the ac-current and the Bloch oscillations match each other $I_n = n(2e)f_{ac}$. Single electron oscillations, with frequency $f_{qp} = 1/2f_B$, should co-exist with the "2e" Bloch oscillations. The quasi-particle tunneling causes the bands to be e-periodic, but opens no further gaps.[54]

2.3.6 Zener tunneling

Previously we've discussed only the situation when the system always stays in the lowest energy state. However if the quasicharge is increased non adiabatically $\hbar\frac{dQ_x/2e}{dt} > \delta E_1$, Zener transitions can excite the system to higher energy bands (fig.8).[55] Originally, Zener tunneling have been studied in context of the motion of an electron in a perfect crystal under the influence of an applied electric field [56]. The discussed similarity of a small JJ dynamics with motion of a Bloch electron in periodic crystal lattice, makes the analogy with Zener process quite obvious. When reaching the boundary of the Brillouin zone $Q_x \to e$, the system makes a transition to the adjacent band n $\pm$ 1 with probability $P^Z_{n\leftrightarrow n+1}$ or it remains in the band with probability $1 - P^Z_{n\leftrightarrow n+1}$. In the limit $E_C \gg E_J$ the probability of Zener tunneling from energy level $(n-1)$ to level n is

$$P^Z_{n-1\leftrightarrow n} = \exp\left(-\frac{\pi}{8}\frac{(\delta E_n)^2}{nE_c}\frac{e}{\hbar I}\right) = \exp\left(-\frac{I_{Zener}}{I}\right), \tag{62}$$

where the gaps between the energy levels are given by equation (56). Thus we can define the Zener breakdown current $I_Z = -\pi(\delta E_n)^2 e/(8nE_c\hbar)$. In the opposite limit $E_J \gg E_C$ the gaps δE_n are large and the probability of transitions to higher bands are vanishingly important. Given the reduction of the energy gaps δE_n (56) with increase of the band number "n", if the system can tunnel from the ground state n = 0 to the first excited state n = 1, then all transitions to higher states will happen with high probability. The system will "climb" to higher states until assuming the energy spectrum given by equation (54). With further increase of the current $I = dQ/dt$ the I-V characteristics eventually switches to quasiparticle branch. The Zener tunneling can be suppressed by adding parallel shunt resistor which provides energy dissipation enabling the system to relax to the ground state.

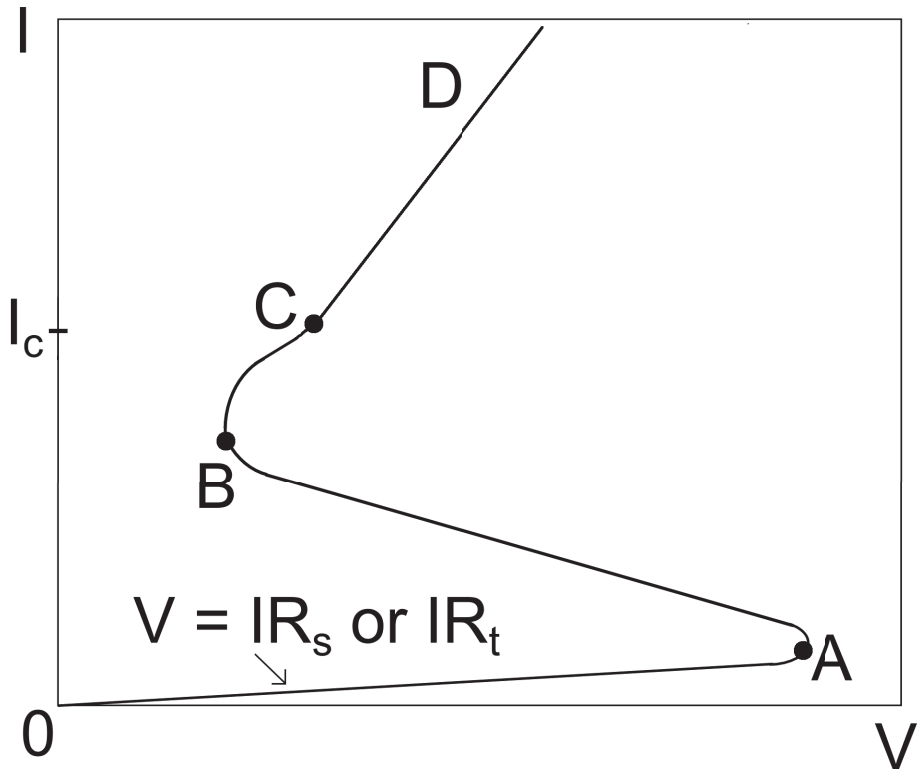

FIGURE 9 Schematics of low temperature (T $\rightarrow$ 0) I-V characteristic of a small resistively shunted (or with finite quasiparticle tunneling) JJ with $E_C \gg E_J$ in the current biasing regime. Region 0A corresponds to Coulomb blockade: JJ is in insulating mode and the current completely flows through the resistive shunt R_s or through the quasiparticle channel characterized by R_t. Region AB corresponds to Bloch oscillations: periodic charging and discharging of the junction. Region BC corresponds to Zener tunneling. And finally region CD at high current above the critical current I_c corresponds to quasiparticle tunneling.

2.3.7 Current-voltage characteristics of shunted junction

Let us first consider at low temperature, $T \approx 0$, a current biased small JJ with $E_C \gg E_J$ and a parallel resistive shunt. The current flows completely through the shunt resistor at small currents when

$$I < I_{th} = \frac{e}{R_s C} \tag{63}$$

and the time averaged voltage is $V = I/R_s$. This limit corresponds to Coulomb blockade (region 0A in fig. 9) When the current is increased above the threshold I_{th}, the system is driven to the regime of Bloch oscillations: and the current increases while voltage over the junction decreases. This back-bending of the V(I) is often called "Bloch nose" (region AB in fig. 9). Above $I > I_{th}$ the current-voltage characteristics can be expressed as:

$$\frac{V}{R_s} = I - \frac{2I_{th}}{\ln\left(\frac{I+I_{th}}{I-I_{th}}\right)}. \tag{64}$$

The Bloch oscillation frequency depends on the current and the current flowing through the parallel resistor reduces the current though the junction $\frac{V}{R_s}$ thus the oscillations are expected at $f_B = \frac{I_{dc}-V/R_s}{2e}$. Region BC (fig. 9) with positive derivate corresponds to Zener tunneling. At high currents, exceeding the critical value I_c, the system switches to the quasiparticle branch (region CD in fig. 9).

2.3.8 Current-voltage characteristics of unshunted junction with weak quasiparticle tunneling

If to take into account the effect of single electron tunneling the situation changes compared to a parallel resistive shunt. Weak tunneling can be treated perturbatively, allowing transitions between states $Q_x \pm e$ (fig. 8). In a simplified picture, the quasiparticle tunneling current can be approximated by $I_{qp}(V) \approx V/R_t$, where R_t depends on the energy differences $E^{\pm}_{n,n'}(Q_x) = E'_n(Q_x \pm e) - E_n(Q_x)$ compared to the superconducting energy gap Δ. If the energy differences are smaller then $R_t = R_{qp}$ and if the energy differences are larger then $R_t = R_N$.

If the quasicharge Q_x is increased adiabatically, for small current $I \ll e/R_tC$, the Q_x rarely reaches the boundary of the Brillouin zone. Therefore no Bloch oscillations can develop, but single electron oscillations can be observed. For a junction with $E_C \gg E_J$ at small bias currents $IR_tC/e \ll 1$ the time averaged voltage is

$$V = \sqrt{\frac{\pi I_{dc} R_t e}{2C}}. \tag{65}$$

When the current is relative large $I \geq \frac{e}{R_tC}$ the quasicharge is frequently driven to the edge of the Brillouin zone. If the probability for the Zener tunneling is small, Bloch oscillations will develop and the quasiparticle tunneling is less important. Due to Bloch oscillations the system spends part of time in states with negative voltage and, if tunneling from $-e < Q_x < e$ happens, it increases the charge. This leads to negative differential current: voltage decreases with increase of current.

For large currents, the current-voltage characteristics of the system have an analytic form, which can be obtained by solving master equation for the system [47]

$$V = \frac{E_C}{12 I_{dc} R_t C}. \tag{66}$$

The I-V characteristics of unshunted JJ is qualitatively similar to the resistively shunted one shown in figure 9a. At small voltages the system demonstrates the Coulomb gap. The crossover from the single electron tunneling region to Bloch oscillations causes the back bending of the I-V characteristics: the Bloch

nose. In the opposite limit $E_J \gg E_C$ the same crossover can be observed but at much smaller voltage scales defined by the bandwidth Δ_0 (58).

It should be noted that only in case of large R_t, the probability of Zener tunneling is small. This is reversed when compared to the shunt resistor case, where the small shunt resistor decreases the probability of Zener tunneling. When the R_t is large the Bloch oscillations suppress the quasiparticle tunneling more effectively compared to the case of small R_t. The strength of the quasiparticle tunneling can be quantified by parameter $\alpha_t = \frac{h}{\pi^2 e^2 R_t}$. The probability of Zener tunneling and thus the expression for the I_Z can be obtained from equation (62) by replacing the relevant parameters and assuming $E_J \ll E_C$

$$P^Z_{0\leftrightarrow 1} = \exp\left(-\frac{1}{8}\left(\frac{E_J}{E_C}\right)^2 \frac{e}{I_{dc} R_t C} \frac{\pi e^2 R_t}{2\hbar}\right). \tag{67}$$

2.3.9 Bloch oscillations and SET oscillations

Small Josephson junction $E_J << E_C$ embedded in high-ohmic environment should exhibit both single electron and Bloch oscillations. At small currents $I \ll \frac{e}{R_t C}$ the single-electron tunneling overrides the Cooper pair tunneling and 2e Bloch oscillations are suppressed. The oscillations are e-periodic $f_{qp} = \frac{I}{e}$.

At intermediate currents $e/R_t C \ll I \ll I_Z$, the voltage exhibits 2e Bloch oscillations, but the single electron tunneling causes phase shift π in the oscillations. Thus the fundamental oscillation frequency is given by the single electron frequency f_{qp}. This effect hides the 2e Bloch oscillations even when the magnitude of single electron oscillations is small compared to 2e Bloch oscillations. Qualitatively the only difference between a normal metal tunnel junction and a JJ is that in a JJ the range of parameters where the oscillations are observed is wider compared to normal metal tunnel junction. This is due to the gap δE_n in the energy spectrum reducing the Zener transitions to the higher bands which limits the process in the normal metal tunnel junctions.

Synchronization of internal 2e Bloch oscillations with external drive can be observed if the system is driven by dc and ac currents $I = I_{dc} + I_{ac} \sin(2\pi f_{ac} t)$: resonances happen at $m f_{ac} = \frac{I_{dc}}{2e} n_{2e}$, where the n_{2e} and m are the number of harmonics. At the V(I) characteristics those resonances should manifest themselves as current steps with differential conductance $\frac{1}{R_t}$. In addition to 2e Bloch singularities there should be single electron resonances $m f_{ac} = \frac{I_{dc}}{e} n_e$. For larger currents (but still $I < I_Z$) the single electron steps have negligible amplitude, while the 2e Bloch resonances remain observable.

The step-width in voltage depends on the RF-amplitude

$$V(Q_x(0)) = -\frac{e}{C} \sum_{s=1}^{\infty} \frac{(-1)^{s(n+m)}}{\pi n s} J_{ms}\left(\frac{ms I_{ac}}{I}\right) \sin\left(\frac{2\pi n s Q_x(0)}{e}\right), \tag{68}$$

where J_{ms} are Bessel functions.[57]

2.4 Physics of QPSJ illustrated with devices

To our best knowledge, so far the comprehensive model describing the quantum dynamics of a QPSJ has not been yet developed. Postulating the equivalence of Cooper pair tunneling in a conventional JJ and a QPS event in a superconducting nanowire one can use duality transformations 'mapping' the extensively studied Josephson physics on QPSJ.[45] However, one should always keep in mind that the analogy between a JJ and a QPSJ is qualitative. There are at least two points, which should be taken into consideration in projecting the results of conventional JJs to a QPSJ. First, while a conventional JJ is a zero dimensional system, a QPSJ is an essentially 1D object with 'distributed' parameters. Second, already analyzing the effect of Zener tunneling in small JJs, we have noticed the qualitative difference between parallel resistive shunt and a tunnel resistance. In case of a QPSJ the origin of finite dissipation is still an open question. We strongly believe that our experiments can stimulate theory development.

In the following section we'll describe some applications that have been proposed to verify the duality between JJ and QPSJ.[58, 59, 60] We have realized two of those: QPS-transistor and synchronization of Bloch oscillations with external RF-irradiation. The latter can be considered as a candidate for the quantum standard of electric current in analogue to the voltage standard based on Shapiro effect [61]. Several groups are currently actively working on various QPS applications: QPS-transistor [62, 63] and QPS-qubit [12, 64].

2.4.1 Coherent QPS

Coherent quantum phase slip is the magnetic counterpart for charge tunneling a JJ: instead of charge tunneling through electrically insulating layer the magnetic vortexes tunnel through the superconductor (magnetic insulator). The effect is as fundamental as Josephson effect.

In coherent tunneling single events can not be discerned and the phase slips are characterized by quantum amplitude E_s. The amplitude depends exponentially on the instanton action which is typically dominated by the core action [65]

$$S_{core} = \alpha\left(\frac{R'\xi e^2}{\pi\hbar}\right), \tag{69}$$

where R' is a wire normal state resistance per unit length and α is a numerical prefactor which depends on the core profile. Exact estimation of the QPS amplitude is difficult due to the uncertainty in α and the strong exponential dependence of $E_s \propto \exp(-S_{core})$.[65]

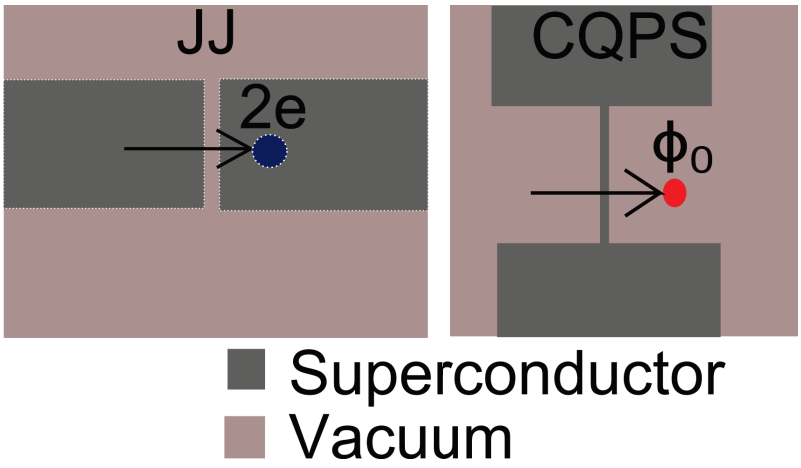

FIGURE 10 Qualitative picture of tunneling processes in Josephson junction (left side) and coherent quantum phase slip (right side).

2.4.2 QPS qubit

The QPS qubit utilizes coherent QPS and consist of a superconducting loop where part of the loop is a narrow nanowire in the regime of QPS.[58] The equivalent circuit and illustration of the circuit is presented in figure 11. Neglecting the geometric capacitance and spatial distribution of the phase-slip events so that the tunneling between different phase-states of the nanowire can be described by a single amplitude we can define the Hamiltonian of the QPS qubit.

$$\hat{H} = E_L(n-f)^2 - \frac{E_{QPS}}{2}\sum_n(|n+1><n| + |n><n+1|), \tag{70}$$

where $f = \phi/\phi_0$ is the applied flux normalized by the flux quantum, $E_L = \frac{\phi^2}{2L}$ the inductive energy of the loop and $E_{QPS} = h\Gamma_{QPS}$ is the energy associated with the quantum phase slips. The energy spectrum E(ϕ) consists of parabolas intersecting at semi-integer values of flux ϕ/ϕ_0 = n + 1/2. The QPS coupling mixes the states with adjacent fluxoid numbers, enabling formation of the two-level quantum system. The level splitting equals E_{QPS}, provided that $E_{QPS} \ll E_L$. Through the duality transformation the QPS qubit can be shown to be dual to a Cooper pair box.[45]

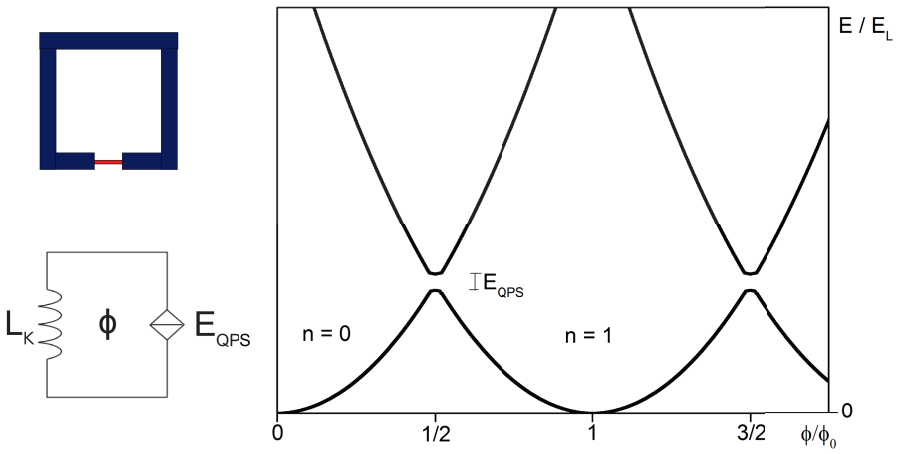

FIGURE 11 In the left upper corner is a typical layout of a QPS flux qubit. It consists of a superconducting (thicker) loop and a narrow superconducting nanowire in the regime of QPS. In the lower left corner the equivalent circuit is presented characterized by the kinetic inductance of the loop L_K and the QPS amplitude E_{QPS} of the narrow nanowire. The qubit is flux biased with ϕ. In the right side is the energy diagram of the qubit as a function of applied flux. The coherent QPS processes open the gap in the spectrum at the 'anti-crossing' points $\phi/\phi_0 = \mathrm{n} + 1/2$.

2.4.3 QPS transistor

The QPS transistor (QPST) is a single electron transistor based on the charge-phase duality of a superconducting nanowire circuit. It is dual to a DC SQUID. As DC SQUID is sensitive to phase across the JJs, the QPS transistor is sensitive to the charge through the QPS elements. The charge sensitivity of the QPS transistor depends on the voltage across the QPSJ and inductances of the QPS elements, and requires high-impedance environment to suppress charge fluctuations.

QPST is equivalent to a single electron transistor (SET) or a Cooper pair transistor (CPT). In conventional SET or CPT charge isolation is maintained by static in space and time (tunnel) junctions. QPST can be considered as a dynamic equivalent of the above devices, where delocalized QPSs enable charge isolation. The structure of the QPST is presented in figure 12. When compared to the QPS qubit (fig. 11), the QPS-transistor is defined by same energies: inductive energy E_L and the phase-slip energy E_{QPS}. In full analogy with the dual system, voltage biased Josephson junction, demonstrating the text-book current-phase relation $I = I_c \sin(\phi/\phi_0)$, the current biased QPSJ demonstrates periodic voltage-charge relation [62, 63]

$$V_{QPS}(q) = V_C sin(\frac{\pi q}{e}), \tag{71}$$

where the V_C is the critical voltage (45).

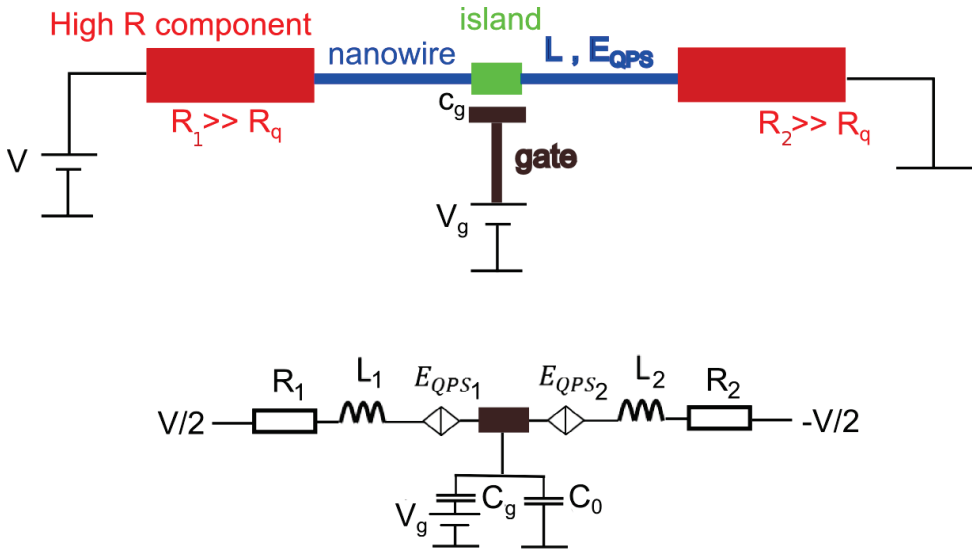

FIGURE 12 Schematics of the QPS-transistor. The high-impedance environment can consist of various elements: e.g. metallic resistors or SQUID-arrays. The equivalent circuit is presented below.

In Kirchhoff presentation the equivalent circuit (fig. 12) has the form

$$V_i = L\frac{q_i^2}{dt} + R_i\frac{q}{dt} + V_{QPSi}(q_i), \;\; i = 1, 2. \tag{72}$$

For symmetric configuration $V_1 = V_2$ and $V = V_1 + V_2$. Through the charge conservation relation one obtains

$$q_1 - q_2 = -C_g V_g - (C_g + C_0)(V_1 - V_2) = 0, \tag{73}$$

where C_g is the capacitance between the gate electrode and the island, and the C_0 is the parasitic capacitance between the island and the ground. In small capacitance limit $C_g, C_0 \ll e/V_C$, the charge difference solely depends on the gate voltage $V_g = \frac{Q}{C_q}$. The voltage over the QPS transistor is the result of coherent interference of individual QPS events controlled by the gate charge

$$V = V_{QPS1} + V_{QPS2} = V_m(Q_q)sin(\pi Q/e), \tag{74}$$

where Q is the "average" charge, which in symmetric case is $Q = q_{1,2} \pm \frac{Q_g}{2}$ and $V_m = 2V_C|cos(\pi Q_g/e)|$ is the maximum amplitude of the Coulomb blockade. In case of an asymmetric circuit the modulation amplitude significantly decreases.

2.4.4 Quantum standard of electric current

For a long time quantum standard of electric current has been a 'dream' device under development. For the moment the most promising methods are related to superconducting tunnel junction based charge pumps driven with ac-drive. To obtain reasonable noise level for the metrological triangle experiment [66] the

current should be of the order 1 nA (or higher) with relative level of uncertainty of about 10^{-8}. Reaching these parameters utilizing charge pumps have been challenging over the last 20 years and so far has not been demonstrated.

With QPS based structures current outputs of few nA should be possible.[63, 67] The QPS based current standard consist of a QPSJ operating in the regime of Bloch oscillations. The oscillations are synchronized with external RF-drive. At positions $I_n = n(2e)f_{ac}$ the V(I) dependencies should demonstrate plateaus of constant voltage(or $V_{step} = IR_t$, see section 2.3.8). The region of the Bloch oscillation depends on the shunting resistance or the strength of the quasiparticle tunneling, as discussed earlier. In case of the shunt resistor corrections to the step positions need to be made (see section 2.3.7). The synchronization of the Bloch oscillations have also been observed in ultra-small Josephson junction but so far only rather broad and very weak n = 1 singularities have been reported.[68]

For the current standard relatively high values of the QPS rate Γ_{QPS} are required so that the value I_n is as high as possible, but it should be less than the superconducting energy gap. The last requirement originates from the assumptions of existing models considering quantum fluctuations as small perturbation of a superconductor. One should not exclude the possibility that in the limit of strong fluctuations $h\Gamma_{QPS} \gg \Delta_0$ some interesting phenomena develop. The environment should maintain it's high impedance over the frequency range up to few GHz.

If the high-impedance environment is made out of a normal metal, the electron heating might be an issue.[63] The electron temperature T_e and the phonon temperature T_{ph} in a mesoscopic-size normal metal conductor at ultra-low temperatures might differ significantly:

$$T_e^5 = T_{ph}^5 + \frac{P}{\Sigma\Omega}, \tag{75}$$

where $P = I^2R$ is the power dissipated in the resistor with resistance R, Ω is the volume of the resistor and the Σ is the electron-phonon coupling constant. For example, the Joule heating in bismuth resistors, used in our experiments, with length 20 μm, cross section 1500 nm^2, resistance ~ 1 $MOhm$ and typical electron-phonon coupling constant $\Sigma \sim 10^9 Wm^3K^{-5}$ at the phonon temperature 20 mK and 1 nA current rises the electron temperature up to T_e = 0.67 K. The estimation gives the upper limit for the electron temperature T_e as it only takes into account the volume of the resistor and the dissipation within. Heat escape to wider electrodes and to the substrate (though suppressed by Kapitza interface thermal resistance) somehow relaxes the constrain, while still keeps the overheating of the current-biasing electrodes a serious problem. Our research related to the current standard [69] has been mainly focused on optimization of the high-impedance environment and the coupling of the RF-drive to QPSJ.(section 4.3)

3 SAMPLE FABRICATION AND MEASUREMENTS

For investigation of QPS effect thin superconducting nanowires with effective diameter of few tens of nm have to be fabricated and characterized. This limit can be reached by modern e-beam lithography, but reproducible fabrication is still challenging. The resolution at sub-20 nm scales can be obtained in small structures, but for the nanowires of lengths with tens of micrometers maintaining the geometrical homogeneity of the nanowire is rather challenging. For some materials the T_c increases as the dimensions are smaller(for example In[4] and Al[9, 24]), and for others the effect is reverse(Nb[70], MoGe[5] and Ti[71, 72]). The origin of the phenomenon is still unclear but models exits predicting either enhancement[73] or suppression[74] of the critical field with reduction of the dimensions. Either way the T_c size dependence leads to broader R(T) transition in realistically fabricated nanowires of finite length and containing wider node sections. For example the effect of varying aluminum nanowire cross section between 5000 to 6500 nm^2 (effective diameter varying between $\sim$70 to 80 nm) leads to larger contribution to the R(T) characteristics than the TAPS.[75] The small variations of the diameter of the nanowire resulting in deviations in the T_c within the nanowire length can be misinterpreted in the R(T)-measurements as fluctuation effect.

For observation of the coherent QPS effects on-chip high-impedance environment for proper current biasing is required in addition to a narrow (and preferably homogeneous) nanowire. Typically both the superconducting nanowire and the high-impedance environment were fabricated in one fabrication cycle without breaking the vacuum. If to use two or more cycles the surface of the previous cycle evaporated metal needs to be carefully cleaned before the new layer is added. The treatment varies between materials. In noble metals gentle oxygen plasma cleaning is sufficient, but for the materials that oxidize, for example titanium and aluminum, the oxide layer should be removed. This is possible by sputtering the oxide layer away with directional Ar^+ plasma before evaporation of the next layer but the process requires formation of protective layer on top of the PMMA. Unfortunately plasma sputtering affects the PMMA mask even with the protective layer. Typically the linewidth is increased, and even some PMMA

residues can be accumulated on the surface of the substrate. Alternative is to cover the pre-fabricated bottom layer with noble metal prior to deposition of the top material. However, we found that for our studies this approach introduced too much undesired disturbance: even 2 to 3 nm thickness layers of gold or platinum noticeably altered the T_c of titanium $\sim 30nm$ thick nanowires.

We used boron doped <100> P-type silicon as substrate for the structures. It has noticeable conductivity at room temperature, while already at liquid nitrogen temperature (77 K) can be considered as good insulator. Utilization of a conducting substrate has two major advantages. First, it helps to avoid charge accumulation during the ion beam processing which would have otherwise created problems with homogeneous ion milling. Secondly, conducting substrate serves as shunting platform for a fragile nanostructure. This significantly aides the experiment since the same nanostucture has to survive several measurement/ion milling cycles and sustain inevitable static charge accumulation.

3.1 Lithography process

Samples were fabricated utilizing standard lift-off electron beam lithography technique. Either thin single layer PMMA resist (Microchem 950k PMMA in anisole), or two layer resist with co-polymer (Microchem MMA(8.5)MAA in ethyl lactate) as the bottom layer and PMMA on top were used. The total thickness of the resist layer varied between 100 nm and 700 nm. The resist composition and thicknesses were altered depending on the complexity of the structure, the required size of undercut region or the alignment accuracy between the process steps. Better resolution can be obtained with thinner resist, but the thicker multilayer mask enables fabrication of more complex structures employing shadow (multiple) angle evaporation technique.

The patterning was made with Raith e-LiNE electron beam writer with resolution below 20 nm feature size. Typical linewidth obtained for long geometrically homogeneous nanowires varied between 25 to 45 nm depending on the resist thickness. The narrowest samples fabricated had width of about 15 nm but geometrical homogeneity of such structures was significantly worse than of the wider samples. Fabrication of slightly larger diameter nanowires also allows use of two layer resist (Copolymer - PMMA) with undercut region which based on limited sample number seemed to improve evaporated material quality. The undercut region reduces the direct physical contact between the evaporated material and the resist and also allows less evasive lift-off.

After patterning samples the PMMA mask was developed with 1:3 MIBK to IPA developer and cleaned in reactive ion etching (RIE) chamber using low energetic oxygen plasma. The cleaning step appeared to have high impact on superconducting properties of the nanostructures. Presumably without plasma cleaning certain amount of resist residues were left on surface of the substrate. Samples fabricated without RIE cleaning (or with too low power cleaning) showed clear

signs of contamination: e.g. the titanium nanowires were not superconducting down to T = 20 mK.

3.2 Metal deposition and lift-off

Metal deposition was made in UHV electron beam evaporator with residual pressure about 1 to $5 * 10^{-9}$ mbar. The superconducting material utilized for the 'body' of all structures was titanium. Even at these clean conditions, ultra high vacuum pumped with cryopumping and the residual gas mainly consisting of hydrogen and helium, evaporation of good quality titanium is challenging. High angle slow rate evaporated titanium or titanium that was evaporated at high angles into the undercut regions of the PMMA/co-polymer mask didn't show any signs of superconductivity down to 20 mK. The slow evaporation rate allows more impurities to be introduced to the metal during the deposition. When the evaporation goes to underneath the resist mask the partial pressure might be higher due to desorption of gases from the PMMA/co-polymer mask. Also the surface cleaning with RIE is not efficient for the undercut area.

With proper substrate cleaning, relatively high evaporation rate 1 Å/s and small angle evaporation(so that the nanowire was aligned along the pattern in the PMMA/co-polymer mask), the titanium nanostructures had critical temperatures between 350 to 400 mK which is comparable to the one of bulk titanium. The resistivity of deposited metal could be varied to some extent without dramatic reduction of T_c and leading to higher QPS-rates (eq. 24). The superconducting energy gap of titanium nanowires fabricated under similar conditions measured with tunneling spectroscopy was found to be 60 ± 10 μeV.

Variation of the evaporation parameters allowed us to utilize titanium in two ways: as the 'body' of superconducting nanostructures and as highly resistive normal metal. The sheet resistances of the wires varied between 300 to 1000 $\Omega/\square$. That property was used in hybrid nanostructures requiring on-chip high-ohmic electrodes.

Lift-off was typically done in heated acetone and occasionally supported by ultrasonic cleaner. Typical time for the lift-off varied between one minute to several minutes. Lift-off with ultrasonic seemed to produces better results: no metal residues are left on the substrate and the lift-off is always complete. Samples with tunnel barriers or with materials with poor adhesion were treated more gently during the lift-off. Yet no differences between the samples having lift-off process in room temperature acetone and the typical ones in heated acetone were noticed.

3.3 Ion beam milling

As it has been explained in previous sections, our e-beam lithographic equipment does not allow reproducible fabrication of sub-20 nm nanowires. Hence, to study gradual development of a size dependent phenomenon a complementary approach should be used. The lithographically fabricated structures were further processed using ion beam milling. This allows gradual and highly controllable way to reduce sample dimensions.[7] Low energetic ions collide with the sample. Momentum exchange between the incident ions and the sample atoms results in slow etching of the sample. If the kinetic energy of the colliding ions is small, the penetration depth into the target is small. For example typical penetration depth of 1 keV Ar^+ ion into titanium is about 1.5 nm, being comparable to the thickness of the native oxide layer.

The flux of the ions is kept small. This limits the etching rate. Typically utilized etching rate was about few nanometers per hour. The accuracy of sputtering can be made as small as one nanometer. The sputtering rate depends on the intensity of the ion beam, the sputtering yield and the redeposition rate. The sputtering yield gives the amount of ejected atoms per incident ion and can be estimated with Monte Carlo simulations: for example, using SRIM software by James Ziegler.[76] After the calculation of the sputtering yield, derivation of the sputtering rate is trivial:

$$S = \frac{I}{e}Y, \tag{76}$$

where I is the ion current per unit area, e is the elementary charge, Y is the sputtering yield. The equation gives the sputtering rate in units of atoms per unit area per second, which can be directly converted into "nm/s" if the density of the sputtered material is known.

The calculated etching rate typically has high error margin and can only be used as a guideline because it lacks corrections for re-deposition of the sputtered material and electron cascades generated by the incident ions. In practice accurate calibration of the milling rate can be obtained by comparing AFM measurements before and after the etching giving a system dependent correction factor for expression (76). The shape of the cross section of a typical nanowire can be approximated with a trapezoid. The phenomenological expression for evolution of a nanowire cross section σ has been found [8]:

$$\sigma = \sigma_0(1 - \frac{\phi}{\phi_0})^2, \tag{77}$$

where σ_0 is the initial cross section, ϕ_0 the fluence needed to sputter away the whole structure and ϕ is the applied fluence.

3.4 Low temperature experiment

When measuring electron transport properties of nanoscale superconductors at ultra-low tempratures a good electromagnetic shielding and filtering is mandatory. Interference of external noise coming from either the external electromagnetic radiation or from the measuring electronics itself can cause noisy signal at the sample. That noise is almost temperature independent and as such can be erroneously misinterpreted as contribution of quantum fluctuations.

The samples were measured in a electromagnetically shielded room. The connections to/from the room were made through low pass filters, the “noisy” ground was disconnected, and the sensitive electronics were connected to the "clean" ground. Inside the shielded room solely battery powered analogue preamplifiers were used.

Two different cryostats were employed. Self-made dilution refrigerator(PDR) was designed and built locally in the NSC of university of Jyväskylä.[77] The refrigerator is capable of reaching the base temperature 60 ± 5 mK and has an option to be inserted into a vacuum can with a superconducting solenoid. The measuring lines contain Amobead inductive filtering from room temperature down to liquid helium temperature. Low-pass T-filtering, stabilized at 4 K (fig. 13a) capacitively shunt the probe pairs. At the mixing chamber, just before the sample, either microstrip meanders with large capacitance to ground or inductive filters were used (fig. 13c). In addition the filter chamber was filled with copper powder. The filtering was designed exclusively for dc-measurements or low frequency ac-measurements.

The samples were glued using conductive (at low temperatures) varnish on a copper sample holder (fig. 13d) and contacted with aluminum wires using ultrasonic bonder. A copper cap was tightened over the sample (fig. 13b) to shield the sample from radiation coming from the vacuum can walls which are at contact with 4.2 K liquid helium bath.

Another cryogenic system used in the experiment is a more powerful commercial dilution refrigerator Kelvinox-100 from Oxford Instruments. Three stage filtering system was custom built. The base temperature of the cryostat with all experimental connections (24 dc-lines, 3 rf-lines and diagnostic lines) was about 20 mK. At the base temperature the electron temperature determined from the V-I dependence of a NIS junction could be as small as 30 mK. [78]

For the RF-measurements three co-axial lines were installed in the cryostat. The RF-lines were first thermalised to 4 K using an 20 dB attenuator to reduce the noise coming from room temperature. At 1 K stage the RF-lines were again thermalised using 3 dB attenuators.

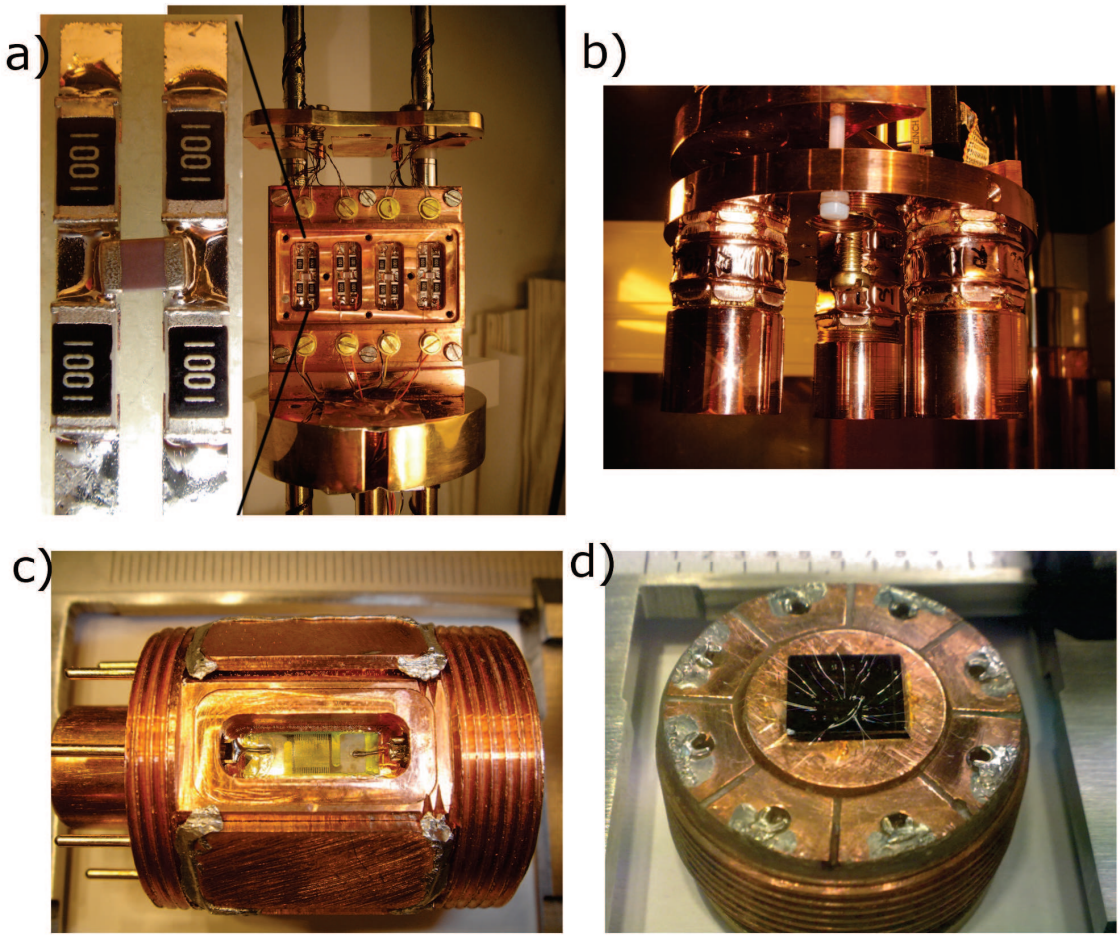

FIGURE 13 The cryostat hardware. a) T-filters thermalised to 4K-plate(in KNOX 1K-plate). The T-filters capacitively couple each of pair of dc lines shunting ac-signals. b) Image of the sampleholder, sample insert and a copper cap protecting the sample from external radiation coming from the vacuum can walls which are at 4 K temperature (in KNOX 1 K). c) The sample holder and the microstrip filter located inside the insert. d) The sample stage with sample attached.

3.5 Measurement methods

Typically for R(T)-measurements small low frequency ac-bias current was used. The current was chosen to be so small that its increase/reduction by factor of ten didn't affect the shape of the R(T) transition. Normally currents below 50 pA were used. The temperature in both cryostats was measured with pre-calibrated RuO-crystal using AVS-4-probe resistance bridge.

The dc-measurements were made utilizing either current or voltage bias. The voltage/current sources used in the experiments were mainly Keithly 238 analogue current/voltage source or Keithly 6221 current source. For current biasing a room temperature 10 or 100 MΩ resistor, connected in series with the sample, was used to stabilize the current. The $1/RC$ of the system depended on the sample (and the bias point) and the pre-resistor varying between 0.1 s to several minutes leading to relatively long measurement times for the high-impedance samples. Battery powered analogue amplifiers Itacho 1211 current amplifier and Itacho 1201 voltage amplifier or Femto DDPCA-300 current amplifier and Femto DLPVA-100 voltage amplifier were used at the first amplification stage. The Femto voltage amplifier has input impedance 1 TΩ enabling measurement of the high-impedance samples.

In addition to dc-measurements, while recording I-V characteristics, normally the derivative dV/dI or dI/dV was also measured using modulation technique. A small ac-signal, with amplitude much smaller than the step of the dc sweep, was mixed with dc bias. The signal was measured with lock-in amplifiers. Typical values for the ac-modulation frequency and amplitude were few Hz and 0.1 to 1 pA.

4 RESULTS AND ANALYSIS

4.1 Material quality and sample homogeneity analysis

Critically oriented reader might always argue that any deviation from 'conventional' superconductivity, e.g. broadening of R(T) transition, is the result of sample inhomogeneity. Thus homogeneity is important issue in interpretation of data. In addition, existing QPS models are designed for homogeneous superconducting wires with uniform cross section σ.

In our experiments at all fabrication stages special care has been taken to obtain the best possible quality of titanium nanostructure. After patterning and development samples were cleaned with low-powered O_2 plasma before the evaporation to remove PMMA residues left from the development stage. Titanium was deposited at a typical rate ~ 0.1 nm/s in cryopumped UHV e-beam evaporator at residual pressure $\sim 5 * 10^{-9}$ mbar. The described procedure should ensure low concentration of foreign impurities.

To reveal the issue of geometrical constrictions the samples were carefully analyzed with first with SEM and then with AFM. Combination of these two methods enables determination of variations of the wire diameter with accuracy 2 nm. Figure 14 shows a typical AFM image of ion milled titanium nanowire which has very smooth surface with roughness being about $\pm$ 1 nm. Note that the error $\pm$ 3 nm in definition of the effective diameter of ion milled samples originates not from the physical roughness, which can measured with AFM with accuracy $\pm$ 1 nm, but from the uncertainty in definition of the interface between the metal and the substrate.(fig. 14 and 16b)

The structural inhomogeneity of a $\sim$ 30 nm nanowire is rather demanding to be measured. Obviously all real samples do have a certain level of structural inhomogeneity originating from various sources: grain boundaries, finite size of the sample, proximity effect at the interface with wider parts of the structure, etc. All the samples, including the thinnest wires, demonstrated sheet resistance $R = 200 - 1000\ \Omega/\Box$, and are still comfortably on the metal side of the metal-

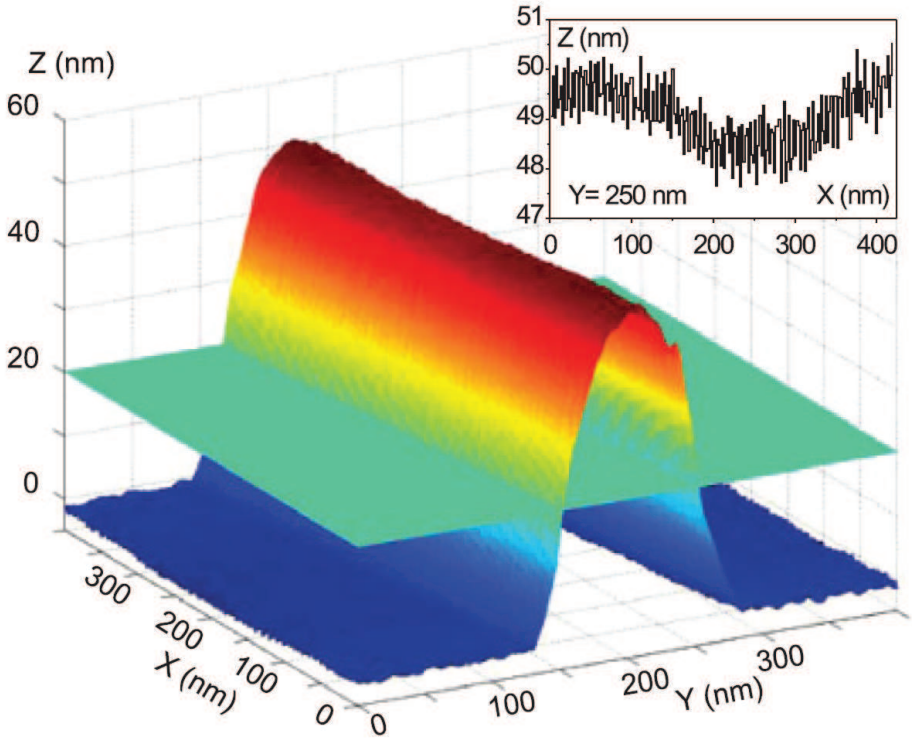

FIGURE 14 Typical AFM-image of a titanium nanowire showing no obvious defects and very smooth surface. Horizontal plane indicates the interface between the metal and the sputtered Si substrate. Inset shows profile of the top part of the wire.[71] (A. I)

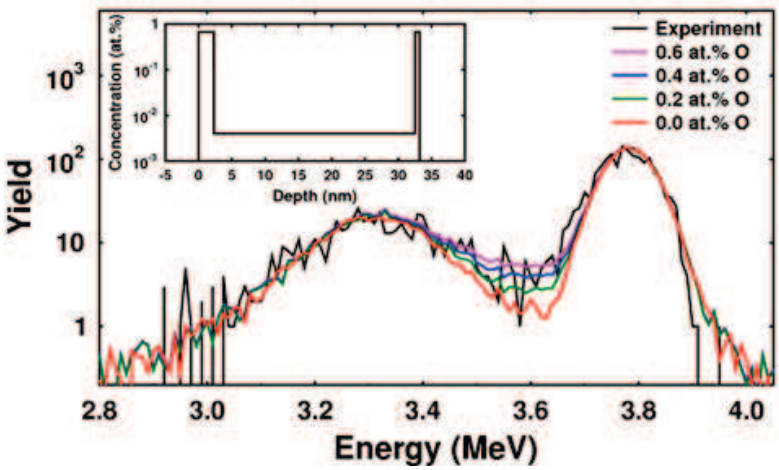

FIGURE 15 ToF-ERDA analysis and Monte Carlo simulations to determine concentration of oxygen in Ti matrix. The best fit is obtained with about 0.3 at. % concentration of oxygen. In the inset the depth profile of oxygen concentration shows that oxygen impurities are mainly localized at the interfaces Ti/vacuum and Ti/Si.[71] (A. I)

insulator transition. Formation of arrays of JJs in titanium has been observed in deliberately anodized thin films with noticeably higher sheet resistivity.[79]

To characterize elemental homogeneity of our titanium nanostructures the co-evaporated films were analyzed with time of flight elastic recoil detection analysis (ToF-ERDA) [80] and the results were analyzed with Monte Carlo simulations.[81] The method enables quantitative determination of impurities of impurities with 0.1% at. accuracy. The ToF-ERDA analysis was done in Physics department of University of Jyväskylä by Dr. T. Sajavaara.

The ToF-ERDA analysis revealed that the highest concentration of impurities can be attributed to oxygen to be about 0.3% at. If to assume that the oxygen impurities are equally distributed inside the Ti-matrix, this would mean that for each titanium grain with characteristics size 2-3 nm, there is only 1 to 2 oxygen atoms. With this low concentration it is obvious that there is not enough oxygen to form insulating barriers between the grains capable to form a JJ blocking the supercurrent between metal grains. The depth profile of the oxygen concentration (fig. 15) makes the conclusion even more convincing. Excluding the interfaces Ti/vacuum and Ti/Si, oxygen appears to be equally distributed in the Ti-matrix.

To obtain information about crystallinity of Ti-matrix TEM analyses were made by Dr. A Vasiliev in Kurchatov Institute, Moscow. The TEM studies showed that the wires are polycrystalline with crystal size between 2 to 3 nm which nicely correlates with the information obtained with SEM and AFM analyses, and the values determined for the mean free path from resistance measurements in normal state utilizing the ρl product for titanium known from literature. The TEM studies of Ti films revealed compactly packed and highly uniform metal matrix showing no obvious defects.

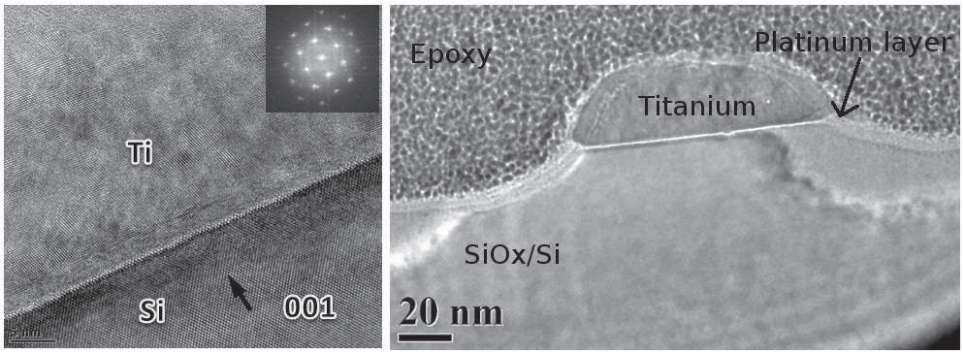

FIGURE 16 Transmission electron microscope image of titanium nanowires, a) high resolution TEM image showing the crystallinity of the Ti-matrix and b) cross-section of heavily ion-milled nanowire.[71] (A. I)

The TEM images were also taken from a nanowire that had been ion milled.(fig. 16b) The ion flux during the sputtering is so small that no gas bubbles or charging effects are possible. The TEM images confirm the hypothesis. No structural damage was found after ion milling.

Even if there would be some unknown hypothetical mechanism affecting the wire homogeneity it would be reasonable to assume that the mechanism should manifest itself individually for each particular sample leading to a unique fingerprint on R(T) and the I-V dependencies. However, the large statistics obtained on multiple samples states the opposite: The shape of the broadened R(T) transitions is universal and reproducible for different samples of the same effective diameter. Moreover the V(I) characteristics of neighboring parts of the same multiterminal nanostructure are quantitatively indistinguishable (fig. 17). The shape of the R(T) dependencies is also the same for all sections of the same nanostructure. All samples above the critical temperature demonstrate I-V dependencies without any nonlinearities, which otherwise might indicate the existence of weak links. At low temperatures $T \sim 50$ mK $\ll T_c$ the IV-dependencies, measured at high magnetic field suppressing superconductivity, also reveal no nonlinearities, which might otherwise originate of single electron effects if tunnel barriers have been unintentionally formed.

To summarize, the extensive structural and elemental analyses reveal no obvious inhomogeneities. The studied titanium nanostructures can be considered as decent quality dirty limit superconductors $l \ll \xi$. The inevitable imperfections are quite moderate and cannot account for deviations from 'conventional' superconductor behavior to be associated with low quality of the studied structures.

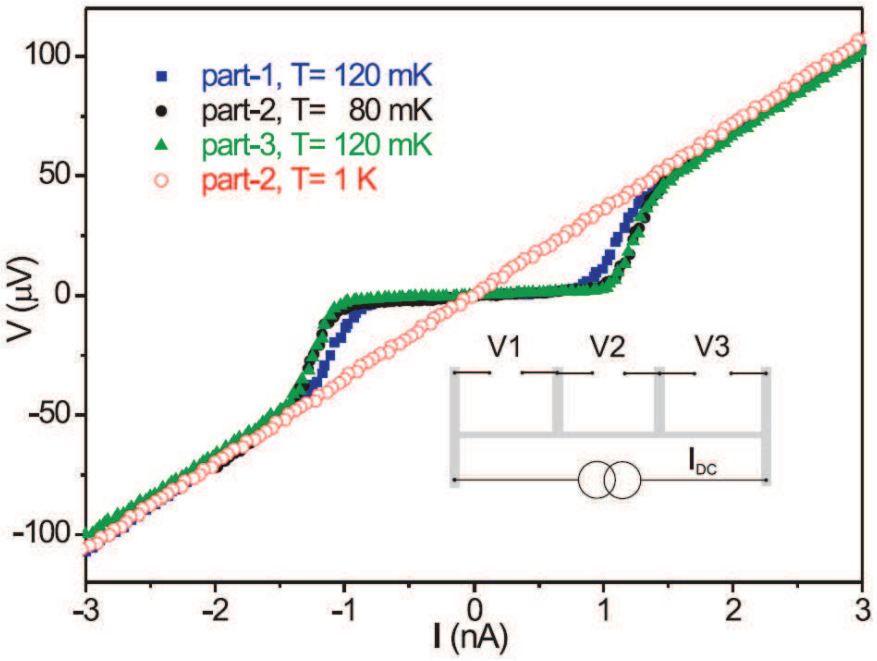

FIGURE 17 V(I) characteristics of the three neighboring parts with equal lengths L = 20 μm of the same nanowire with the effective diameter $\sqrt{\sigma} = 38 \pm 2$ nm. Above the critical temperature $Tc \geq 300$ mK within the scale of the image the Ohmic V(I) characteristics (open circles) are quantitatively indistinguishable between the different parts. Below the critical temperature the V(I) dependencies are also very similar (filled squares, circles, and triangles). Note the absence of the true zero resistance state manifesting itself as a finite slope below the residual critical current ~ 1.2 nA. Inset shows the layout of the sample and the measurement.

4.2 Titanium nanowires in low-ohmic environment

The QPS has been observed in a rather limited number of experiments studying the transport properties of ultranarrow nanowires made of various superconducting materials, amorphous MoGe[20, 5, 21], In and In-Pb[4, 22, 23], and Al[9, 10, 24]. In Pb[25] and InOx[26] nanowires broad R(T) have been observed, while no clear claims about the link with QPS were made. The material selection has an important role in the QPS-experiments. The characteristic diameters of the nanowire where the QPS related broadening of the transition have been observed in the above experiments is about 10 nm. At these scales reliable analysis of the sample homogeneity is difficult. The uncertainty leaves room to attribute the broadening of the transition to structural or geometrical inhomogeneities.

Following equation (31) one may conclude that proper material selection is crucial for observation of QPS phenomena.[82] In clean superconductors with $T_c \geq 4$ K the QPS effects can be observed only at wire diameters of few nanometers. Consideration of a realistically achievable superconducting nanostructures in dirty limit $l \ll \xi$, the QPS rate (eq. 24) reduces to a form $\Gamma \sim exp(-A^* \sqrt{T_c}\sigma/\rho_n)$, where A^* is a constant of proper dimensionality, T_c is the critical temperature, ρ_n normal metal state resistivity and σ is nanowire cross section. Hence, materials with low T_c and high resistivity in normal metal state are of advantage, given that fabrication of structures with minimal feature size $\sigma^{1/2}$ is limited by available nanotechnology hardware. For majority of our experiments titanium has been selected as the most suitable material. The T_c of bulk Ti is about 400 mK, it is high-ohmic metal which is easy to deposit on various substrates using e-beam UHV evaporation.

4.2.1 R(T) and I-V characteristics

The R(T)-measurements were made with 50 pA 7 Hz AC current at zero DC-bias utilizing lock-in technique and four-probe measurements configuration in a dilution refrigerator with base temperature down to 17 mK and extensive filtering of EM noise. SEM image of a typical sample for the R(T)-measurements is presented in the figure 18.

To study the dependence of the QPS rate on the nanowire cross section we used method of low energy ion milling.[6, 7] capable to reduce the effective diameter $\sigma^{1/2}$ in $\sim$ 1 nm steps. In the figure 19 R(T)-measurements of a same nanowire that have been progressively ion milled between the measurements are presented. To compare the results to the existing models the corresponding fittings for thermal and quantum phase slips were made. The fits were made utilizing equations (8) and (13) for thermally activated and (31) for the quantum phase slips. For thermal phase slips the only fitting parameter, that wasn't obtained directly from the experiment was the critical magnetic field H_c. The larger the H_c, the sharper the slope. The fits have been made assuming the Ginzburg-Landau enhancement of the parallel critical field $H_{c||} \sim H_c^{Bulk}\lambda/d$, where λ is the

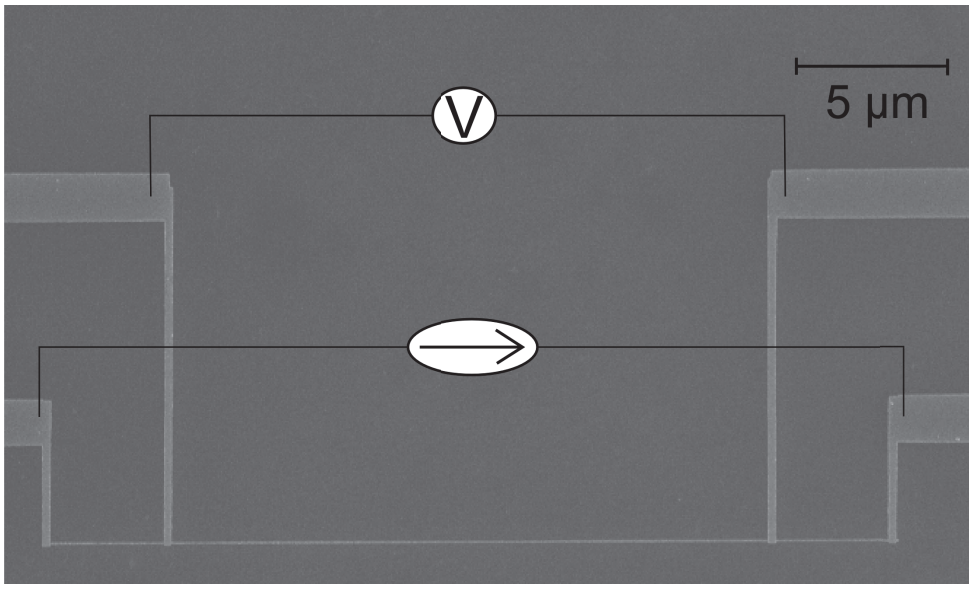

FIGURE 18 SEM-image of a typical sample for R(T)-measurements. Inner probes are used for voltage sensing and the outer probes are used for current biasing of the nanowire.

field penetration depth, and d is the film thickness. In our estimations we considered $d = \sigma^{1/2}$. No set of realistic parameters of the TAPS model can provide a reasonable fit to broad experimental R(T) dependencies.

In the Golubev and Zaikin QPS-model[30] the only fitting parameter is the numeric constant A, which should be of the order of unit. The mean free path for the wires can be evaluated within reasonable accuracy from the material constant $l\rho_N \approx 10 * 10^{-16}\ \Omega m^2$ for bulk titanium, which slightly varies between different literature sources.[83] This approach gives for our samples the mean free path around 1 nm. The result agrees well with TEM measured grain size of roughly 2 - 3 nm. Within the dirty limit, coherence length for the superconductor can be calculated $\xi \simeq \sqrt{l\xi_0(T)}$, where $\xi_0 \simeq \hbar v_F/\Delta(T)$ is the coherence length in the clean limit $\xi_0 >> l$ and $v_F = 1.79 * 10^6 m/s$ is the Fermi velocity for bulk titanium. The normal state resistance R_N can be obtained directly from the measurement data.

For titanium the superconducting critical temperature decreases with the decrease of the cross-section. The origin of the effect, typical for several materials, is still unclear. For some materials, for example aluminum, the effect is reverse: the critical temperature increases with the decrease of cross-section. Definition of a critical temperature T_c from a R(T) transition with finite width is always a question of a convention. For example, one may define T_c from $R(T_c) = R_N/2 \equiv R(T \gg T_c)/2$. For extremely narrow nanowires, where the QPS effect dramatically flattens the R(T) transition (fig. 20a), only a rough estimation for the T_C can be obtained from the data. In the fits (fig. 19 and 20) the critical temperature affects mainly only the shift of the fit in temperature scale, not the slope of the R(T) transition at $T \ll T_c$. It should be noted that QPS-fits are only valid when $T << T_c$, or formally where the QPS action S_{QPS} (eq. 20) is

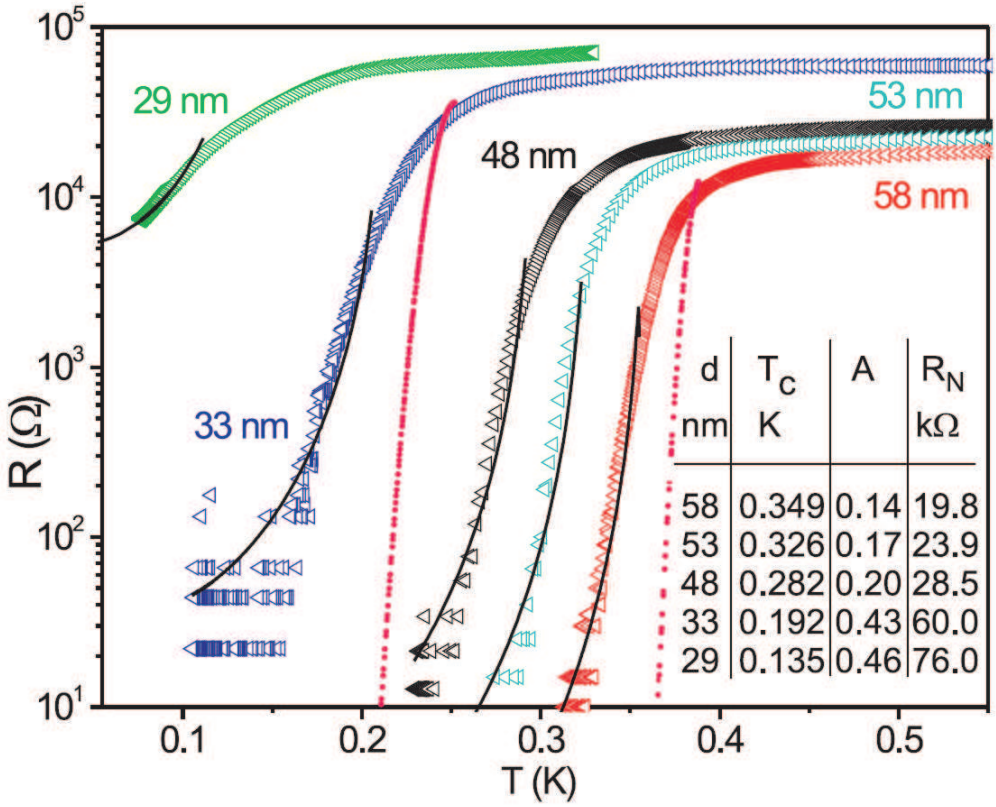

FIGURE 19 Resistance vs temperature for the same titanium nanowires with length L = 20 μm and progressively reduced effective diameter $\sqrt{\sigma}$ indicated in the plot and specified with accuracy $\pm$2 nm. The measuring currents were from 50 to 200 pA for the thinnest and the thickest samples, respectively. Fits using the QPS model are shown with solid lines; TAPS estimates for 33 nm and 58 nm samples are shown with dashed lines. The variable fitting parameters are indicated in the inset. For all samples the mean free path is of the order l = 1 nm.[71] (A. I)

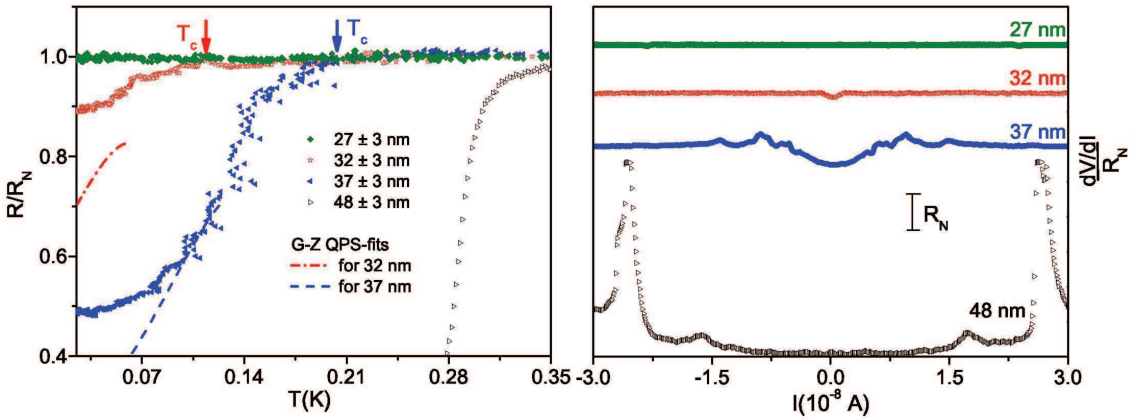

FIGURE 20 Left panel demonstrates typical temperature dependence of the resistance R(T) of four titanium nanowires with length L = 10 μm. Calculations based on equation (31) using the realistic model parameters l = 1 nm, v_F = 1.79 * 10^6 m/s, A = 0.098 and the critical temperature T_c = 200 mK and 115 mK for the 37 nm and 32 nm samples, respectively, are plotted with dashed lines. Best fit T_c's are indicated with arrows. In the limit $R(T) \ll R_N$, the G-Z QPS model fails to provide any acceptable fits for the thinnest samples. Right panel shows the dV/dI(I) dependencies of the same nanowires as in the left panel. For clarity the curve are vertically shifted and the value of the normal states resistance R_N is indicated with the bar. [72] (A.II)

much larger than one.

In figure 20a the sub-40 nm nanowires reach the limit of the applicability of the model.[30] Below diameter 37 $\pm$ 2 nm the theory [30] cannot be applied to the transitions. It should be noted that the resistivity of titanium nanostuctures vary greatly depending on the deposition rate. Thus the observable impact of QPS in titanium varies between 30 to 40 nm depending on the resistivity of particular sample. In the narrowest samples the zero resistivity state $R(T \ll T_c) \to 0$ conventional for superconductor is not observed (fig. 19 and 20).

At temperatures well below the critical temperature the I-V dependencies of the same nanowires as in figure 20a are presented in figure 20b. The thickest sample demonstrates the conventional characteristics: The zero resistance state quenched by application of current exceeding the critical value I_c. The double shape of the transitions (two values of critical current) is presumably due to the node regions where the diameter of the wire is slightly larger. With decrease of the cross-section the zero-resistance state disappears and only peculiarities associated with residual critical current are observed. In thinner samples the differential resistance does not vary with bias current: dV/dI = R_N. In the thinnest structures at $I \to 0$ slight increase of differential resistance is observed associated with weak Coulomb blockade. Observation of pronounced Coulomb blockade requires high-impedance environment described in the following section.

Tunneling spectroscopy of nanowires with small diameters, well within the regime of quantum fluctuations, reveals that the mean value of the modulus of the superconducting order parameter $|\widetilde{\Delta}|$ doesn't change significantly as the wire

diameter is reduced. This is an important fact to realize, the 'superconductivity' doesn't disappear due to phase slips though R(T $\rightarrow$ 0) does not tend to zero. BCS model predicts linear correspondence between critical temperature and the magnitude of the order parameter $T_c \approx 3.52 k_B \Delta(0)$. Our recent results, where R(T) and tunneling I-V characteristics (Al-AlOx-Ti(nanowire)) have been measured on same nanowires.[84] In figure 21 four different sets of nanowires with various effective diameters have been measured: the superconducting energy gap $|\widetilde{\Delta}|$ is determined at temperature 20 mK with tunneling spectroscopy utilizing S-I-S tunnel junction, and the R(T) transition of the same nanowire is measured in a separate experiment. The $|\widetilde{\Delta}|$ of titanium nanowires varies slightly between different samples, but even for the thinnest samples remains finite. The T_c's of the same set (identical fabrication conditions) nanowires are heavily suppressed by reduction of the wire diameter just by few nanometers.

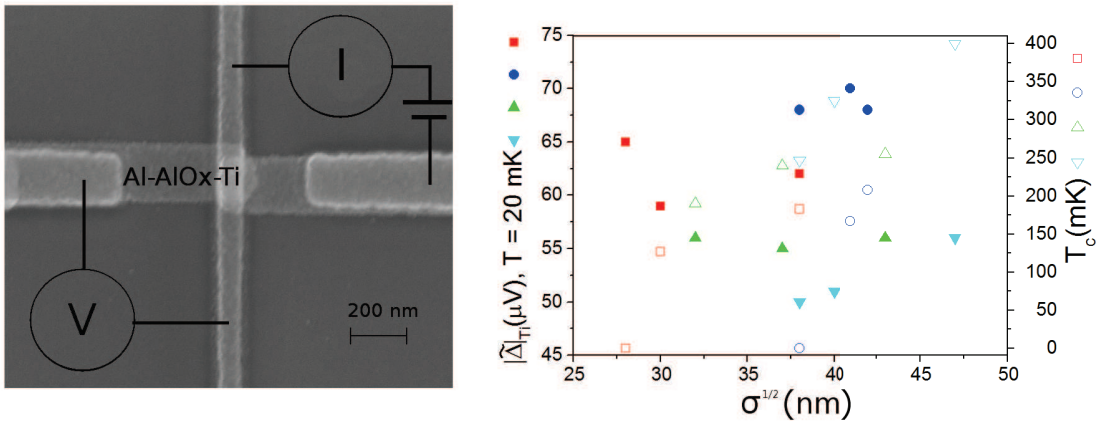

FIGURE 21 Left panel: schematics of the sample enabling simultaneous determination of $|\widetilde{\Delta}|$ and T_c. Right panel: same symbol and color indicate that the wires have been co-fabricated and have comparable properties, resistivity, impurity concentration, etc. The plot contains data for twelve nanowires where both the mean value of the superconducting energy gap Δ(T = 20 mK) and the transition temperature, defined as the point where the drop of resistance is noticeable R(T_C)/R_N = 0.9, are indicated with solid and open symbols respectively. The length of the wires is 4 μm for the squares and circles, and 20 μm for the face-up/down triangles. The error in definition of the energy gap is $\pm$ 3 μeV and for the transition temperature $\pm$ 10 mK.

Though the variation of the wire diameter doesn't affect significantly the order parameter mean value $|\widetilde{\Delta}|$, it affects the magnitude of fluctuations.[84] In sufficiently narrow nanowires, with the same diameters when the quantum phase slips are observed, the fluctuations of the order parameter amplitude $\frac{\delta|\Delta|}{|\Delta|}$ can reach 50%,[32] which should be easily detectable experimentally. Analysis of the shape of the I-V dependence provides the direct information about the 'smearing' of the energy gap $\delta|\Delta|$ associated with the quantum fluctuations. Note that these fluctuations should be distinguished from the phase slip process when the phase changes by 2π and the magnitude of the order parameter momentary nulls

$|\Delta| \rightarrow 0$.

4.2.2 Negative magnetoresistance

Transport measurements of our nanowires in low-ohmic environment revealed unusual effect: negative magnetoresistance (nMR). The phenomenon was mostly pronounced in thin samples with clear QPS contribution (fig. 22). The effect increases with lowering the temperature. Similar phenomenon has been reported in aluminum[10], MoGe and niobium[85] and lead[86] nanowires. The origin of the nMR in these quasi-1D channels is still under debates. In case of niobium and MoGe it was conjected that some rogue magnetic moments might be present, and their pair breaking contribution, active at lower magnetic fields, is suppressed by higher fields leading to the observed nMR.[85] It is a well-known fact that hypothetic magnetic impurities can have a non-negligible magnetic moment in aluminum (likely also in titanium) matrix only at relatively high concentrations [87] and thus this explanation is not likely in our case. Our titanium nanowire samples were carefully characterized in ToF-ERDA experiments, and it is highly improbable that high enough concentration of rogue magnetic impurities could be left undetected.

More likely explanation for the phenomenon is that the magnetic field suppresses the charge imbalance accompanying each phase slip event.[88] The suppression of the charge imbalance by magnetic field would result in shorter relaxation time and thus, decrease the effective resistance associated with quasi-normal region within the locus of each PS at low magnetic fields. Another possibility, also capable to explain the nMR, is that magnetic field more effectively suppresses superconductivity in wider superconducting electrodes, compared to thinner 'QPS-body' of a nanowire. This affects the phase slip formation in the nanowire [89] or the heat escape from the nanowire: it is known fact that a superconductor (=electrodes) are ideal thermal insulators compared to normal metals [8, 90]. However, applicability of model [89] to our structures studied at $T \ll T_c$ is not clear.

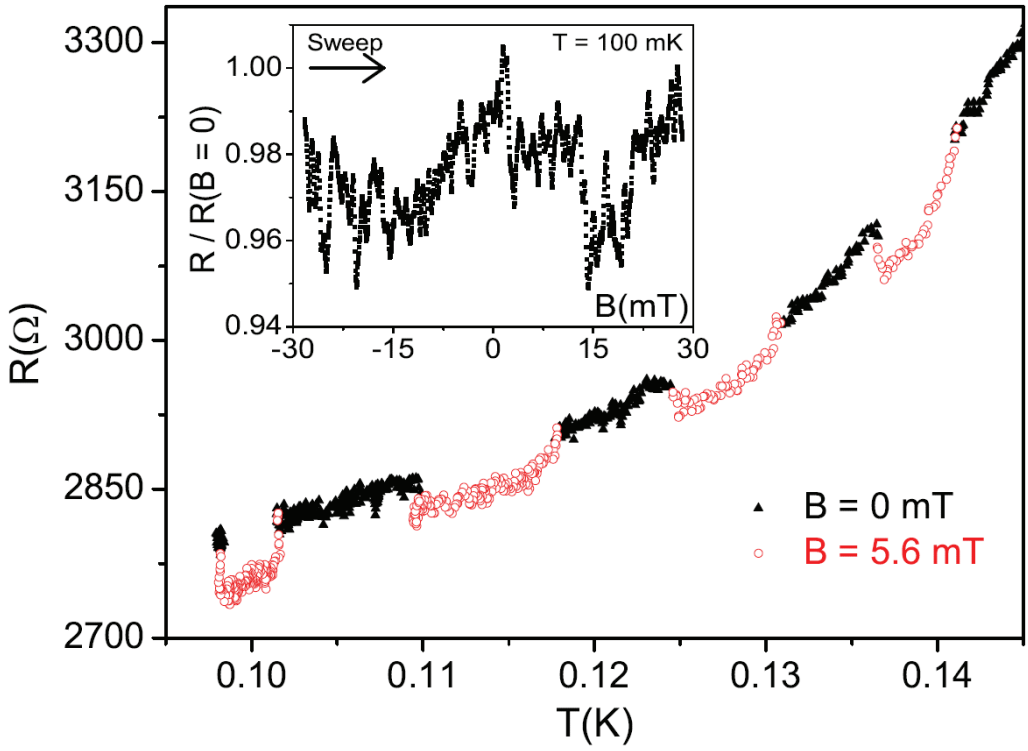

FIGURE 22 Temperature dependence of resistance of titanium nanowire with length L = 30 μm and the effective diameter 39 $\pm$ 3 nm measured at zero magnetic field (filled triangles) and in perpendicular magnetic field $B = 5.6$ mT (open circles). Both data were obtained while the same slow temperature sweep just by switching on and off the magnetic field. The inset shows the representative region with the negative magnetoresistance, measured at a constant temperature $T = 100$ mK.[72] (A. II])

4.3 Titanium nanowires in high-ohmic environment

Previous section refers to a conventional case when transport through a mesoscopic-scale superconductor is studied utilizing low-ohmic probes: typically consisting of the same superconductor, but with wider line-width. In this section we'll deal with the limit, when charge is the relevant quantum variable. Electronic charge passing through the system per unit time should be constant: charge fluctuations are suppressed. To enable realization of this limit, the system should be current biased.

In section 2.3 we have outlined that a QPS process in a superconducting nanowire is qualitatively similar to a Josephson tunneling. The corresponding system, current biased small JJ with $E_c \gg E_J$, exhibits essentially periodic electron transport process: Bloch oscillations. Given that the characteristic frequency of Bloch oscillations is of the order of 3 GHz, "true" current biasing should be applicable in this high frequency regime. The current biasing circuit should have relatively low capacitance not to shunt the RF signal. The characteristic scale, which the system "sees", the electromagnetic horizon, can be roughly estimated

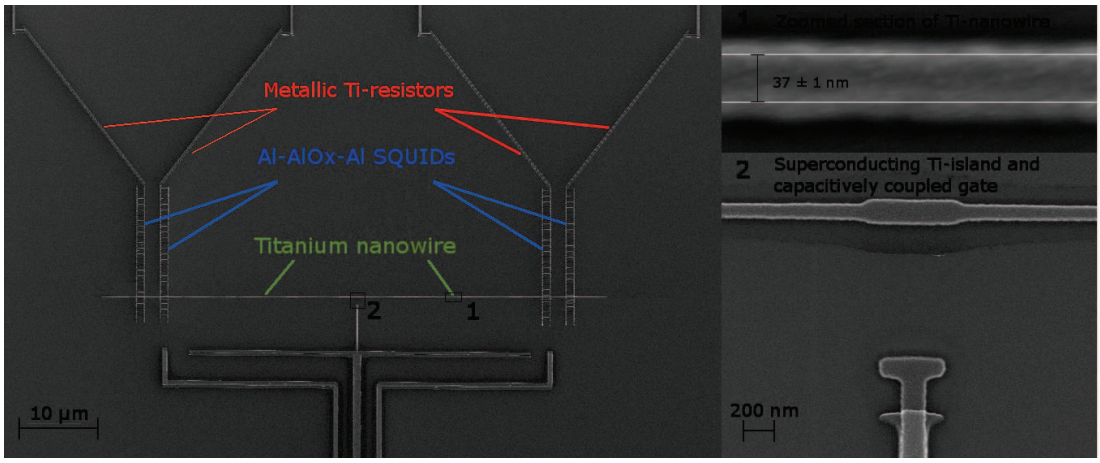

FIGURE 23 SEM image of a typical nanostructure with high-impedance electrodes of 'dirty' non-superconducting titanium and 1D arrays of Al-AlOx-Al SQUIDs. The right panel shows the zooms of the structure: upper image shows a section of the nanowire and lower image shows the central island.

as the wavelength of the Mooij-Schön mode at characteristics frequency. Estimation gives for our case the scale of the order 100 μm. Hence, to enable reliable current biasing (at high frequency!) one should fabricate on-chip high impedance probes with low cross-capacitance and low capacitance to ground.

4.3.1 QPS transistor

Coherent superposition of QPS leads to charge localization.[60] Hence, in a full analogy with a conventional single electron transistor (or Cooper pair transistor), where tunnel barriers from both sides of a central island enable charge localization at the island, two QPS nanowires, connecting the island to external circuit, should provide charge localization acting as dynamic equivalent of a conventional tunnel (Josephson) junctions.[60, 62]

Several versions of QPS transistors were studied in this work. All the samples had possibility for four probe measurement. In the first demonstration showing the transistor effect we used rather high-ohmic bismuth electrodes in current biasing circuit. In the next sample generation the high-impedance probes providing current bias, consisted of metallic resistors and arrays of Al-AlOx-Al SQUIDs. In figure 23 is the SEM image of such QPS transistor. In later design voltage probes consisted of only normal metal resistors to eliminate nonlinearities in voltage sensing circuit. All sufficiently narrow titaniun nanowires in high enough impedance environment demonstrated the Coulomb blockade. The blockade width varied between few μV to few mV depending on the diameter of the measured sample and the impedance of the environment.

Utilization of dissipationless elements SQUIDSs[52] in the high impedance environment has an advantage compared to dissipative high-ohmic metallic contacts[62] as it eliminates the Joule heating of the latter and reduces the associated Johnson noise.[63]

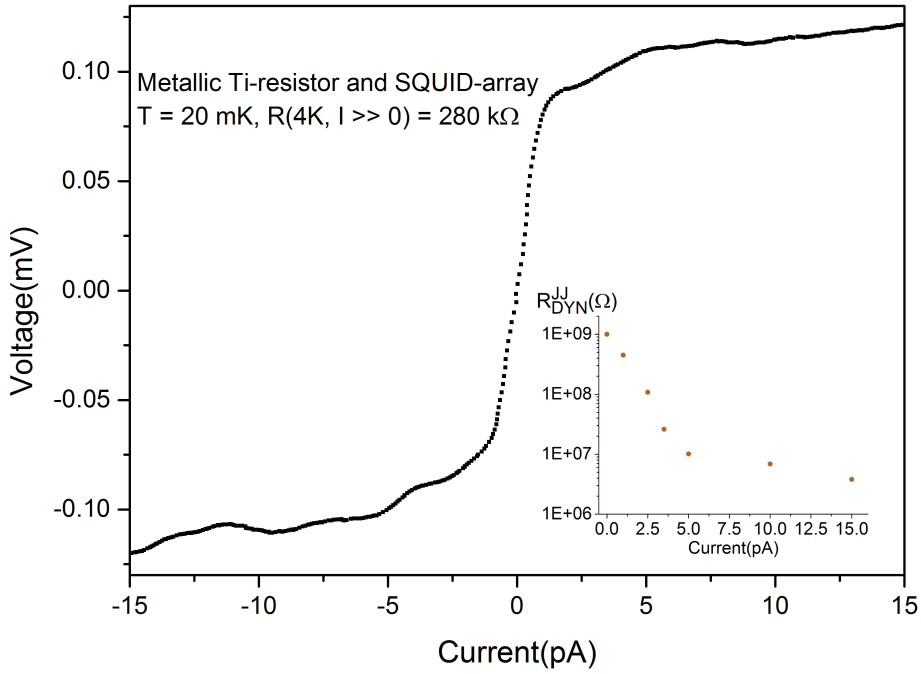

FIGURE 24 V(I)-measurement of the SQUID array and metallic resistor at $T = 20$ mK. The dynamic resistance of the high-ohmic environment depends the bias-point (inset). At higher biases the dynamic resistance saturates at $\sim 300\,\mathrm{k}\Omega$.

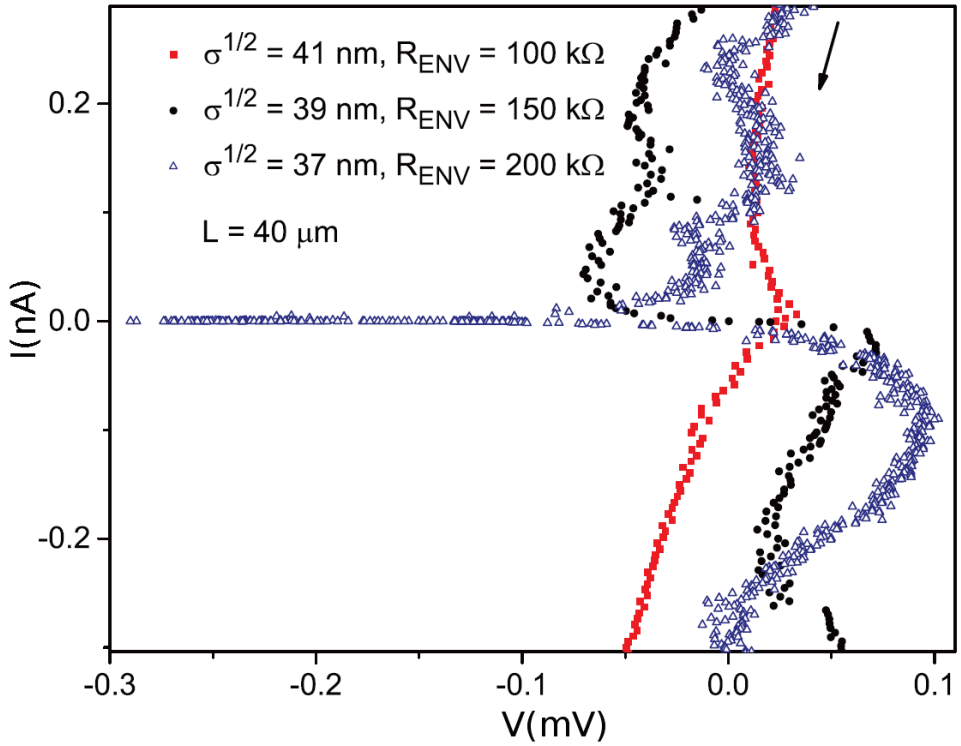

FIGURE 25 V(I)'s of a 40 μm long titanium nanowire with progressively reduced effective diameter $\sigma^{1/2}$ at temperatures $T \ll T_c$. Note that the high bias resistance of the SQUID array and serially connected metallic resistors increases after each sputtering cycle $R_{env} \equiv R|_{resistor} + dV/dI(|I| \gg 0)|_{SQUID}$. The effect should be small at the limit $I \to 0$ because the array dimensions should not significantly affect the differential resistance within the Coulomb blockade region. Note that the reduction of the diameter just by 2 nm ($\sim$ 5% from the effective diameter) increases the blockade dramatically. The arrow indicates the data recording direction.[91] (A. IV)

SQUID-based high-impedance environment utilizes the concept of dynamic resistance of a JJ (or a SQUID) at zero bias $R_{JJ}^{DYN} = dV/dI(V \to 0)$ and the Josephson inductance $L_K = (d^2E_J/\phi^2)^{-1}$. Typical V(I)-characteristics of the high-impedance probe is presented in figure 24. In the inset is the dynamic resistance of the SQUID array. At small biases the dynamic resistance is about 10^4 times higher than the normal state resistance of the array. Hereafter, we define $R_{ENV} \equiv R_{PROBES} + dV/dI(I \gg 0)_{SQUID-array}$. In figure 25 the V(I) characteristics of the same nanowire that has been ion milled to reduce the cross section, is presented between the sessions of ion milling. It is clear that the width of the Coulomb blockade V_{CB} strongly depends on the nanowire diameter. At temperature $T \ll T_C$ the width of the Coulomb gap δV_{CB} indeed should exponentially depend on the nanowire cross section following the expectation $\delta V_{CB} \sim E_{QPS}$ (eq. 45 and 74).

The asymmetry of the IV curves observable in figure 25 has been typical for the studied high-impedance samples. The shape of the back-bending region varies depending on the sweep direction and even sweeps performed in the same direction are not dot-to-dot reproducible when entering or leaving the blockade

region. The asymmetry seems not to be significantly altered between cool downs which to some extent would rule out the association of the effect solely to random access charges. Even if there could be some physics behind the asymmetry, there is an instrumental effect contribution which originates from the high RC-constant of the measurement circuit near the blockade region (several minutes). The effective resistance of the blockade region combined with the high capacitance of the RC filters in dc-lines require the desired sweep rate to be much more slower than is possible realistically. To clarify the issue the RC filters should have been removed from the cryostat which would have dramatically degrade the immunity of the system to environmental EM noise.

The asymmetry of the IV curves observable in figure 25 has been typical for the studied high-impedance samples. The shape of the back-bending region varies depending on the sweep direction and even sweeps performed to same direction are not dot-to-dot reproducible when entering or leaving the blockade region. The asymmetry seems not to be significantly altered between cool downs which to some extent would rule out the effect to be contributed solely to random access charges. Even as there could be physics behind the asymmetry, there is a possibility of instrumental effect originating from the high RC-constant of the measurement circuit near the blockade region (several minutes). The effective resistance of the blockade region combined with the filtered high capacitance dc-lines make the required sweep times longer than realistically is possible. To clarify the issue the RC filters should have been removed from the cryostat which was not possible during the time.

Figure 26 shows the magnetic field dependence of the V_{CB}. The Coulomb gap is suppressed by strong magnetic field at $T \ll T_C$. This supports the presumption that the effect is related to superconductivity. It is well-known that Coulomb phenomena in single-electron systems are immune to magnetic field.[92] Note also the increase of the Coulomb gap at small magnetic field. The observation could be linked to the negative magnetoresistance effect observed in the QPS nanowires (section 4.1.2). Still the origin of the phenomenon is not clear.

Evolution of the Coulomb Blockade with temperature is presented in figure 27. At the lowest temperatures $T \ll T_c$ the Coulomb blockade is very pronounced. The blockade decreases with increase of temperature and completely disappears above the critical temperature of titanium $\sim$ 400 mK. We have discussed the dependence of the Coulomb gap on QPS nanowire cross section (fig. 25), magnetic field dependence (fig. 26) and temperature (fig. 27). The transistor effect can be observed using the gate electrode that is capacitively coupled to the superconducting island. As in case of normal SET or Cooper pair transistor the supercurrent through the transistor can be modulated by changing the gate potential $V_g = \frac{q}{C_g}$, where q = e for a SET and q = 2e for a Cooper pair transistor. For geometry similar to figure 23 estimated $C_g \approx 1.5 * 10^{-17} F$ corresponds to $V_g \approx 20mV$ when q = 2e. The effective resistance of the QPS transistor at constant bias current as function of the gate voltage is shown in figure 29. The measured period $\delta V_g \sim$ 16.6 mV is in a reasonable agreement with the estimated period. At $T = 20$ mK the depth of the gate modulation is about 50%.

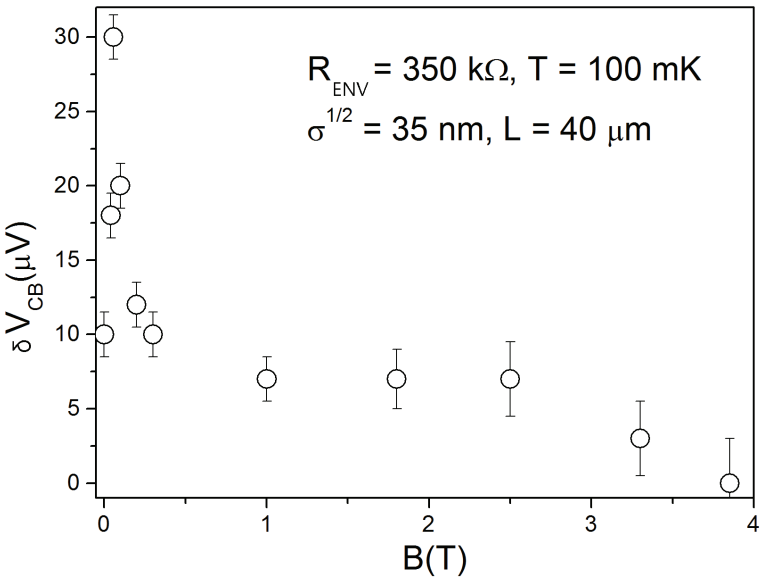

FIGURE 26 Coulomb blockade width V_{CB} of titanium nanowire as function of perpendicular magnetic field B at temperature 100 mK. Increase of the Coulomb gap at small fields may be linked to negative magnetoresistance effect observed in the QPS nanowires, but the origin of the phenomenon is not clear. At high field $B \gtrsim 3.85$ T the Coulomb gap is suppressed. The Coulomb blockade width is determined as region where the current is below noise level (< 0.1 pA) and the error bars correspond to cumulative experimental uncertainty of the voltage measurement. [91] (A. IV)

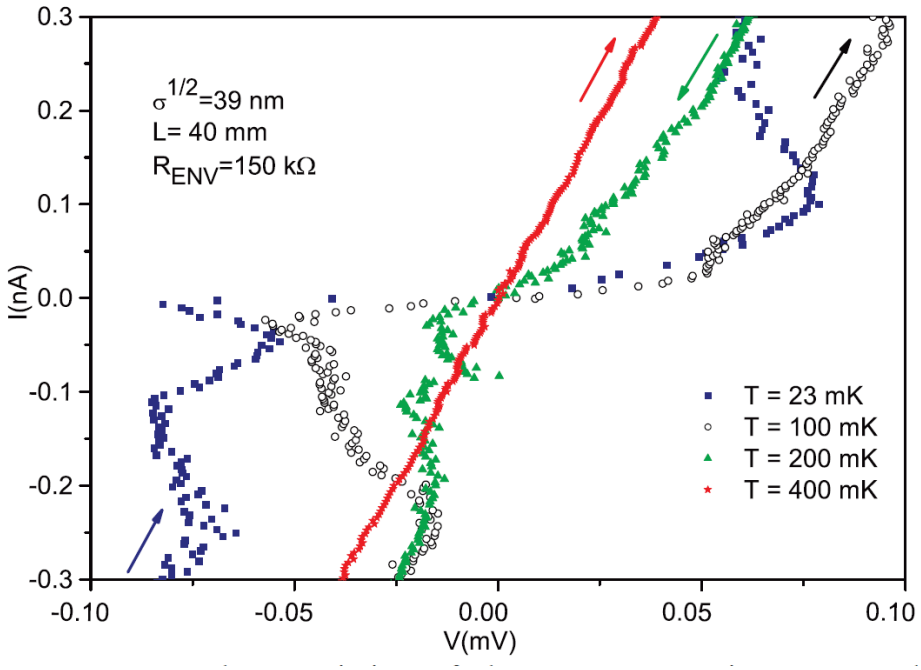

FIGURE 27 Zoom of V(I) dependencies close to the blockade region of a same nanowire at various temperatures. The R_{ENV} is the high bias resistance of the environment (for typical low bias characteristics see figure 24). Arrows indicate direction of the data recording.[91] (A. IV)

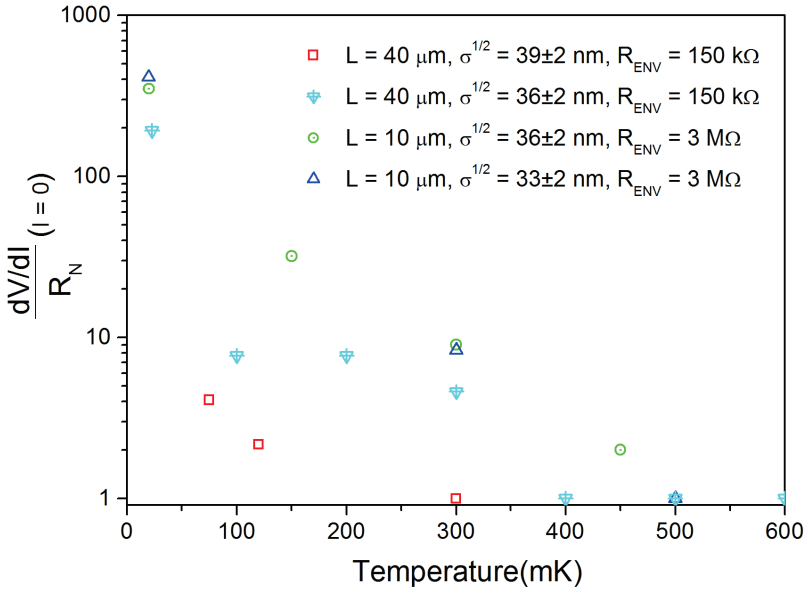

FIGURE 28 Temperature dependence of zero bias dynamic resistance dV/dI(I = 0) normalized by the normal state resistance R_N for several titanium nanowires as function of temperature. The listed high impedance probe resistances R_{ENV} are for high bias limit. Typical low bias characteristics are presented in figure 24. [91] (A. IV)

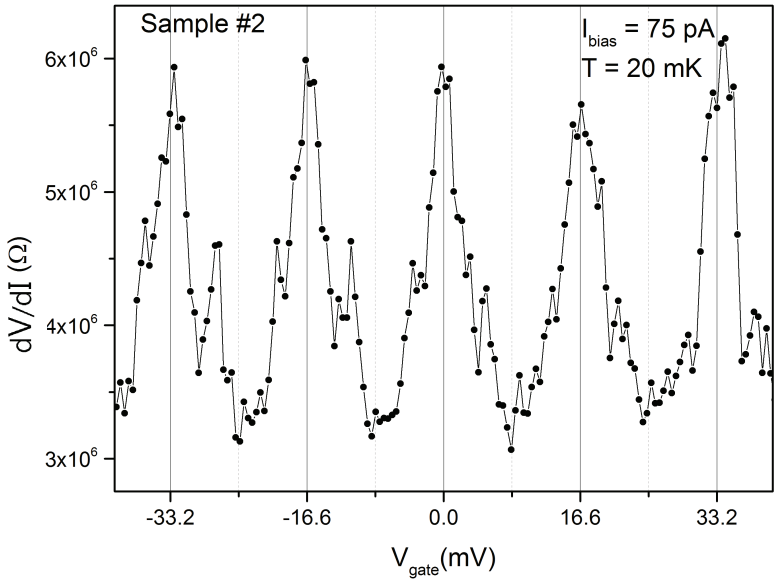

FIGURE 29 Effective resistance of the QPS transistor measured at constant current I = 75 pA as function of the gate voltage. The solid vertical lines are the guides for marking the 2e periodicity.

On some samples single electron contribution is observable even at temperature T = 20mK.(fig. 29) With increase of temperature the contribution of single electron tunneling becomes stronger and pronounced 1e periodicity is observed. The overall magnitude of oscillations drops as the temperature increases and completely disappear between 400 mK and 500 mK, ie. above the superconducting transition temperature of titanium. Note also that the oscillation period doesn't change between the samples with identical gate electrode configuration (fig. 29 and 30).

The 2e transistor effect can be destroyed by relatively small magnetic fields $B \gtrsim 60mT$, presumably corresponding to the critical field of the superconducting island. The SET effect retains finite amplitude even when the superconductivity of the island is completely suppressed by magnetic field. It should be also noted that although the Coulomb gap δV_c increases at small fields (fig. 25 inset), the effective resistance R_{ac} decreases. The blockade width δV_c is larger, but the current at a given voltage is also larger, presumably due to more pronounced contribution of single electron tunneling.

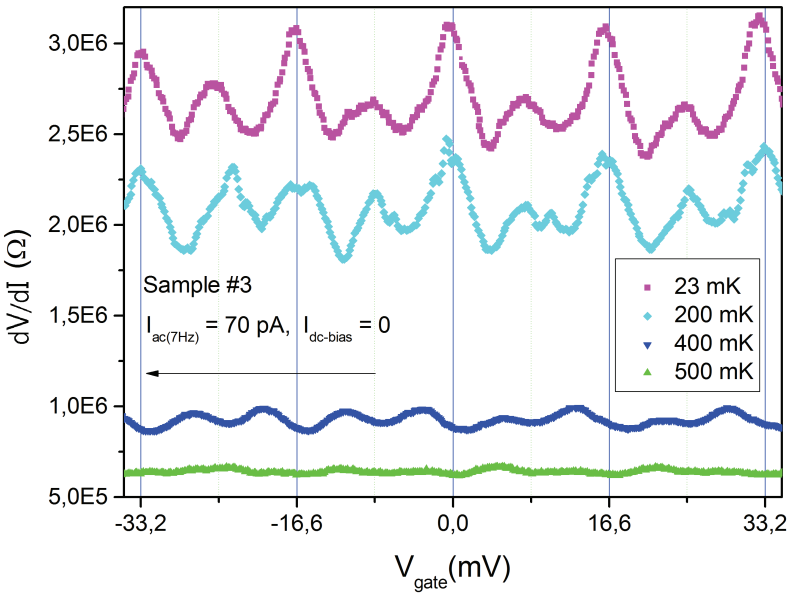

FIGURE 30 Temperature dependency of the effective resistance of the QPS transistor at zero dc bias as function of the gate potential. The effective resistance is measured with $I_{ac} = 70\ pA$ peak-to-peak modulation with frequency 7 Hz utilizing four-probe configuration and lock-in technique. At T = 20 mK the Cooper pair tunneling dominates, but 1e-periodicity is also measurable. At higher temperatures the 1e-periodicity becomes more pronounced. The modulation disappears between 400 mK and 500 mK. The arrow indicates the direction of the V_{gate} sweep and solid vertical lines mark the 2e-periods and dashed lines the e-periods.

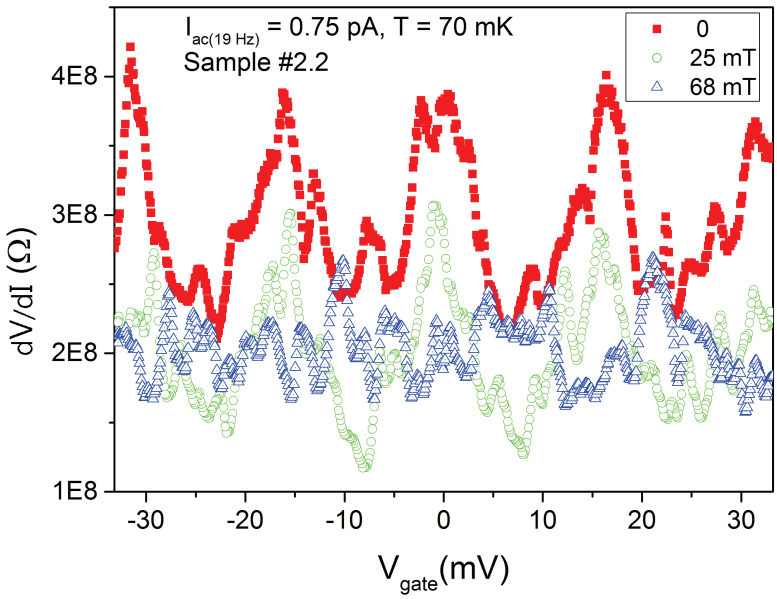

FIGURE 31 Effective resistance R_{ac} of the transistor at $I_{dc} \to 0$ as function of gate potential at various magnetic fields applied perpendicular to the structure. The absolute value of R_{ac} drops already at small fields($\sim$ 25 mT) but relative amplitude of 2e oscillations have higher magnitude compared to $B = 0$. At higher magnetic fields (B $\gtrsim$ 60 mT) the 2e-periodicity is completely suppressed and only weak e-periodicity is left. This is most likely due to the suppression of superconductivity in the island.

4.3.2 Synchronization of the Bloch oscillations

As it has been discussed in section 2.4.4, synchronization of internal Bloch oscillations with external RF drive should lead to formation of current singularities at values I = n(2e)f_{RF}, opening a possibility to use the effect as quantum standard of electric current.(QSC) Illustrating the viability of the QSC to be built based on the QPSJ has been one of the main motivations of the work. The requirements for the standard of metrological quality are strict: at current of about 1 nA the relative accuracy should be of the order of 10^{-8}. We've developed several structures in attempts to realize the standard. The first samples gave promising results with accuracy about 10^{-2} at 1 nA current. In this section I'm going to present the experimental results of two QSC structures we've realized and propose a new structure in which more accurate results should be possible to obtain.

The first generation of samples had high-ohmic environment consisting of normal metal resistors. The metallic resistors were made out of either dirty titanium (few tens of kΩ) or from bismuth (from MΩ to tens of MΩ). In all our titanium structures the resistivity of both the nanowire $\rho_N^{QPS} \leq 300\Omega/\Box$ and the electrodes $\rho_N^{PROBES} \leq 1k\Omega/\Box$ are still on the metal side of the metal-to-insulator transition. In deliberately oxidized nanowires with noticeably higher resistivity Coulomb effects have been observed.[79]. Typical structure is presented in figure 32.

At low temperatures even relatively thick samples $d = 40nm$ with dirty titanium electrodes $R_{ENV} = 30$ kΩ show slight increase of resistance at small bias currents compared to the normal state resistance. With RF-irradiation noticeable traces of the steps were observed in the dynamic resistance dV/dI at positions corresponding to the $I = n(2e)f$.(fig. 33) The first step demonstrates only very slight increase of the dynamic resistance presumably due to overlap with ′stronger′ superconducting region, but second and third steps, closer to the critical current, and correspondingly having higher fluctuation rate, show already measurable traces of the dynamic resistance.

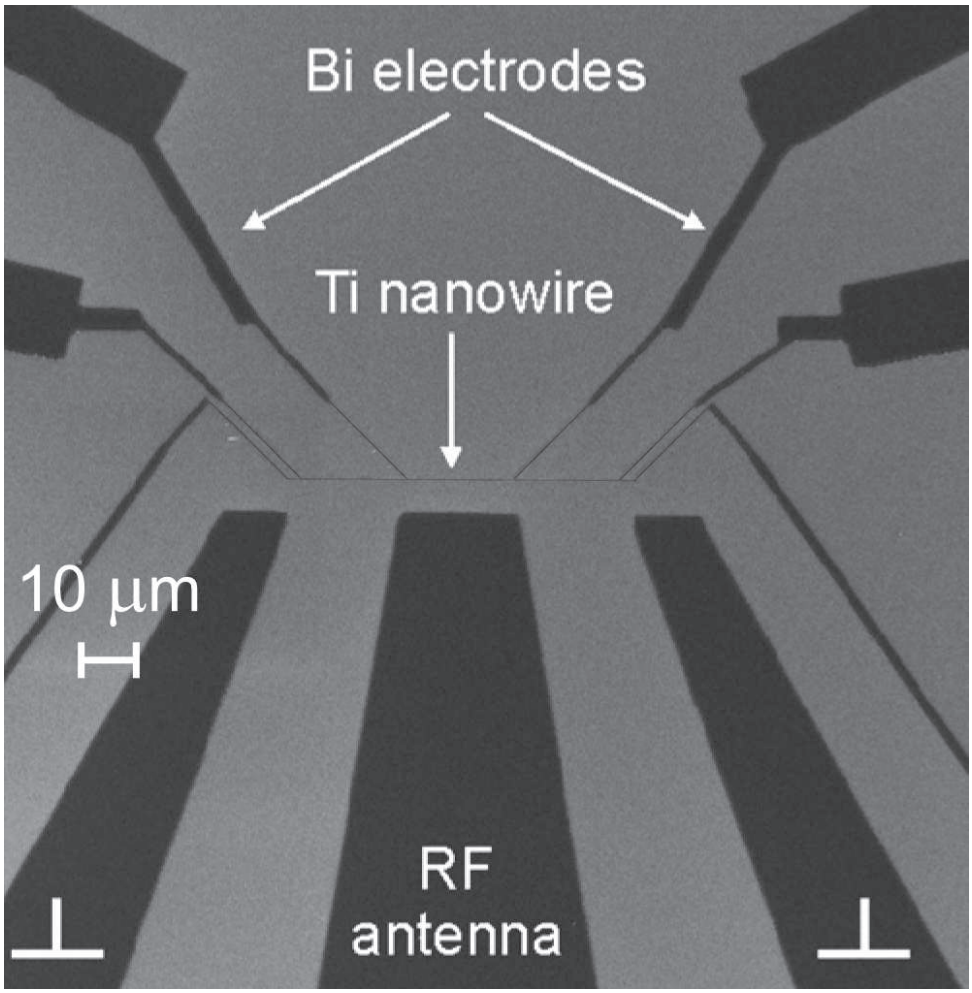

FIGURE 32 SEM image of the nanostructure: high-impedance Bi-probes and superconducting titanium nanowire. The sample consists of three separately measurable titanium nanowires each with length of 20 μm and all measurable in four probe configuration. The separate sections allow comparison be-tween characteristics of identical nanowires to clarify the possibility of inhomogeneity related effects. The capacitively coupled antenna below the nanowire is used for the RF irradiation. The same antenna can be used as a dc gate.[69] (A. III)

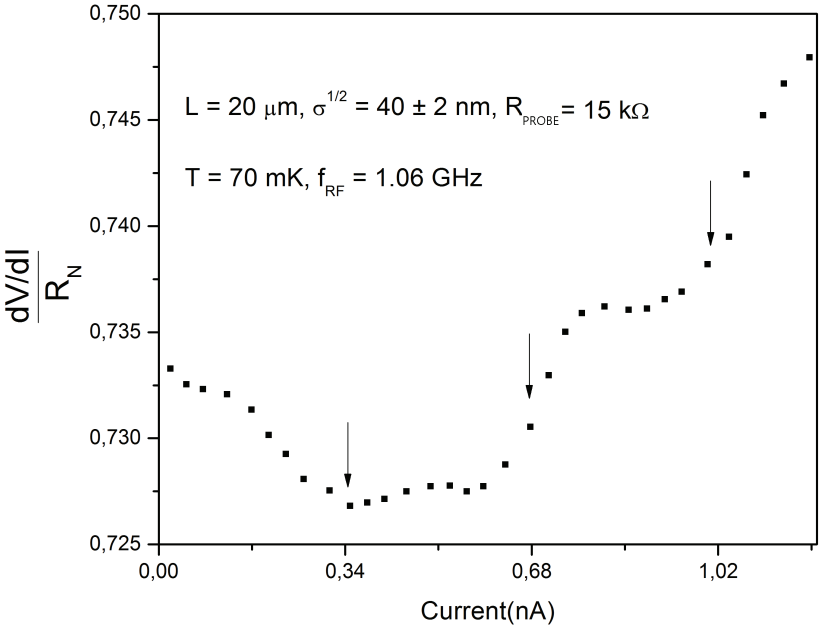

FIGURE 33 dV/dI(I) in the presence of external rf irradiation $f_{rf} = 1.06$ GHz for all-titanium structure: superconducting titanium nanowire $\sigma^{1/2} = 40 \pm 2$ nm, $L = 20$ μm and metallic 'dirty' titanium probes $R_{PROBE} = 15$ kΩ. Expected positions for current singularities $I_n = n(2e)f_{rf}$ are indicated with arrows. Note also the slight increase of the dynamic resistance at $I \to 0$.[69] (A. III)

Thinner nanowires, $d = 24$ nm, exhibit pronounced Coulomb blockade (fig. 34). The Coulomb gap decreases with temperature and disappears at the critical temperature of bulk titanium.(see section 4.3.1) In the multiterminal structure all the neighboring parts have similar V(I)-characteristics yet the blockade width only slightly increases when several structures are measured in series. By applying dc-voltage to the RF antenna the blockade magnitude δV_{CB} can be modulated.

As there is no qualitative difference between electrodynamics of a JJ and a superconducting wire governed by quantum fluctuations, the results should be analyzed from the point of view if the same data can be quantitatively (and qualitatively) explained by 'conventional' system a JJ, before making the claim of QPS-based phenomenon. Support of the QPS scenario is based on four points. Firstly, the wires show no obvious geometric weak links and the material analysis confirms the high quality of the evaporated titanium as discussed in section 4.1. Secondly, even if there would be some unnoticed breaks or oxide layer blocking the metal-to-metal supercurrent along the nanowire, the charging energy corresponding to JJ formation by 1 nm thick oxide barrier and the area $\sim$ 24 x 24 nm^2 would result in capacitive energy $E_c \sim 50$ meV which is almost two orders higher than the observed blockade (fig. 34). Note that the estimation corresponds to the largest capacitor to be formed in the nanowire providing the lowest charging energy $E_c = (2e)^2$ / 2C. Third, if to consider that in the nanowire still exists a hypothetical tunnelbarrier with smaller charging energy of the order of the experimentally observed Coulomb gap $V_{CB} \sim 0.4$ to 1 meV, then the normal state blockade should be noticeable up to temperatures T $\approx$ 4.6 to 11.6 K. On the contrary, in all the samples the Coulomb blockade disappears at temperatures, which correlate well with critical temperature of bulk titanium T = 400 to 500 mK. Fourth, the blockade can be suppressed by magnetic field, which wouldn't be possible with traditional SET as the Coulomb phenomena in single-electron systems are almost immune to magnetic fields[92]. Summarizing, the interpretation of the observed Coulomb phenomena in terms of 'conventional' (static in space and time) JJs, unintentionally formed in out titanium nanowires, is rather improbable.

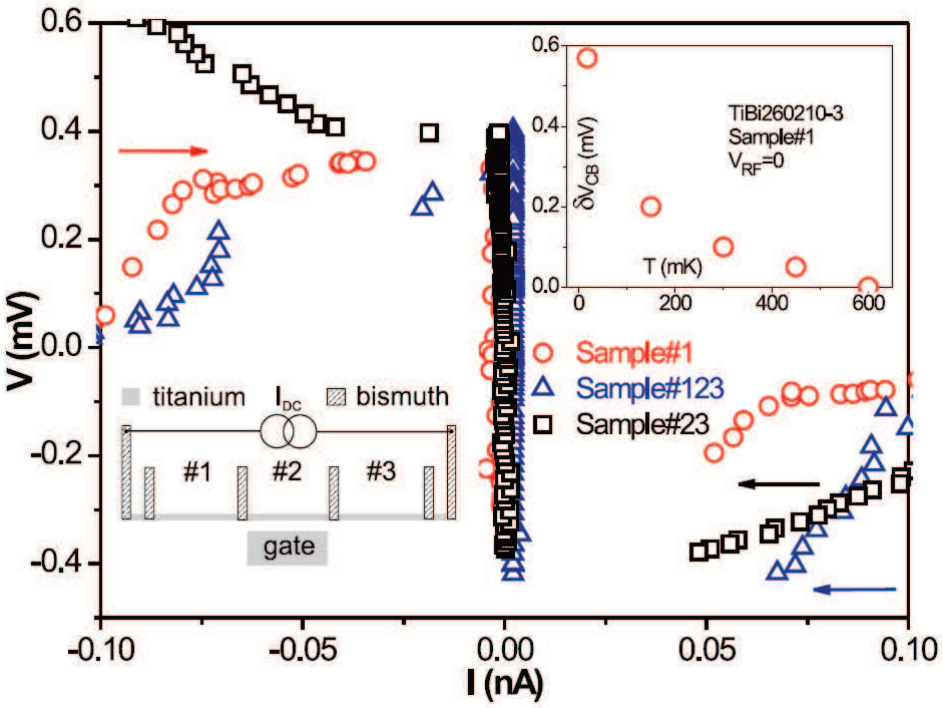

FIGURE 34 Multiterminal titanium nanostructure with three adjacent nanowires each with length L = 20 μm and effective diameter d = 24 $\pm$ 2 nm. All bismuth probes have identical parameters $R_{PROBE} \approx 10$ MΩ and length L = 22 μm. The V(I)s demonstrate the Coulomb blockade for all three neighboring parts of the same nanostructure. Arrows indicate the direction of the current sweep. Inset shows the temperature dependence of the Coulomb gap. δV_{CB} decreases with increase of the temperature and disappears above $\sim$ 450 mK.[69] (A. III)

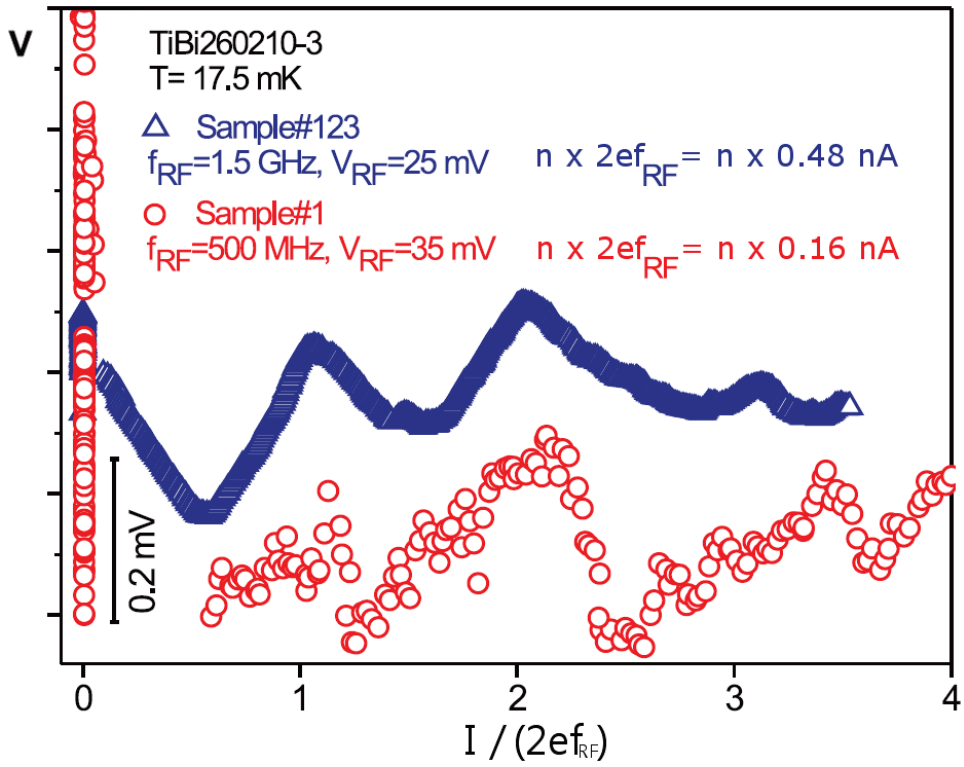

FIGURE 35 Titanium nanowires, effective diameter d = 24 ± 2 nm and length L = 20 μm (red circles) or L = 60 μm (blue triangles), in high-ohmic environment $R_{PROBE} \sim 10$ MΩ irradiated with frequency f_{RF}. The synchronization of the Bloch oscillations is observed at $I = n(2e)f_{RF}$. The maximum 'width' of the Bloch steps $\delta V_C{}^{(n}{}_B{}^{)}$ is observed for sample #123 (blue triangles) at frequency $f_{RF} \approx 1.5$ GHz, which corresponds to $I_1 = 0.48$ nA and for sample #1 (red circles) $f_{RF} \approx 0.5$ GHz, which corresponds to $I_1 = 0.16$ nA.[69] (A. III)

Typical V(I)-characteristics of our samples irradiated with external RF-radiation are shown in figure 35. The external radiation should generate resonances at positions $I_n = n(2e)f_{RF}$ which are observed at the V(I)s as broad plateaus. At higher frequencies the plateaus become even broader. Presumably, the extra broadening originates from he Joule heating of the high-resistive normal metal probes. The impact of Joule heating is mostly pronounced at ultra-low temperatures, and might easily lead to overheating of the current-biasing probes well above the critical temperature of titanium $T_c \sim 450$ mK (eq. 75). Presence of 'hot' electrodes, contacting the QPS nanowire, is undesirable from two points of view. First is the trivial overheating of the nanowire itself, resulting in thermal broadening of the Bloch steps.[93] Second, presence of a 'hot' resistor in the circuit inevitably leads to increase of Johnson noise, which might completely smear the Bloch singularities.[63]

Modulation technique enabling the measurement of the dynamic resistance reveals relatively sharp Bloch singularities up to eighth harmonic (fig. 36). In figure 36 the RF frequency has been selected to be low (and hence the corresponding current $I_n = n(2e)f$) in order to observe multiple harmonics avoiding the heating effects.

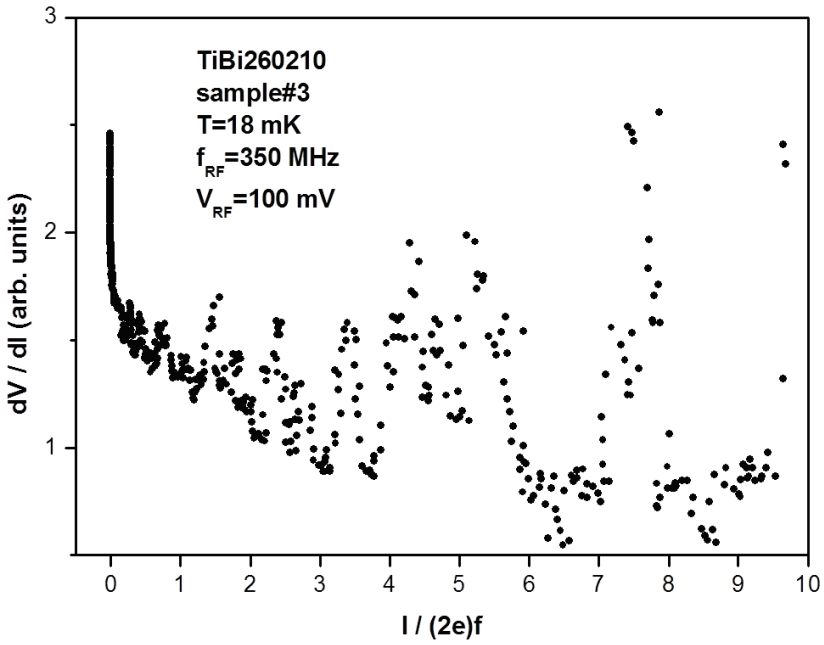

FIGURE 36 Fist derivative of the V(I) characteristics (=dynamic resistance) of titanium nanowire, d = 24 $\pm$ 2 nm and length L = 20 μm, in high-ohmic environment biased with current I and irradiated with RF. At drive frequency f_{RF} = 350 MHz steps up to eighth harmonic are observed. [69] (A. III)

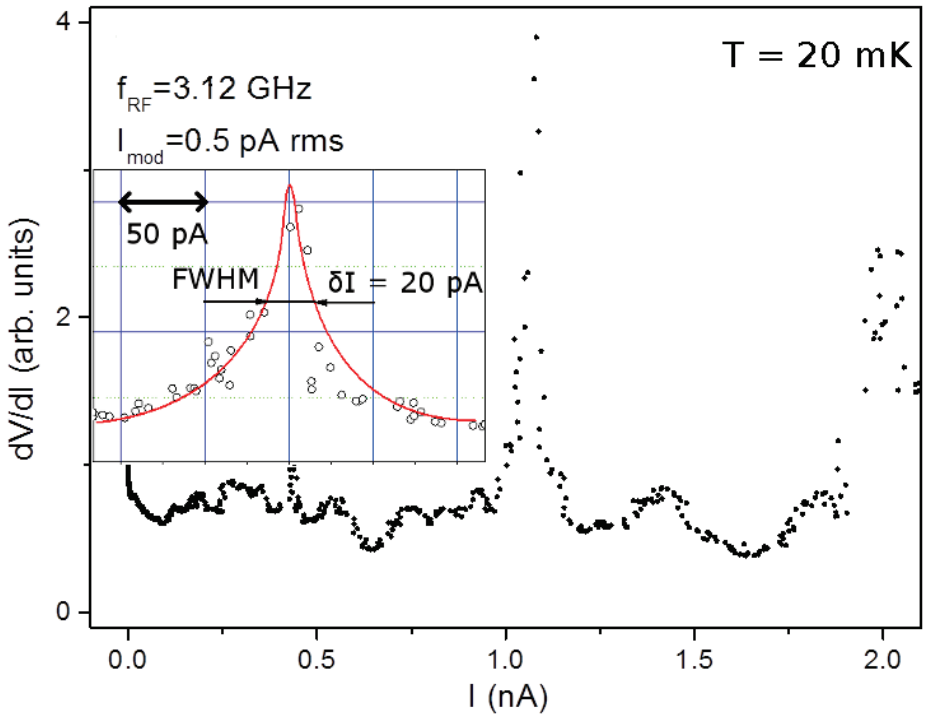

FIGURE 37 Dynamic resistance of current biased titanium nanowire ($\sigma^{1/2}$ = 15±2 nm and L = 20 μm) in high-ohmic environment irratiated with f_{RF} = 3.12 GHz (I = 2ef ≈ 1 nA). Weak single electron peaks and strong 2e peaks are observed. In the inset is the Gaussian fit for the first (n = 1) 2e step. The FWHM of the Gaussian fit is about 20 pA, leading to relative uncertainty of the position of the current singularity $\sim 10^{-2}$.

In figure 38 the positions of the singularities at $I_{n,m}$ are plotted as function of the RF drive frequency. The occurrence of the steps and the harmonics n and m are explained in the section 2.3.9. Both single electron and Cooper pair steps and their harmonics are observed. The frequencies vary from tens of MHz up to several GHz showing the linear dependence of the current - frequency relation for broad frequency range. The amplitude dependence is illustrated in the fig. 39 for the $f_{SET,\ n=2,\ m=1} = f_{Bloch,\ n=1,\ m=1}$. The dependency follows the Bessel-function dependency(eq. 68) supporting the early model derived for the dual system: small current biased JJ.[93]

The realization of the current standard for practical metrological applications requires accuracy of 10^{-8} at 1 nA current. Typical results obtained by us so far are still lacking in the desired accuracy (fig. 37). Even as the accuracy is far from the required value, it should be remembered that these are the first generation devices and further development should be possible with reasonable efforts. In our opinion, at the moment the most limiting factor in improving the accuracy has been the overheating of the samples which probably should be possible to overcome with the approach suggested in the next section.

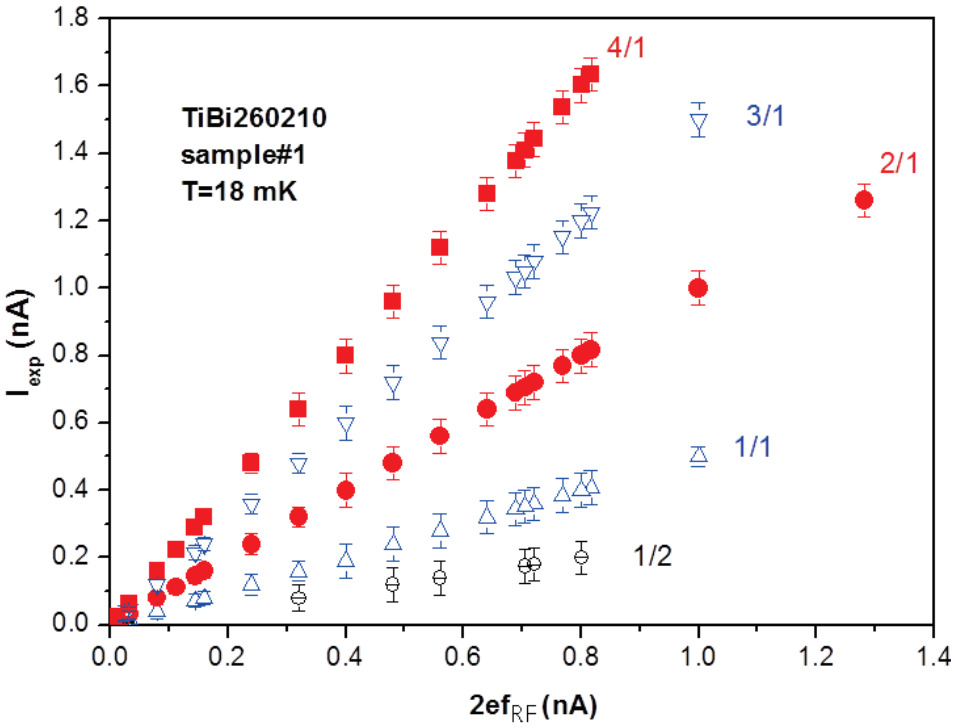

FIGURE 38 The positions of the current singularities at $I_{n,m}$ as function of the frequency (multiplied by 2e). The error bars indicate uncertainty defining the step positions. We believe that the main contribution to the undesired broadening of the plateaus comes from the Joule heating of the high-resistive leads and the associated Johnson noise. Notations of the series are discussed in section 2.3.9.[93]

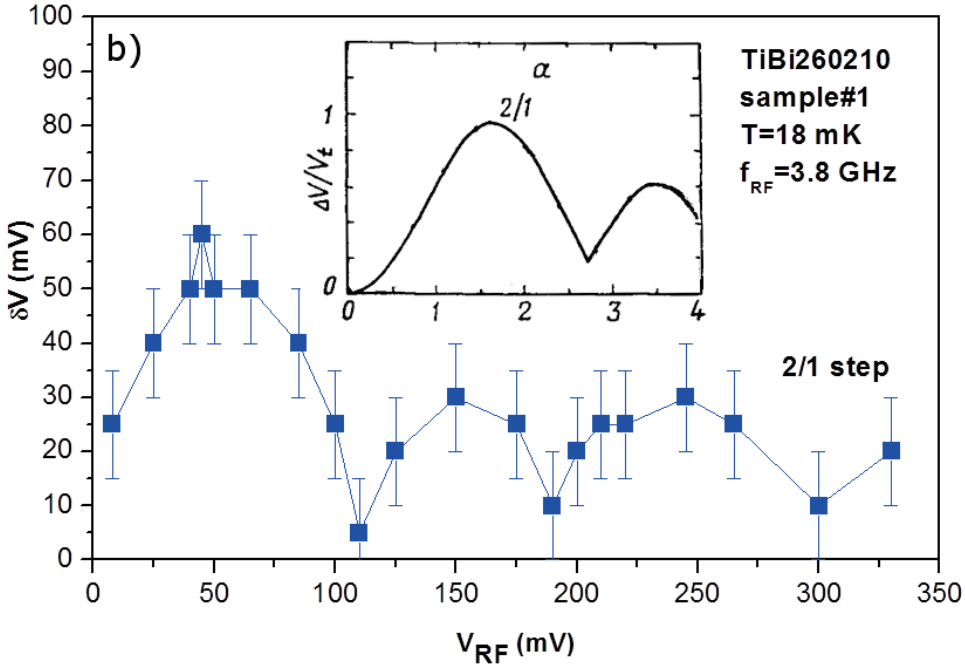

FIGURE 39 The width of the 'principal' Bloch 2/1 step for charge 2e, n = 1 and m = 1 as function of the RF amplitude. The amplitude dependency qualitatively corresponds to the theoretical dependency shown in the inset and derived for the dual system: small current biased JJ. Heating of the high-ohmic contacts with finite measurement current broadens the plateaus causing uncertainty in determination of the Bloch steps (marked with error bars).[93]

4.3.3 Improving the structure

As the most limiting factor of the performance so far obtained for the accuracy of the current standard structure has been the electron heating in the high ohmic resistors, the resistive elements were replaced by superconducting SQUID-arrays, similar to the QPS transistor structure (fig. 23). The solution should have eliminated the heating problems to large extent, however no distinct Bloch singularities were observed, only weak peculiarities. This is presumably due to the fact that the essentially non-linear SQUID-based elements provide high impedance environment only at small currents (fig. 24 inset). The dynamic resistance of the SQUID arrays is essentially current dependent, and is higher than 10^7 Ω only within the range of bias current $I < 10^{-11}$ A, while the current standard would require currents of the order of 1 nA.

The next improvement used in this work was to utilize resonant LC-tank as the high-impedance environment. Two types of structures were studied. In the first set the LC-resonator was made to supply the high-impedance environment for a certain frequency, i.e. to act as a band-reject filter. The high dc resistance was provided by serially connected dirty titanium resistor with LC-tank. For each probe the dc resistance was about 500k Ω to 1 MΩ. Simulated impedances for the LC-tank at the resonance frequency were of the order 10^7 Ω. The structure is presented in figure 40. Voltage was measured either with normal metal or superconducting probes. The LC-tank consists of a long superconducting nanowire with kinetic inductance $L_K \approx 700$ nH and a 'comb-type' capacitor with capacitance C ≈ 20 fF in parallel. One side of the LC-resonator is capacitively coupled to the ground (to prevent damping of the oscillator) and other side is connected to the RF-line and the nanowire (fig. 40a).

The structure has multiple desired properties. At the resonance frequency $f = 1/(2\pi\sqrt{LC})$ the RF-drive is forced to go through the nanowire. Simulation made with 5Spice software for ac-current through the nanowire $I_{ac}(f)$ with constant rf drive demonstrates the performance (fig. 40b). The equivalent ac-circuit used for the simulation is presented in figure 40c. Parasitic capacitances are neglected as the effects would be negligible. For other frequencies the impedance to the ground is small through the tank. From the dc-probe side the structure functions as RC-filter: dc is biased through resistors R1 and R2 forming RC-filters with capacitances C4 and C3 with cut-off frequency $1/RC \approx 1$ kHz. This helps to 'shield' the QPS-nanowire from the external noise coming from the (overheated) high-ohmic normal electrodes by reducing the bandwidth of Johnson noise.

The other LC-structure works in the opposite way: the resonance enhances the drive impact of the RF. At certain frequency (corresponding to the optimal RF-drive) the whole circuit should "ring". The elements of the structure are the same as above but are arranged in different way. The parallel capacitor to the inductance is interchanged to be parallel capacitance to the high-ohmic probe.

Unfortunately in both types of structures with RLC-circuit only very weak Coulomb blockade of about few μV has been observed though the diameter of the QPS nanowire ~ 30 nm corresponds to the scales where in earlier studies

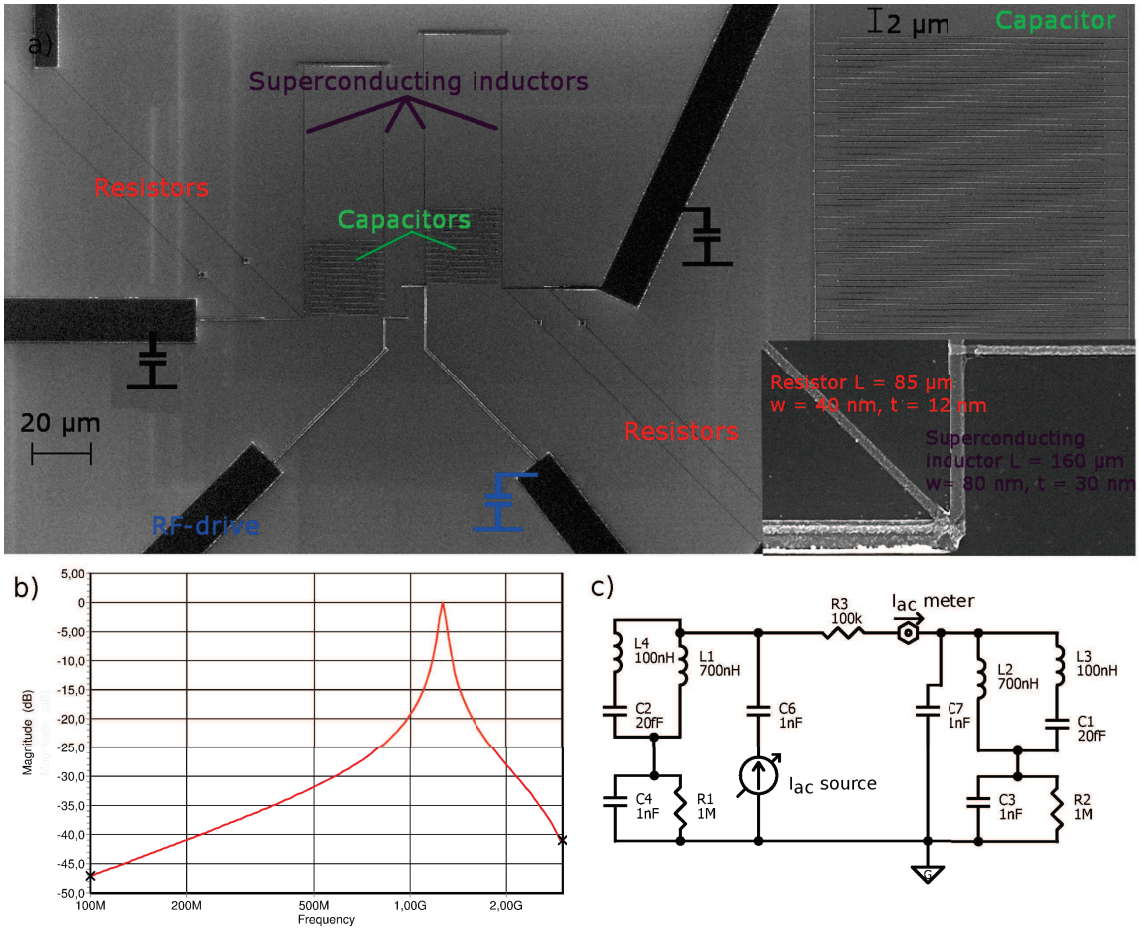

FIGURE 40 a) SEM images of the LC-structure. The structure consists of dirty titanium normal metal resistor current-biasing probes L = 85 μm and R = 500 kΩ to 1 MΩ in series with LC-tank. The LC-circuit consists of long superconducting nanowire with kinetic inductance L = 700 nH and 'finger' capacitor with capacitance C = 20 fF. In the middle, between the LC-tanks, is the QPS-nanowire. Voltage is measured either with normal metal or superconducting probes. b) Simulated $I_{ac}(f)$ through the nanowire. At resonance frequency, the rf-drive is forced to go through the nanowire. c) The equivalent circuit used for the simulation.

pronounced signature of the QPS effect has been observed. Given that for such high-ohmic samples the experimental noise is $\sim$ 100 nV, no definite conclusions on existence/non-existence of Bloch steps could be made.

Several explanations might explain this experimentally unsatisfactory result. First is that the environment is too low ohmic: the dirty normal metal titanium probes have 20 - 100x lower dc resistance than previously used Bi-probes. Second is that the QPS-nanowire might not be within the horizon of the high-impedance environment. The estimations for the scale of the horizon[94, 95, 96] are from tens of μm to hundreds μm. In our earlier structures the high-impedance environment was within $\sim$ 25 μm from the QPS-nanowire. In the LC-designs the length of the high-impedance environment is about 300 μm and it is likely that the QPS-nanowire is not anymore affected by the environment as desired. We cannot also exclude the possibility, that due to some uncontrolled factors in these latest generation samples, we unintentionally managed to fabricate cleaner titanium nanowires. Given the exponential dependence on the resistivity of the sample (eq. 24) $\sigma^{1/2} \equiv 30$ nm might appear insufficient to provide decent QPS rate.

Third reason might be related to undesired Zener tunneling. As discussed in section 2.3.6, the effect of Zener tunneling strongly depends on dissipation in the system. With decrease of dissipation the Zener tunneling starts to dominate the system behavior at smaller currents, effectively reducing the range of currents, where Bloch oscillations can be observed (fig. 9). Hence, the substitution of purely dissipative elements from earlier design (fig. 32) with LC-tank (fig. 40 and 41) might shrink the range of observability of Bloch oscillations.

Unfortunately, the ideas about incorporation of LC resonance tanks in the current biasing circuit came just few months before the expiration of the Ph.D. studies. Due to time limitations we had not much time to solve the mentioned problems.

4.3.4 Suggestions for an improved design

The RLC-structure could be improved by making compact resistor and capacitor elements from tunnel junctions(fig. 41). The structure consists of parallel arrays of tunnel junctions, long superconducting titanium nanowire acting as kinetic inductor and high-ohmic dirty titanium probes each 1 MΩ isolating the ac-circuit from the dc-bias and dc-voltage measurement circuits.

The QPSJ is biased through the tunnel junction array with dc-impedance $>$10 MΩ up to current 1 nA . With small currents the impedance is even higher about 10^8 to 10^9 Ω derived from the results obtained from the tunnel junction arrays on previous samples (fig. 24 inset). To obtain dynamic resistance of the order of $10^7\Omega$, enabling effective current biasing, the critical current through each probe should be at maximum 10 pA. This means that there should be $\sim$ 100 parallel junctions for the 1 nA current. If the distance between each chain is 300 nm, this would require $\sim$35 μm wide array. If each of the tunnel junction chain contains 5 junctions, the length of the each probe is about 1 to 2 μm. For sharp resonance the superconducting kinetic inductor should be placed before the array.

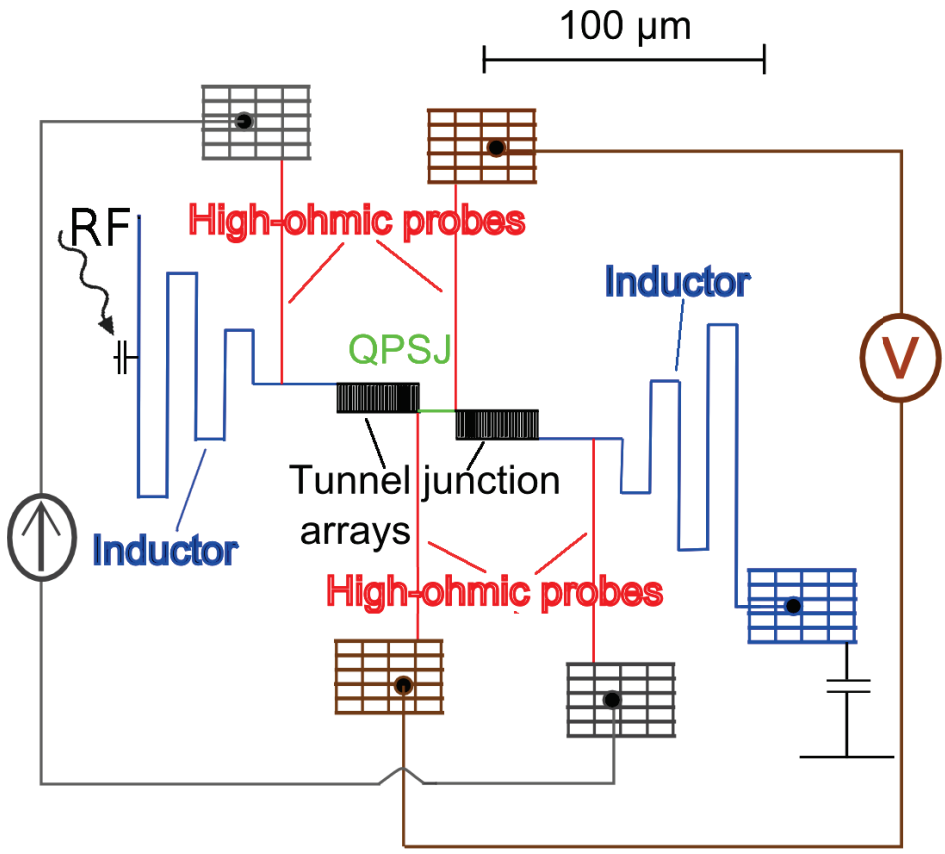

FIGURE 41 Qualitative schematics of improved design for the QSC. The structure consists of long superconducting nanowire acting as inductor, tunnel junction array providing the high impedance (ac and dc) and also the capacitance for the LC-resonator, high-ohmic resistors isolating the structure from the parasitic capacitances of the pads and the measurement lines, and QPSJ: a thin superconducting nanowire with high QPS rate.

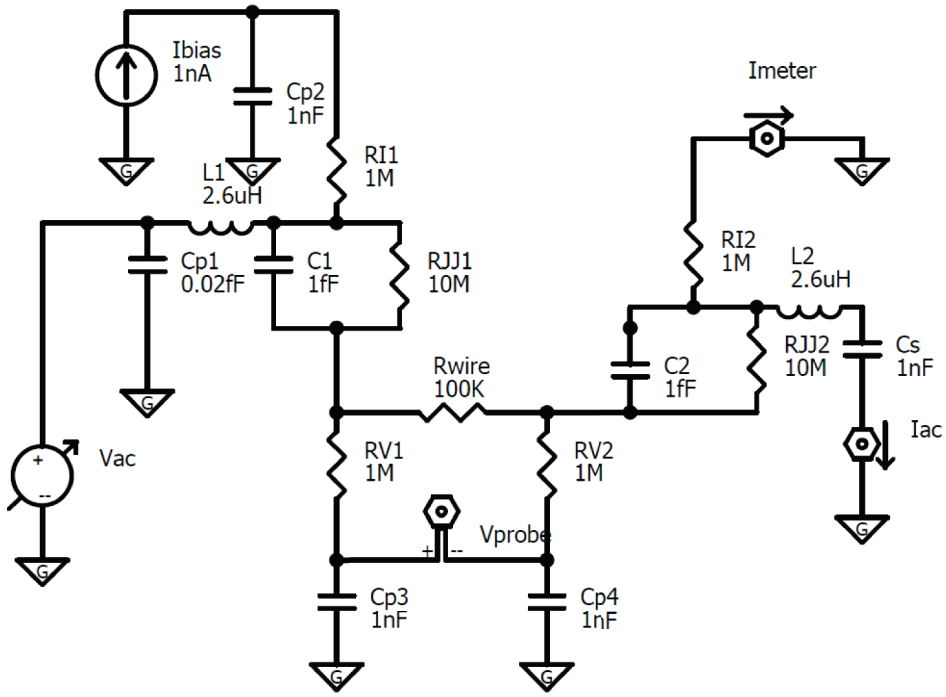

FIGURE 42 Kirchhoff equivalent circuit for structure presented in figure 41. For simulating the circuit capacitance to ground, the effective ground plate, has been added under the structure at distance of 550 μm corresponding to typical thickness of a silicon wafer. The resistors RI1, RI2 and RV1, RV2 isolate the QPSJ from the parasitic (pad) capacitances Cp2, Cp3, and Cp4 of the dc-biasing and dc-voltage measurement circuits, but not from the inductor's parasitic capacitance Cp1. Component parameters that have negligible impact when determining the overall characteristics in the simulation have been neglected.

If the tunnel junctions have thickness 20 nm and width 50 nm the capacitance of 5 junction chain would be of the order 10^{-17} to 10^{-18} F. The cross capacitance between the parallel chains would be of the same order. Thus the total capacitance could be estimated to be at the range $C_{probe} = 100 * 10^{-17} = 10^{-15} F$. The parasitic capacitance to the ground should be negligible in comparison. For the GHz range this would mean impedance of the order of a $M\Omega$.

Let us select the resonance frequency of the oscillator adjusted for obtaining the Bloch step at 1 nA, ie. 3.12 GHz. Then inductance of the oscillator should be $L_K = \frac{1}{4\pi^2 f^2 C} = 2.6$ μH. The kinetic inductance of a superconducting nanowire can be evaluated $L_{K,T=0} = \hbar R_N / \pi \Delta_0$. To have high kinetic inductance superconducting wire needs to have high normal state resistance and small superconducting gap. Typical normal states resistivity of evaporated titanium nanowire is about $\rho = 2 * 10^{-6}$ Ωm and the superconducting energy gap $\Delta_0 = 60$ μeV. The wire cross-section needs to be high enough to have negligible quantum phase slip rate at low temperatures. For obtaining the kinetic inductance 2.6 μH with $\sigma^{1/2} \cong 50$ nm superconducting titanium nanowire the length of the wire should be

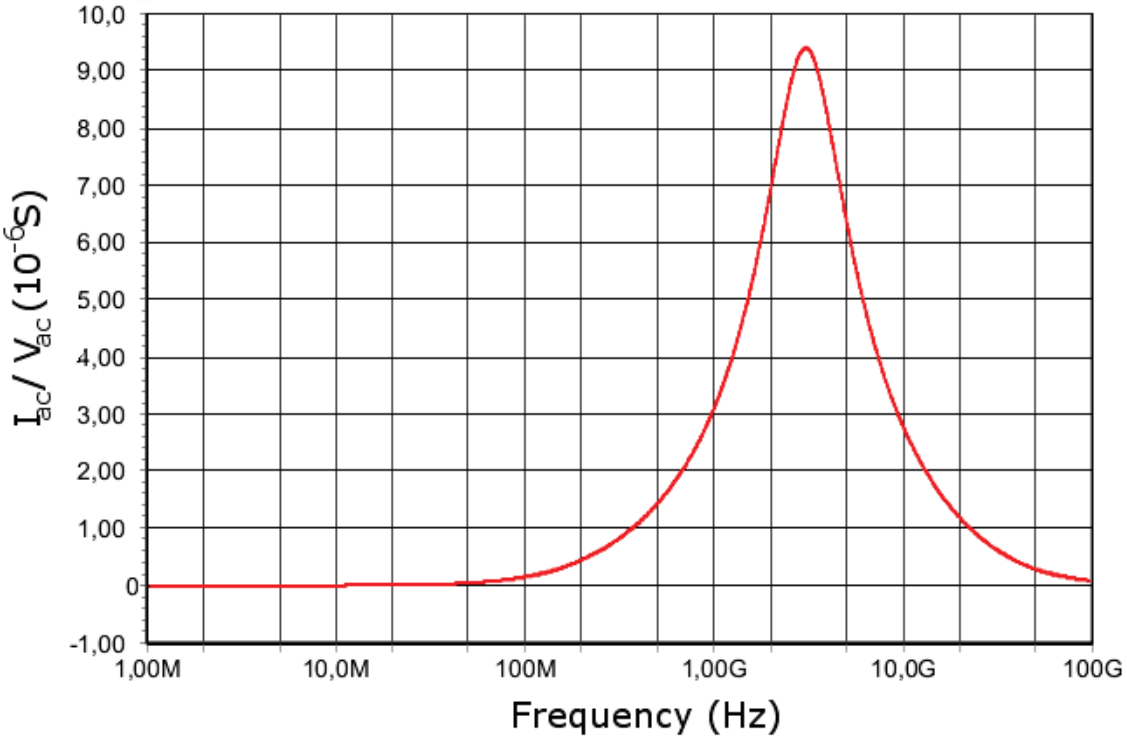

FIGURE 43 Admittance I_{ac}/V_{ac} of the circuit presented in figure 42 as function of frequency of external RF drive f_{ac}. The RF signal can be introduced through capacitive coupling with the on-chip inductor. At the resonance frequency $1/\sqrt{LC} = 3.12$ GHz the admittance has maximum.

$$l = \frac{\pi\sigma L_K \Delta_0}{\hbar\rho} \approx 370\mu m. \tag{78}$$

The long superconducting nanowire acting as the element with high inductance can be incorporated within the RF-antenna structure.

Figure 42 the Kirchhoff equivalent circuit used to simulate the ac-performance of the structure. The circuit has parasitic capacitances from the inductors, connection pads and the measurement lines incorporated. When the parasitic capacitances were calculated, it was assumed that the structure is made on Si-chip that has thickness 550 μm and the chip has been glued on the ground-plate. The capacitances and inductances of the resistors and the QPSJ and also the cross-capacitance ($\sim$few aF, depends on the geometry) between left and right parts of the circuit are neglected. The result of the simulation, done with 5Spice software, for the ac-impedance of the structure is presented in figure 43.

The circuit filters well the frequencies below 1 GHz and above 10 GHz. For MHz range the ac-impedance is $\gtrsim$ 10 MΩ. At the resonance of the LC-circuit the impedance is about 100 kΩ. Small external drive at the resonance frequency should make the system "ring".

Realization of the circuit depicted in figure 41 with proper parameters is feasible and is compatible with the processes and materials used in our earlier structures. The resonance frequency of an LC-resonator has a square root depen-

dency of the capacitance and inductance and thus even relatively large changes in either parameter should result in only minor tuning of the resonance frequency. Certain technological efforts would be necessary to realize the optimized circuit. Note that the suggested circuit is designed not to perform an extended 'academic' study of the QPS phenomenon. The circuit is optimized to solve exclusively the applied problem: to obtain sharp current singularities (Bloch steps) $I_n = n(2e)f_{RF}$ at the pre-defined frequency f_{RF} corresponding to the resonant frequency of the LC-tank.

5 CONCLUSIONS

We have studied superconducting highly uniform polycrystalline titanium nanowires with progressively reduced cross sections using low energy ion milling. All samples are in the quasi-1-dimensional limit $l \ll \sigma^{1/2} < \xi \ll L$, where σ is the nanowire cross section, l is the mean free path, ξ is the dirty limit coherence length, and L is the wire length. For nanowires with diameters <50 nm the width of the R(T) transition broadens well above the limits which can be explained by the TAPS model[15, 16] with a realistic set of parameters. On the other hand the G-Z QPS-model[30] gives good agreement for the shape of R(T) transitions for samples with diameters between 30 to 50 nm. For thinner samples with diameters $\lesssim$30 nm the experimentally measured R(T) dependency is weak, and for the thinnest samples we've observed complete flattening of the superconducting transition $R(T \ll T_c) \approx R(T_c) = R_N$. The observation of the size-dependent broadening of the R(T) dependencies in superconducting titanium supports the conjecture about the universality of the QPS effect earlier observed in other materials to be present in a quasi-one-dimensional superconductor of sufficiently small cross section.

To verify the high quality of the evaporated material and to address to the skepticism related to sample homogeneity the extensive microscopy and elemental analyses were performed. The analyses revealed no obvious structural or geometrical imperfections. The transport properties of 'conventional' structures with low-ohmic probes, neither in normal, nor in superconducting state, revealed any signature of a non-ohmic behavior, which could be associated with hidden structural defects.

The configuration enabling current biasing of a QPS superconducting nanowire through on-chip high-impedance electrodes demonstrates intuitively controversial effect: the insulating state of a 1D superconductor. The phenomenon originates from the fundamental quantum duality between a Josephson junction and a superconducting nanowire governed by quantum fluctuations – quantum phase slips junction. The magnitude of the Coulomb gap increases with decrease of the nanowire cross section, and disappears above certain temperature and/or magnetic field supporting the relation of the effect to superconductivity.

The insulating state of the quantum phase slip junction can be utilized to realize a quantum phase slip transistor: a transistor without any dielectric barriers. The QPS effect provides the dynamic equivalent of a conventional (static in space and time) JJ. The charge of the island can be monitored by application of a static potential by capacitively coupled gate electrode. The dynamic resistance of the transistor at small bias $dV/dI(I \to 0)$ oscillates periodically with gate voltage. Application of small magnetic field, much smaller than the critical, increases the value of the Coulomb gap. Note that in superconducting QPS nanowires with low-ohmic probes application of small magnetic field also leads to observation of negative magnetoresistance. The origins of both effects are not clear, but likely are linked.

The I-V characteristics of a QPS nanowire in high-ohmic environment demonstrates at small biases the insulating states (Coulomb blockade), while with increase of the bias the specific back-bending ('Bloch nose') is observed. This peculiar region of the I-V dependence is characterized by transition from the insulating state to current-carrying state. Electron transport at this region with negative differential resistance is maintained by coherent motion of Cooper pairs, similar to the well-know single electron effect. Coherent superposition of $\pm 2\pi$ quantum phase slips enables periodic charging/discharging by 2e happening at a Bloch frequency $f_{Bloch} = I/2e$.

With application of external RF drive the Bloch oscillations of a QPSJ can be synchronized leading to formation of current singularities at values $I_n = n(2e)f_{RF}$, n = 1,2,3,... The effect could be utilized to build the quantum standard of electric current (QSC). Our realization for the QSC structure demonstrated clear signature of Bloch oscillations, and we've been first to report in QPSJ the observation of synchronization of the Bloch oscillations with the external RF drive. Compared to conventional small JJs, a QPSJ (with proper parameters enabling observation of Bloch oscillations) should sustain much higher currents, being of clear advantage for practical metrology. In our experiments the relative accuracy in positions of the Bloch steps $\delta I_n/I \approx 10^{-2}$ presumably is limited by the undesired Joule heating of the high-ohmic current biasing electrodes. However, the high absolute value reaching the nA range of the current is very encouraging. Further improvements aimed at solving the heating problem and optimizing the high-impedance environment of the QSC-structure were tested.

In addition to the importance for the basic knowledge about of nanoscale superconductivity, the subject of quantum fluctuations has lead to a new class of devices: QPS flux qubit[12], quantum standard of electric current[69, 63], and QPS-transistor[62]. The absence of conventional tunnel barriers formed of dielectrics, undesired for such applications as quantum computing, open new horizons for corresponding utilization of QPS-based devices. The exponential dependence of the QPS rate on diameter enables realization of almost arbitrary ratio between the characteristic energies(E_{QPS}, E_C and E_L), compared to conventional JJs, where E_J and E_C are somehow entangled by the geometry of the junction.

It would be very desirable if the studies of the QPS phenomenon will be continued. The topic is interesting offering numerous intriguing applications.

REFERENCES

[1] J. Bardeen, L. N. Cooper, and J. R. Schrieffer, "Microscopic theory of superconductivity," *Physical Review*, vol. 106, pp. 162–164, Apr. 1957.

[2] J. Bardeen, L. N. Cooper, and J. R. Schrieffer, "Theory of superconductivity," *Physical Review*, vol. 108, pp. 1175–1204, 12 1957.

[3] W. A. Little, "Decay of persistent currents in small superconductors," *Phys. Rev.*, vol. 156, pp. 396–403, 1967.

[4] N. Giodano, "Evidence for macroscopic quantum tunneling in one-dimensional superconductors," *Phys. Rev. Lett.*, vol. 61, pp. 2137–2140, 1988.

[5] A. Bezryadin, C. N. Lau, and M. Tinkham, "Quantum suppression of superductivity in ultrathin nanowires," *Nature*, vol. 404, pp. 971–974, 2000.

[6] M. Savolainen, V. Touboltsev, P. Koppinen, K.-P. Riikonen, and K. Y. Arutyunov, "Ion beam sputtering for progressive reduction of nanostructures dimensions," *Applied Physics A*, vol. 79, pp. 1769–1773, 2004.

[7] M. Zgirski, K.-P. Riikonen, V. Tuboltsev, P. Jalkanen, H. T. T., and K. Y. Arutyunov, "Ion beam shaping and downsizing of nanostructures," *Nanotechnology*, vol. 19, no. 5, pp. 055301–1–055301–6, 2008.

[8] M. Zgirski, "Experimental study of fluctuations in ultra-narrow superconducting nanowires," *PhD. Thesis, University of Jyväskylä*, 2008.

[9] M. Zgirski, K.-P. Riikonen, V. Touboltsev, and K. Arutyunov, "Size dependent breakdown of superconductivity in ultranarrow nanowires," *Nano Letters*, vol. 5, no. 6, pp. 1029–1033, 2005.

[10] M. Zgirski, K.-P. Riikonen, V. Touboltsev, and K. Y. Arutyunov, "Quantum fluctuations in ultranarrow superconducting aluminum nanowires," *Phys. Rev. B*, vol. 77, p. 054508, 2008.

[11] K. Arutyunov, T. Hongisto, J. Lehtinen, L. Leino, and A. Vasiliev, "Quantum phase slip phenomenon in ultra-narrow superconducting nanorings," *Sci.Rep.*, vol. 2, p. 213, 2012.

[12] O. V. Astafiev, L. B. Ioffe, S. Kafanov, Y. A. Pashkin, K. Y. Arutyunov, D. Shahar, O. Cohen, and J. S. Tsai, "Coherent quantum phase slip," *Nature*, vol. 484, pp. 355–358, 2012.

[13] K. H. Onnes, "Investigations into the properties of substances at low temperatures, which have led, amongst other things, to the preparation of liquid helium," *Nobel lecture series*, 1913.

[14] M. Tinkham, *Introduction to superconductivity: second edition*. McGraw-Hill New York, 2004.

[15] J. S. Langer and V. Ambegaokar, "Intrinsic resistive transition in narrow superconducting channels," *Phys. Rev.*, vol. 164, pp. 498–510, 1967.

[16] D. E. McCumber, "Intrinsic resistive transition in thin superconducting wires driven from current sources," *Phys. Rev.*, vol. 172, pp. 427–429, 1968.

[17] D. E. McCumber and B. I. Halperin, "Time scale of intrinsic resistive fluctuations in thin superconducting wires," *Phys. Rev. B*, vol. 1, pp. 1054–1070, Feb 1970.

[18] J. E. Lukens, R. J. Warburton, and W. W. Webb, "Onset of quantized thermal fluctuations in "one-dimensional" superconductors," *Phys. Rev. Lett.*, vol. 25, pp. 1180–1184, 1970.

[19] R. S. Newbower, M. R. Beasley, and M. Tinkham, "Fluctuation effects on the superconducting transition of tin whisker crystals," *Phys. Rev. B*, vol. 5, pp. 864–868, 1972.

[20] J. M. Graybeal, P. M. Mankiewich, R. C. Dynes, and M. R. Beasley, "Apparent destruction of superconductivity in the disordered one-dimensional limit," *Phys. Rev. Lett.*, vol. 59, pp. 2697–2700, Dec 1987.

[21] C. N. Lau, N. Markovic, M. Bockrath, A. Bezryadin, and M. Tinkham, "Quantum phase slips in superconducting nanowires," *Phys. Rev. Lett.*, vol. 87, p. 217003, Nov 2001.

[22] N. Giordano, "Superconducting fluctuations in one dimension," *Physica B*, vol. 203, no. 3-4, pp. 460–466, 1994.

[23] N. Giordano and E. R. Schuler, "Macroscopic quantum tunneling and related effects in a one-dimensional superconductor," *Phys. Rev. Lett.*, vol. 63, pp. 2417–2420, Nov 1989.

[24] F. Altomare, A. M. Chang, M. R. Melloch, Y. Hong, and C. W. Tu, "Evidence for macroscopic quantum tunneling of phase slips in long one-dimensional superconducting Al wires," *Phys. Rev. Lett.*, vol. 97, p. 017001, 2006.

[25] F. Sharifi, A. V. Herzog, and R. C. Dynes, "Crossover from two to one dimension in in situ grown wires of Pb," *Phys. Rev. Lett.*, vol. 71, pp. 428–431, Jul 1993.

[26] A. Johansson, G. Sambandamurthy, D. Shahar, N. Jacobson, and R. Tenne, "Nanowire acting as a superconducting quantum interference device," *Phys. Rev. Lett.*, vol. 95, p. 116805, Sep 2005.

[27] N. Giordano, "Superconductivity and dissipation in small-diameter Pb-In wires," *Phys. Rev. B*, vol. 43, pp. 160–174, Jan 1991.

[28] J.-M. Duan, "Quantum decay of one-dimensional supercurrent: Role of electromagnetic field," *Phys. Rev. Lett.*, vol. 74, pp. 5128–5131, Jun 1995.

[29] S. R. Renn and J.-M. Duan, "Nonuniversal metallic behavior of superconducting wires," *Phys. Rev. Lett.*, vol. 76, pp. 3400–3403, Apr 1996.

[30] A. D. Zaikin, D. S. Golubev, A. van Otterlo, and G. T. Zimányi, "Quantum phase slips and transport in ultrathin superconducting wires," *Phys. Rev. Lett.*, vol. 78, pp. 1552–1555, 1997.

[31] J. E. Mooij and G. Schön, "Propagating plasma mode in thin superconducting filaments," *Phys. Rev. Lett.*, vol. 55, pp. 114–117, Jul 1985.

[32] K. Arutyunov, D. Golubev, and A. Zaikin, "Superconductivity in one dimension," *Physics Reports*, vol. 464, no. 1, pp. 1 – 70, 2008.

[33] M. Remeika and A. Bezryadin, "Sub-10 nanometre fabrication: molecular templating, electron-beam sculpting and crystallization of metallic nanowires," *Nanotechnology*, vol. 16, no. 8, p. 1172, 2005.

[34] A. T. Bollinger, R. C. Dinsmore, A. Rogachev, and A. Bezryadin, "Determination of the superconductor-insulator phase diagram for one-dimensional wires," *Phys. Rev. Lett.*, vol. 101, p. 227003, Nov 2008.

[35] S. Chakravarty, "Quantum fluctuations in the tunneling between superconductors," *Phys. Rev. Lett.*, vol. 49, pp. 681–684, Aug 1982.

[36] A. Schmid, "Diffusion and localization in a dissipative quantum system," *Phys. Rev. Lett.*, vol. 51, pp. 1506–1509, Oct 1983.

[37] S. A. Bulgadaev, "Phase diagram of a dissipative system," *JETP Lett.*, vol. 39, p. 315, 1984.

[38] H. P. Büchler, V. B. Geshkenbein, and G. Blatter, "Quantum fluctuations in thin superconducting wires of finite length," *Phys. Rev. Lett.*, vol. 92, p. 067007, Feb 2004.

[39] D. Meidan, Y. Oreg, and G. Refael, "Sharp superconductor-insulator transition in short wires," *Phys. Rev. Lett.*, vol. 98, p. 187001, May 2007.

[40] G. Refael, E. Demler, and Y. Oreg, "Superconductor to normal-metal transition in finite-length nanowires: Phenomenological model," *Phys. Rev. B*, vol. 79, p. 094524, Mar 2009.

[41] B. Josephson, "Possible new effects in superconductive tunnelling," *Physics Letters*, vol. 1, no. 7, pp. 251 – 253, 1962.

[42] R. Feynman, "The feynman lectures on physics (online)," *http://www.feynmanlectures.caltech.edu/ (retrieved 21.11.2013)*.

[43] V. Ambegaokar and B. I. Halperin, "Voltage due to thermal noise in the dc Josephson effect," *Phys. Rev. Lett.*, vol. 22, pp. 1364–1366, Jun 1969.

[44] T. A. Fulton and L. N. Dunkleberger, "Lifetime of the zero-voltage state in Josephson tunnel junctions," *Phys. Rev. B*, vol. 9, pp. 4760–4768, Jun 1974.

[45] J. Mooij and Y. V. Nazarov, "Superconducting nanowires as quantum phase-slip junctions," *Nature Physics*, vol. 2, pp. 169–172, 2006.

[46] R. F. Voss and R. A. Webb, "Macroscopic quantum tunneling in 1-μm Nb Josephson junctions," *Phys. Rev. Lett.*, vol. 47, pp. 265–268, Jul 1981.

[47] G. Schön and A. Zaikin, "Quantum coherent effects, phase transitions, and the dissipative dynamics of ultra small tunnel junctions," *Physics Reports*, vol. 198, no. 5-6, pp. 237 – 412, 1990.

[48] A. O. Caldeira and A. J. Leggett, "Influence of dissipation on quantum tunneling in macroscopic systems," *Phys. Rev. Lett.*, vol. 46, pp. 211–214, Jan 1981.

[49] J. M. Martinis, M. H. Devoret, and J. Clarke, "Experimental tests for the quantum behavior of a macroscopic degree of freedom: The phase difference across a Josephson junction," *Phys. Rev. B*, vol. 35, pp. 4682–4698, Apr 1987.

[50] K. Likharev and A. Zorin, "Theory of the Bloch-wave oscillations in small Josephson junctions," *Journal of Low Temperature Physics*, vol. 59, no. 3-4, pp. 347–382, 1985.

[51] D. Haviland, L. Kuzmin, P. Delsing, K. Likharev, and T. Claeson, "Experimental evidence for the Coulomb blockade of cooper pair tunneling and Bloch oscillations in single Josephson junctions," *Zeitschrift für Physik B Condensed Matter*, vol. 85, no. 3, pp. 339–347, 1991.

[52] M. Watanabe and D. B. Haviland, "Coulomb blockade and coherent single-cooper-pair tunneling in single Josephson junctions," *Phys. Rev. Lett.*, vol. 86, pp. 5120–5123, May 2001.

[53] A. Widom, G. Megaloudis, T. D. Clark, H. Prance, and R. J. Prance, "Quantum electrodynamic charge space energy bands in singly connected superconducting weak links," *Journal of Physics A: Mathematical and General*, vol. 15, no. 12, p. 3877, 1982.

[54] F. Guinea and G. Schön, "Coherent charge oscillations in tunnel junctions," *Europhys. Lett.*, vol. 1, no. 11, p. 585, 1986.

[55] K. Mullen, E. Ben-Jacob, and Z. Schuss, "Combined effect of Zener and quasiparticle transitions on the dynamics of mesoscopic Josephson junctions," *Phys. Rev. Lett.*, vol. 60, pp. 1097–1100, Mar 1988.

[56] C. Zener, "A theory of the electrical breakdown of solid dielectrics," *Proc. R. Soc. A*, vol. 145, p. 523, 1934.

[57] D. V. Averin and A. A. Odintsov, "Coherent oscillations in small tunnel junctions: tight-binding limit," *Fiz. Nizk. Temp.*, vol. 16, pp. 16–25, 1990.

[58] J. E. Mooij and C. J. P. M. Harmans, "Phase-slip flux qubits," *New Journal of Physics*, vol. 7, no. 1, p. 219, 2005.

[59] A. M. Hriscu and Y. V. Nazarov, "Model of a proposed superconducting phase slip oscillator: A method for obtaining few-photon nonlinearities," *Phys. Rev. Lett.*, vol. 106, p. 077004, 2011.

[60] A. M. Hriscu and Y. V. Nazarov, "Coulomb blockade due to quantum phase slips illustrated with devices," *Phys. Rev. B*, vol. 83, p. 174511, 2011.

[61] S. Shapiro, "Josephson currents in superconducting tunneling: The effect of microwaves and other observations," *Phys. Rev. Lett.*, vol. 11, pp. 80–82, Jul 1963.

[62] T. T. Hongisto and A. B. Zorin, "Single-charge transistor based on the charge-phase duality of a superconducting nanowire circuit," *Phys. Rev. Lett.*, vol. 108, p. 097001, 2012.

[63] C. H. Webster, J. C. Fenton, T. T. Hongisto, S. P. Giblin, A. B. Zorin, and P. A. Warburton, "NbSi nanowire quantum phase-slip circuits: dc supercurrent blockade, microwave measurements, and thermal analysis," *Phys. Rev. B*, vol. 87, p. 144510, Apr 2013.

[64] J. T. Peltonen, O. V. Astafiev, Y. P. Korneeva, B. M. Voronov, A. A. Korneev, I. M. Charaev, A. V. Semenov, G. N. Golt'sman, L. B. Ioffe, T. M. Klapwijk, and J. S. Tsai, "Coherent flux tunneling through NbN nanowires," *Phys. Rev. B*, vol. 88, p. 220506, Dec 2013.

[65] M. Vanević and Y. V. Nazarov, "Quantum phase slips in superconducting wires with weak inhomogeneities," *Phys. Rev. Lett.*, vol. 108, p. 187002, May 2012.

[66] F. Piquemal and G. Genevès, "Argument for a direct realization of the quantum metrological triangle," *Metrologia*, vol. 37, no. 3, p. 207, 2000.

[67] C. H. Webster, S. Giblin, D. Cox, T. J. B. M. Janssen, and A. Zorin, "A quantum current standard based on phase slip," *CPEM Precision Electromagnetic Measurements Digest*, pp. 628–629, 2008.

[68] L. S. Kuzmin and D. B. Haviland, "Observation of the bloch oscillations in an ultrasmall Josephson junction," *Phys. Rev. Lett.*, vol. 67, pp. 2890–2893, 1991.

[69] J. S. Lehtinen, K. Zakharov, and K. Y. Arutyunov, "Coulomb blockade and Bloch oscillations in superconducting Ti nanowires," *Phys. Rev. Lett.*, vol. 109, p. 187001, Oct 2012.

[70] A. Rogachev and A. Bezryadin, "Superconducting properties of polycrystalline Nb nanowires templated by carbon nanotubes," *Applied Physics Letters*, vol. 83, no. 3, pp. 512–514, 2003.

[71] J. S. Lehtinen, T. Sajavaara, K. Y. Arutyunov, M. Y. Presnjakov, and A. L. Vasiliev, "Evidence of quantum phase slip effect in titanium nanowires," *Phys. Rev. B*, vol. 85, p. 094508, 2012.

[72] J. S. Lehtinen and K. Y. Arutyunov, "The quantum phase slip phenomenon in superconducting nanowires with a low-ohmic environment," *Superconductor Science and Technology*, vol. 25, no. 12, p. 124007, 2012.

[73] A. A. Shanenko, M. D. Croitoru, M. Zgirski, F. M. Peeters, and K. Arutyunov, "Size-dependent enhancement of superconductivity in Al and Sn nanowires: Shape-resonance effect," *Phys. Rev. B*, vol. 74, p. 052502, 2006.

[74] Y. Oreg and A. M. Finkel'stein, "Suppression of T_c in superconducting amorphous wires," *Phys. Rev. Lett.*, vol. 83, pp. 191–194, 1999.

[75] M. Zgirski and K. Y. Arutyunov, "Experimental limits of the observation of thermally activated phase-slip mechanism in superconducting nanowires," *Phys. Rev. B*, vol. 75, p. 172509, May 2007.

[76] J. F. Ziegler, "Srim - the stopping and range of ions in matter," *www.srim.org*, retrived 11.12.2013.

[77] J. Pekola and J. Kauppinen, "Insertable dilution refrigerator for characterization of mesoscopic samples," *Cryogenics*, vol. 34, pp. 843–845, 1994.

[78] K. Y. Arutyunov, H.-P. Auraneva, and A. S. Vasenko, "Spatially resolved measurement of nonequilibrium quasiparticle relaxation in superconducting Al," *Phys. Rev. B*, vol. 83, p. 104509, 2011.

[79] V. Schöllmann, J. Johansson, K. Andersson, and D. B. Haviland, "Coulomb blockade effects in anodically oxidized titanium wires," *J. Appl. Phys.*, vol. 88, no. 11, pp. 6549–6553, 2000.

[80] M. Putkonen, T. Sajavaara, L. Niinistö, and J. Keinonen, "Analysis of ald-processed thin films by ion-beam techniques," *Analytical and Bioanalytical Chemistry*, vol. 382, no. 8, pp. 1791–1799, 2005.

[81] K. Arstila, T. Sajavaara, and J. Keinonen, "Monte Carlo simulation of multiple and plural scattering in elastic recoil detection," *Nuclear Instruments and Methods in Physics Research Section B: Beam Interactions with Materials and Atoms*, vol. 174, pp. 163 – 172, 2001.

[82] J. C. Fenton, C. H. Webster, and P. A. Warburton, "Materials for superconducting nanowires for quantum phase-slip devices," *Journal of Physics: Conference Series*, vol. 286, no. 1, p. 012024, 2011.

[83] B. A. Sanborn, P. B. Allen, and D. A. Papaconstantopoulos, "Empirical electron-phonon coupling constants and anisotropic electrical resistivity in hcp metals," *Phys. Rev. B*, vol. 40, pp. 6037–6044, Sep 1989.

[84] T. Rantala, "Size dependent quantum fluctuations of the superconducting gap," *MSc Thesis, University of Jyväskylä*, 2013.

[85] A. Rogachev, T.-C. Wei, D. Pekker, A. T. Bollinger, P. M. Goldbart, and A. Bezryadin, "Magnetic-field enhancement of superconductivity in ultranarrow wires," *Phys. Rev. Lett.*, vol. 97, p. 137001, 2006.

[86] P. Xiong, A. V. Herzog, and R. C. Dynes, "Negative magnetoresistance in homogeneous amorphous superconducting Pb wires," *Phys. Rev. Lett.*, vol. 78, pp. 927–930, Feb 1997.

[87] P. Jalkanen, V. Touboltsev, H. Koivisto, P. Suominen, T. Suppula, K. Y. Arutyunov, and J. Raisanen, "Superconductivity suppression in Fe-implanted thin Al films," *Journal of Applied physics*, vol. 98, no. 1, p. 016105, 2005.

[88] K. Arutyunov, "Negative magnetoresistance of ultra-narrow superconducting nanowires in the resistive state," *Physica C: Superconductivity*, vol. 468, no. 4, pp. 272 – 275, 2008.

[89] D. Y. Vodolazov, "Negative magnetoresistance and phase slip process in superconducting nanowires," *Phys. Rev. B*, vol. 75, p. 184517, 2007.

[90] M. Meschke, W. Guichard, and J. Pekola, "Single-mode heat conduction by photons," *Nature*, vol. 444, p. 187, 2006.

[91] J. Lehtinen, T. Rantala, and K. Arutyunov, "Insulating state of a quasi-1-dimensional superconductor," *arXiv:1311.3202*, 2013.

[92] F. Giazotto, T. T. Heikkilä, A. Luukanen, A. M. Savin, and J. P. Pekola, "Opportunities for mesoscopics in thermometry and refrigeration: Physics and applications," *Rev. Mod. Phys.*, vol. 78, pp. 217–274, Mar 2006.

[93] D. V. Averin, A. B. Zorin, and K. K. Likharev, "Coherent oscillations in small tunnel junctions," *Zh. Eksp. Teor. Fiz.*, vol. 88, pp. 692–703, 1985.

[94] Y. V. Nazarov, "Anomalous current-voltage characteristics of tunnel junctions," *JETP*, vol. 68, no. 3, p. 561, 1989.

[95] P. Wahlgren, P. Delsing, and D. B. Haviland, "Crossover from global to local rule for the Coulomb blockade in small tunnel junctions," *Phys. Rev. B*, vol. 52, pp. R2293–R2296, Jul 1995.

[96] J. P. Kauppinen and J. P. Pekola, "Charging in solitary, voltage biased tunnel junctions," *Phys. Rev. Lett.*, vol. 77, pp. 3889–3892, Oct 1996.